A Comprehensive study on Heterogeneous Single Atom Catalysis: Current Progress, and Challenges

Swarnalata Swain,[a] Ali Altaee,[b] Manav Saxena, [a*] Akshaya K. Samal[a]*

[a]Centre for Nano and Material Sciences, Jain University, Jain Global Campus, Ramanagara, Bangalore - 562112, India

[b]Centre for Green Technology, School of Civil and Environmental Engineering, University of Technology Sydney, 15 Broadway, NSW 2007, Australia

Email: s.akshaya@jainuniversity.ac.in; manavsaxena19@gmail.com

Contents

Abstract

The production of suitable catalytic materials has expanded considerably in recent years. Now a days, single atom catalysts (SACs) are becoming a new fundamental research area because of the availability of a greater number of active sites and high catalytic activity. However, when particle size decreases, the surface activity of metals upsurges, facilitating the aggregation and sintering. As a result, an appropriate strategy is necessary for the synthesis and stability of SACs. Meanwhile, a large quantity of catalysts is needed for industrial scale production and practical applications. Therefore, manufacturing a high yield of SACs remains challenging. The development of bimetallic SACs is crucial since bimetallic and ternary catalysts have become more comprehended. Herein, the review opens a broad portfolio towards the development of SACs in the fields of electrocatalysis (HER, OER, ORR, N_2 reduction, CO oxidation etc.), photocatalysis (H_2 generation, CO_2 reduction etc.) and organic transformation (C-C, C-X bond formation, oxidation of alcohol-aldehyde and alkane-alcohol) focusing on different types of metal-support co-ordination. A comprehensive summary of the different synthesis protocols of SACs (impregnation, co-precipitation, ALD, pyrolysis, etc.) over several substrates and large-scale manufacturing strategies are highlighted. Furthermore, the current review will concentrate on SAC stability, dual site performance, and the growth of bimetallic SACs to date. Finally, the potential future opportunities are discussed.

Keywords: Single atom catalyst, bimetallic catalyst, ternary catalyst, HER, OER, ORR

1. Introduction

Catalysts have great importance great importance in manufacturing a huge mainstream of drugs, chemicals, materials, and fuels which are crucial for human beings and other organisms [1]. Mainly, it has categorized into three types: homogeneous, heterogeneous, and enzymatic. Enzymatic and homogeneous catalysts, on the other hand, have some limitations, such as stability, reusability, product separation, and industrial scale application, despite their great performance. As a result, heterogeneous catalysts, which often contain transition metal series mostly noble metals and metal oxide nanocatalysts, have played an important role in many of the major industrial chemical revolutions [2, 3]. However, their high cost and less abundance in the earth's crust limit their widespread use in industrial scale applications. To address these limitations, supported metal nanoparticles (NPs) were developed for several applications, where a minor part is involved in the catalysis process and out of that a tiny amount of catalyst is served as the active centre in the reaction [4]. Even though this technique minimizes the catalyst loading, there are several disadvantages like irregular morphology distribution, agglomeration of metal nanocatalysts, and individual catalysts may possess different active sites exhibiting different performances [5]. Hence the search for an ideal catalyst which can be stable, recyclable and work consistently without altering its activity and selectivity under different working conditions is required.

According to the proverb, "There is strength in numbers", researchers have done massive hard work to expand the outcomes of sustained metal nanocatalysts by decreasing the size of the catalysts [6]. In this context, single atom catalysts (SACs) have recently headed as a fundamental research interest in the field of catalysis. In theory, SACs offer the possibility of increasing catalytic centre efficiency while maintaining the advantages of typical heterogeneous catalysts, such as stability and recyclability [7]. SACs have several advantages over metal nanocatalysts and supported metal nanocatalysts as shown in Fig.1. Maschmeyer et al. were the first to find SACs by grafting titanium (Ti) species onto the inner walls of mesoporous silica MCM-41 to obtain well dispersed Ti active sites [8]. The authors confirmed that because no visible NPs were formed, Ti species may be separately disseminated. Further Dmitry et al. proposed the formation of ammonia by reducing N_2 under mild circumstances at a single molybdenum (Mo) centre [9]. Afterward some other reports of SACs have been established by several authors for different catalytic applications [10, 11]. It was observed that even though all these articles present the importance of SACs, but the restricted

characterization tools during that period was unfeasible for the schematic characterization of the catalysts. Fortunately, the advanced progress of the research techniques made it possible to overcome the characterization hurdle. On the other hand, Qiao et al. deeply studied Pt_1/FeOx SACs through different characterization techniques such as atomic resolution aberration-corrected high-angle-annular-dark-field scanning transmission electron microscopy (AC-HAADF-STEM), X-ray absorption spectroscopy (XAS), and in situ diffuse reflectance infrared Fourier transform spectroscopy (DRIFTS) [12].

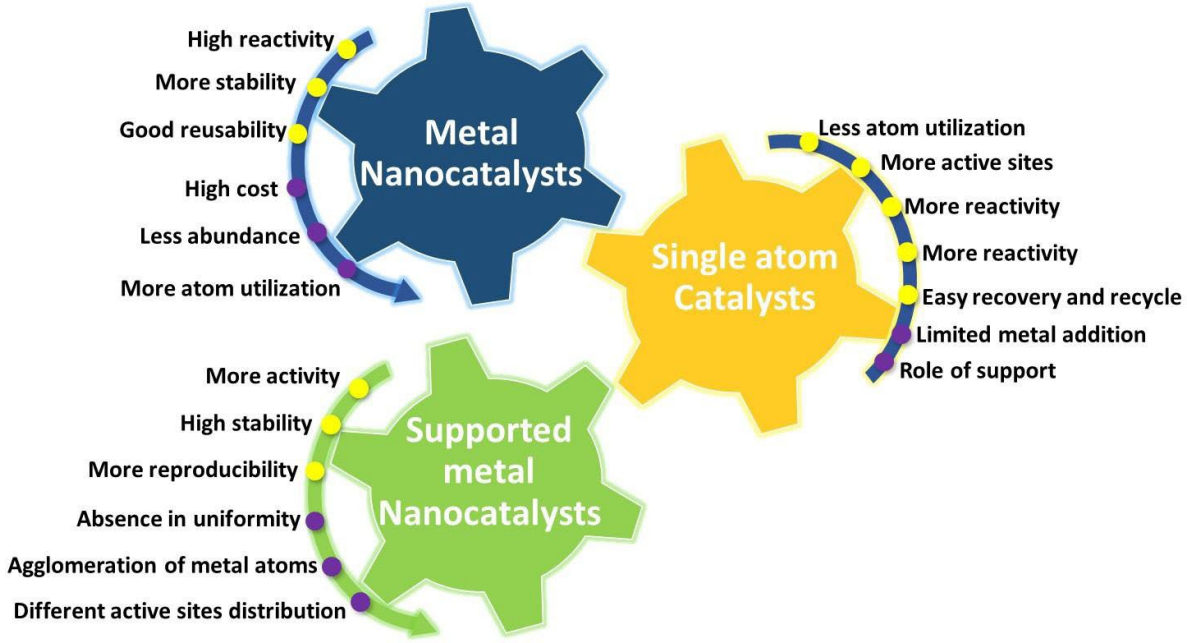

Figure 1. Schematic representation of the advantages and disadvantages of metal nanocatalysts, supported metal nanocatalysts and SACs.

Another advantage to consider is the cost effectiveness of SACs. Enhancing the atom efficiency of precious metals may be a cost-effective strategy to maintain the robust catalytic behaviour while reducing the amount of pricey metals used. Meanwhile the first noble-metal SAC Pt_1/FeOx catalyst was reported [12], many reports have discussed the active site modification of noble metal SACs on various supports such as Au_1/Co_3O_4, [13] Au_1/CeO_2, [14] $Pt_1/q\text{-}Al_2O_3$, [15] and Pd_1/FeOx [16] and performed for several applications. Yang et al. created single Pt atoms on TiN NPs and established the two-electron approach for selective large output of H_2O_2 under feasible condition [17]. The authors observed distinct Pt atoms were successfully bounded by N-vacancies on the TiN support due to the low Pt loading of 0.35 wt%, which was favourable for the production of SACs. Moreover, using a photochemical synthesis method, Liu et al. [18] described the distribution of Pd atoms on the surface of TiO_2 (Pd_1/ TiO_2) with a Pd loading of 1.5 wt %. The Pd_1/TiO_2 catalyst revealed efficient catalytic performance towards

the hydrogenation of C–C bonds via the activation of H_2 in a heterolytic system. In comparison to the commercial Pd catalysts, the clearly dispersed Pd_1/TiO_2 on ethylene glycolate (Pd_1/TiO_2 -EG) to have nine times better catalytic performance. The hydrogenation of aldehydes was also improved by a factor of more than 55, and there was no drop-in activity for 20 consecutive cycles.

Rather than employing noble metals, it is more practicable to develop SACs that store inexpensive metal atoms for a variety of uses to avoid the cost issue. Such as a support sacrificial strategy was implemented by Liu et al. [19] to produce the CoN_4C_8–1–$2O_2$ SAC of 3.6 wt% of Co loading. Further, excellent catalytic performance of the SAC was observed for the chemoselective hydrogenation of nitroarenes to form azo molecules. Li et al. [20] used a low annealing rate to produce an atomically distributed Zn–N–C catalyst with an ultrahigh Zn loading of 9.33 wt %. The Zn–N–C catalyst displayed exceptional oxygen reduction reaction (ORR) performance with good stability. Babucci et al. [21] followed a typical air exclusion synthesis protocol to form an atomically distributed Ir atoms fabricated on the reduced graphene aerogel (rGA) having the Ir loading of 14.8 wt%. However, currently Cheng et al. [22] described about the formation of nitrogen-doped carbon nanotubes (NiSA–N–CNTs) following a multistep pyrolysis procedure. It was seen that the Ni atoms distributed individually with high amount (20 wt %) of Ni loading. An outstanding catalytic output was observed for the electro reduction of CO_2 to CO by NiSA-N-CNTs with turnover frequency (TOF) of 11.7 s^{-1} at - 0.55 V (vs. RHE).

The dispersion of isolated single metal atoms onto suitable support material is a precondition for SACs. However, due to the energetically preferred agglomeration of metal atoms during reaction treatment, SAC manufacturing is difficult. As a result, to accomplish widespread usage of SACs, suitable synthetic processes must be developed. Recently, several reviews reported the importance of SACs for variety of applications. Singh et al. explained the Fe based SACs synthesis using various techniques on different supports and their applications for several organic reactions and electrocatalysis. In another report, Wei et al. explained SACs and their applications for thermoelectric, electrocatalysis, and photocatalysis. Similarly, Singh and co-workers discussed the electrocatalysis applications of SACs. Gawande et al. gathered thorough knowledge about the carbon-based SACs synthesis and their role towards electrocatalysis and organic coupling reactions. Moreover, Wang et al. explained the importance of SACs for several aspects, including the dynamic behaviour mechanism [23-28]. Despite the fact that

these articles have presented a positive outlook on SAC synthesis, properties, and applications, however, there are still a lot of scientific questions that need to be answered for the future development of SACs in the catalysis field. Looking into the current scenario, this review is designed to understand the SACs through the effective strategy for the synthesis of SACs and their role for electrocatalytic, photocatalytic and organic synthesis applications. Apart from this, there are a few significant scientific queries about SACs that are addressed in depth are outlined below

i) The stability: Single atoms tend to assemble as they approach stability due to an increase in surface energy with decreasing the atomic size. But the aggregation tendency of single metal atom during the synthesis produces a great threshold for the fabrication and formation of clearly dispersed SACs. A strong metal-support interaction and a stable co-ordination effect must be accomplished to lift such limitations**.**

ii) Large-scale production: There are several synthetic approaches reported previously to form SACs including mass selected soft handling, coprecipitation, impregnation and many more. [29-31]. However, some techniques are widely and frequently considered as the most promising procedures for large scale production of SACs is discussed [32, 33].

iii) Dual site behaviour: It is well known that transition metals can have multiple oxidation states depending upon their electronic state. If only a single electronic state is required for a certain reaction, what will happen if the SAC is spread in a mixed valency state? The role of mixed valency state of single metal atoms in a specific reaction is another issue which is addressed in the present review.

iv) Bimetallic SACs: From a very long time, it was observed that the bimetallic nanocatalyst boost the activity as compared to monometallic NPs for several applications [34, 35]. As a result, by introducing the notion of bimetallic SAC formation, the activity of SACs can be improved. Bimetallization can advance the properties of monometallic SACs and create new properties due to the synergistic effect or inter electronic charge transfer between the two metals which may enhance the stability [36-38]. The several aspects of formation of bimetallic SACs and their catalytic behaviour are discussed here.

Overall, the scope of present review is shown in Fig. 2, which indicates to discuss several synthetic strategy for the production of SACs. The methods for the large-scale production of SACs for industrial uses, different forces responsible for the stability of single atoms on support materials, understand the role of mixed valency state/ dual site behaviour of metal atoms, the most important fact that discussed in the present review is the advance of bimetallic SACs and

finally the role of different SACs for electrocatalysis, photocatalysis and organic transformation. To the end, the implications and problems derived from recent surveys are included.

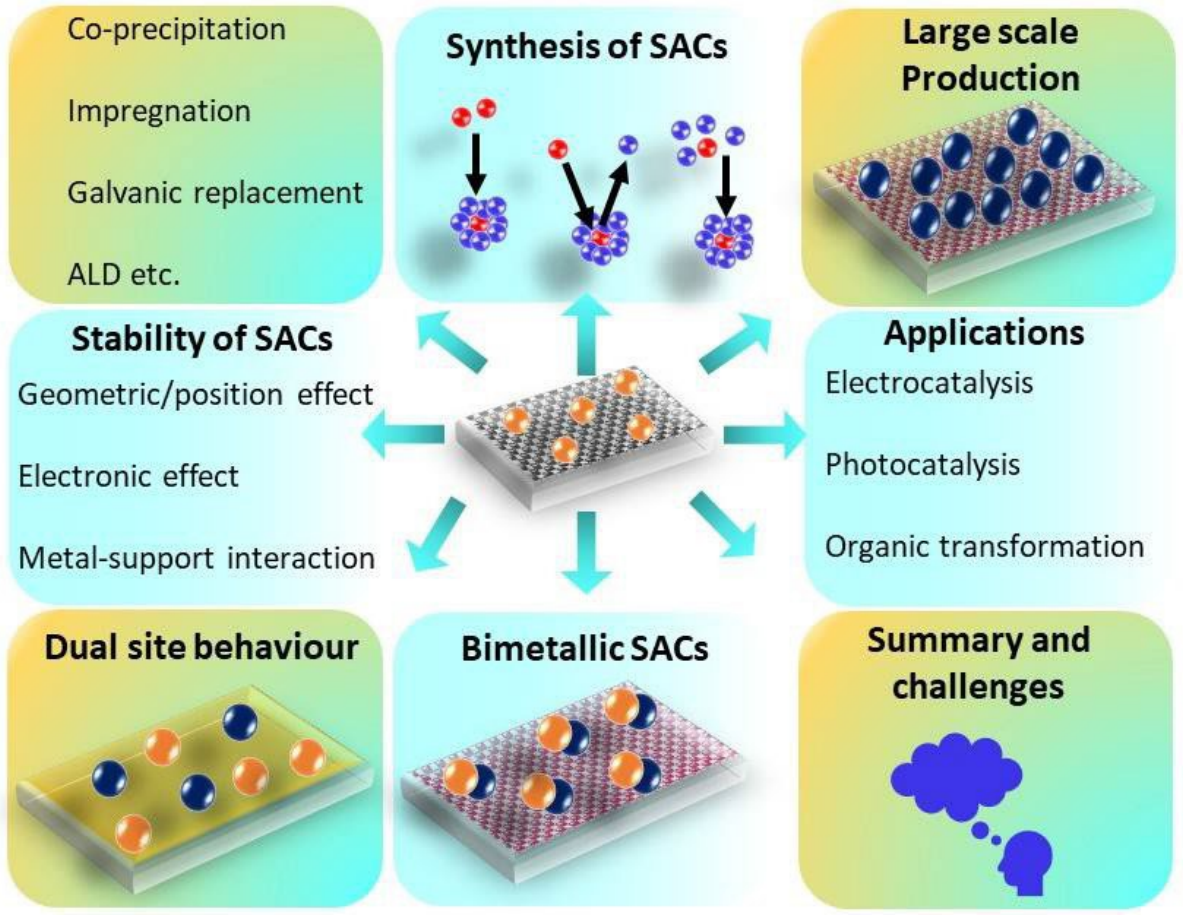

Figure 2. Schematic representation indicating scope of the present review.

2. Synthesis of SACs

The most essential and challenging work is the preparation of highly dispersed SACs on appropriate supports by following a suitable technique. Still, the production of SACs is a main task because of the dynamically privileged accumulation of single metal atoms throughout the manufacturing process or successive handling procedure by following a suitable fabrication technique. In this review, we have discussed various synthesis protocols for SACs including impregnation, mass selected soft handling, atomic layer deposition (ALD), co-precipitation, etc. Apart from that, galvanic replacement reaction, electrostatic adsorption, pyrolysis, and combustion method along with surface reaction are highlighted.

2.1 Impregnation method

Impregnation is a suitable technique to synthesize single atom supported catalysts. In this method, a definite volume of solution mixture carrying active metal precursors and highly porous catalyst support can be mixed properly. After a suitable interval, the required active metals from the precursors will anchor onto the substrate by the process called ion-exchange/adsorption. The metal- support interaction and bonding between them will decide the distribution or formation of SACs. Impregnation is basically two types; wet impregnation (mixture of both the components in a liquid state), which is more appropriate and suitable and dry impregnation (mixture of both the components in solid state). For example, Li et al. synthesized g-C_3N_4 (graphitic carbon nitride) in which single Pt atoms are fabricated on the g-C_3N_4 support, which can ease the contact with metal precursors [37]. The process was followed by the addition of H_2PtCl_6 (Pt precursors) into the aqueous dispersion of g-C_3N_4 solution with vigorous stirring at 70 °C for 4–10 h. The residue was washed with distilled water and ethanol many times to remove the unreacted metal atoms with the g-C_3N_4 support and after that, the obtained mass was subjected for drying at 60 °C followed by annealing at 125 °C for 1 h under argon (Ar) atmosphere. The morphology distribution was observed through TEM analysis as shown in Fig. 3 (a). Similarly, using dry impregnation method, SACs can also be synthesized where there is no strong metal-support interaction. For instance, Yang et al. followed the dry impregnation technique to fabricate single Pt atoms onto a TiN substrate where the Pt precursor solution was well dissolved with acid-treated TiN NPs and kept for drying at 50 °C in a vacuum oven [17]. The resultant SACs formed is shown in Fig. 3 (b). The authors noticed that with the increase in the Pt loading above 0.35 wt%, the formation of Pt clusters rather than SACs prevailed. This happens because of the weaker precursor–support interaction, which obtained during the excess distribution of Pt NPs with loadings higher than 0.35 wt% of impregnated species [39]. Generally, impregnation is cost-effective and modest technique for the synthesis of SACs. However, there is a drawback of producing a high amount of SACs because of the availability of a limited number of functional groups or active sites to react with the metal precursors. To understand this, Choi and co-workers utilized sulfur-doped zeolite-templated carbon with 4 wt% and 7 wt% of sulfur to produce single Pt atom catalysts using a wet-impregnation process and found that the deposition of active Pt atoms can spread effectively at 5 wt% shown in Fig. 3 (c, d) [40].

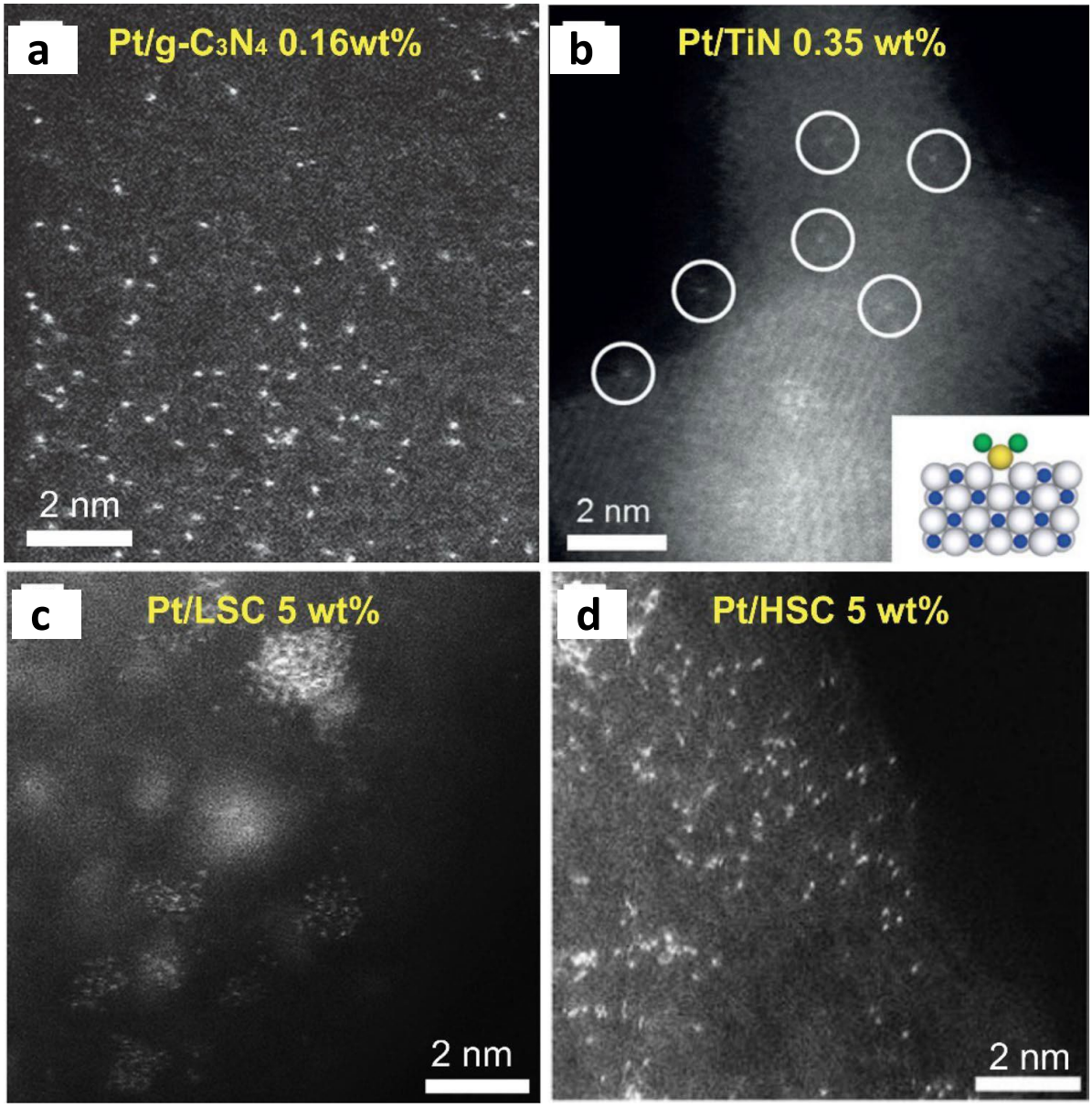

Figure 3. HAADF-STEM images of individual Pt atoms on various substrates: (a) Pt/g-C_3N_4, (b) Pt/TiN, (c) Pt/LSC, and (d) Pt/HSC. Here, (a) Reproduced from Ref. [37] by permission of Wiley-VCH, (b) Reproduced from Ref. [17] by permission of Wiley-VCH, and (c, and d) Reproduced from Ref. [40] by permission of Nature Publishing Group.

2.2 Mass selected soft handling method

SACs can be produced by utilizing the mass selected soft handling methodology, which involves regulating the single metal atom quantity during the reaction. The physical deposition of metal precursors on a flat or porous substrate is used in this process indicating that the metal atom can be soft landed onto the surface with precise addition of metal quantity [41]. To elaborate, this technique involves monitoring the flow of metal ions having a positive charge,

which moves towards the substrate from the vacuum chamber through a quadruple mass filter constructed on mass to charge proportion. Through this, the metal-support interaction and selective distribution of metal ions occur. However, it has some drawbacks over the advantage of precise synthesis of SACs. For example, it entails the use of sophisticated devices and gives less output. Therefore, it is usually difficult to follow industrial scale synthesis or large-scale production of catalysts [42]. Abbet and co-workers in 2000 performed acetylene cyclotrimerization by taking the benefit of mass selected soft handling technique to synthesize different sizes of Pd*n* clusters ($1 < n < 30$) fabricated upon MgO (100) thin films, and DFT study discovered the defects in single inactive Pd atoms from the MgO substrate after the charge transfer [29]. This technique can produce an effective catalyst for basic research into atomic metal-support relationships. However, it has some drawbacks in terms of cost and harvest, and it may not be suitable for real-world engineering applications.

1.1 Atomic layer deposition (ALD)

ALD is a vapour phase deposition technique that plays critical attention for the formation of SACs between metals and metal oxides substrate. It has the capacity to distribute the particles ranging from nano to single atoms over a suitable substrate uniformly in high-aspect-ratio shapes and absorbent materials [43, 44]. In a wide range, the overall process of ALD is completed in four stages [45]. Initially, (1) disclosure to the main precursor; (2) removal of the reaction chamber for vaporisation; (3) contact with the next reactant; and (4) a final purging of the reaction chamber whereby adjusting the ALD cycles the shape, size, mass, and stuffing of deposited materials on supports can be accurately controlled [46]. ALD technology is an appropriate and consistent procedure as it can deliver the necessary SACs to learn the modest steps followed in the catalytic procedure and the influence of particle size, support surface phenomenon and combination of individual atoms, ions, or molecules to form metal or alloy NPs. This synthesis protocol has been employed to distribute single metal atoms on carbon materials like graphene and other sorts of substrate materials and has achieved amazing results in catalysis. For example, Sun and co-workers first defined the useful production of single Pt atoms attached to the graphene nanosheets (GNS) using ALD [47]. The authors proposed a suitable binding mechanism as shown in Fig. 4 and the characterization of SACs through HAADF-STEM and the respective particle size distribution is shown in Fig. 5.

$$Pt - O* + MeCP\ Pt(CH3)3 \rightarrow (CH_3)_2\ Pt\ (MeCP) + CO_2 + H_2O + fragments$$

$$(CH_3)_2\ Pt\ (MeCP)^* + O_2 \uparrow \rightarrow Pt - O^* + CO_2 + H_2O + fragments$$

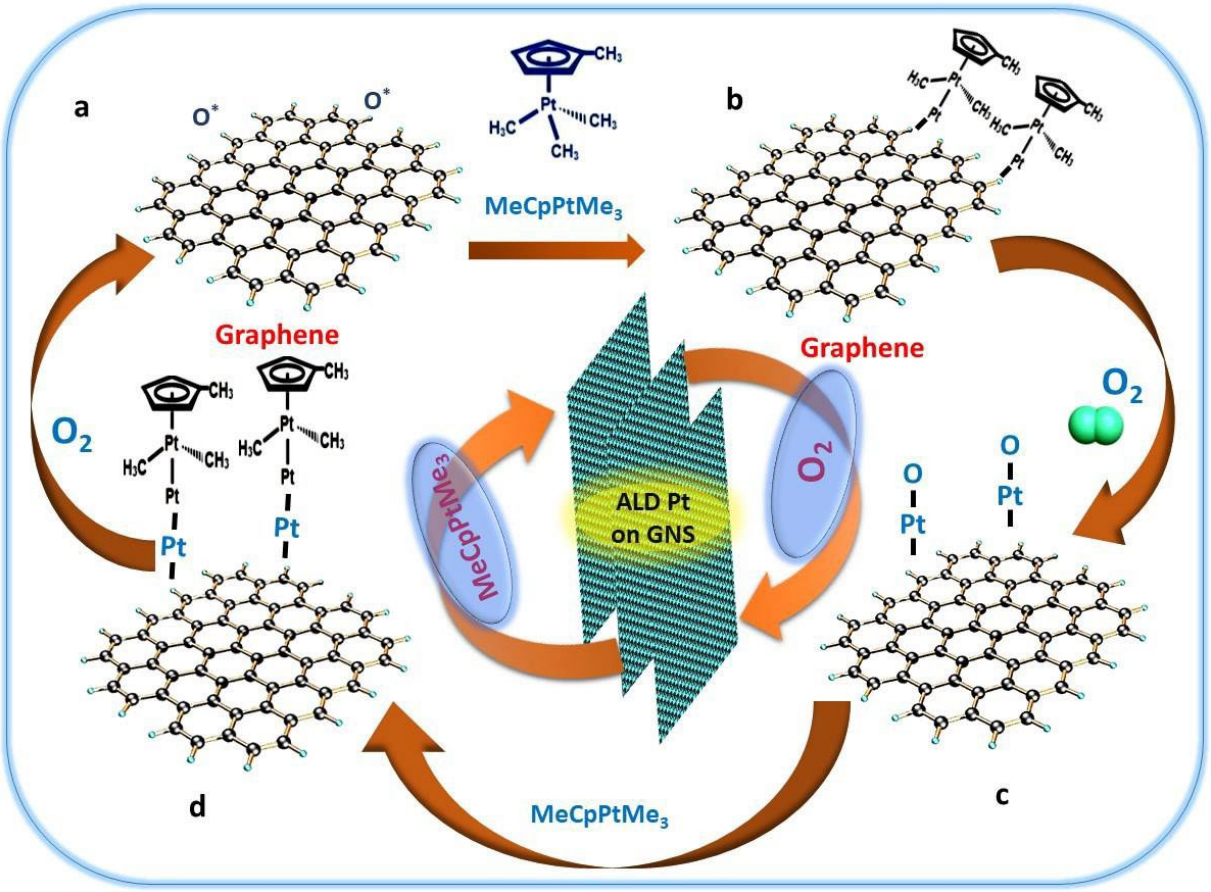

Figure 4. Schematic diagram of Pt ALD mechanism on graphene nanosheets. Reproduced from ref [47].

The above represented diagram illustrates different pathways to complete the reaction. Where (a) denotes the existence of an oxygen comprising monolayer on the graphene nanosheet surface. (b) Some of the forerunner ligands interact with the present oxygen throughout the $MeCpPtMe_3$ revelation, and the restricted source of surface oxygen permits the self-limiting progress essential for ALD to ensue in a Pt-containing medium. Whereas in (c), the succeeding oxygen contact results in the formation of a new adsorbed oxygen layer on the Pt surface; the two methods (b and c) combined create a broad ALD cycle, culminating in a single atomic layer of Pt atoms. The number of ALD cycles can be adjusted to control the amount of Pt deposited (d).

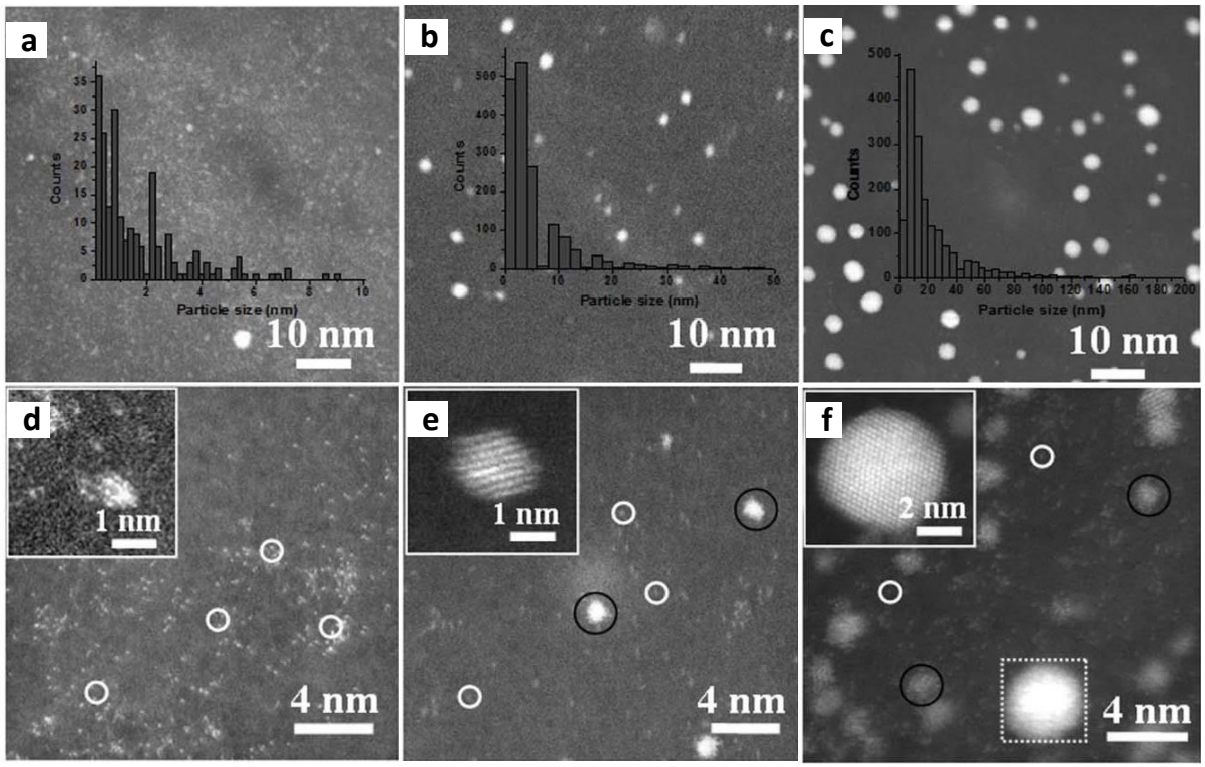

Figure 5. Represents the HAADF-STEM images of Pt/GNS samples at 50,100 and 150 ALD series in (a, b, c), respectively and (d, e, f) displays the zoom images of the consistent outcomes. The applicable Pt on GNS histogram is shown in the inset of individual image. Reproduced from Ref. [47] by permission of Springer Nature Communication.

1.2 Co-precipitation

Co-precipitation is a simple and broadly followed technique to produce nanomaterials. However, compared to the gaseous phase ALD mechanism, this method is cost-effective and easy to operate without the necessity of any sophisticated tools [45, 46]. In this technique, the required metals are deposited on the substrate surface in a precisely accomplished way, associated to the above-mentioned vapour-phase methods. It is a dire challenge to deliver 3D restrained reactive sites that can carry no other than a single metal atom. The 3D deposition of SACs within the suitable porous cross-linked captivity has proven as an essential method to avoid the movement and accumulation of metal atoms. Some of the broadly used porous materials, for example, metal organic frameworks (MOFs), covalent organic frameworks (COFs), and zeolites are some of the relevant supports which allow the three-dimensional and uniform spreading of metal atoms to attain comparatively more SAC loading [48, 49]. Many research groups, such as Zhang and co-workers successively synthesized SACs by following co-precipitation method to perform electrocatalytic CO oxidation, hydrogenation, and water–

gas shift reactions [32, 49-52]. To extend this, Liang et al. organized single Pt atom catalysts over FeO*x*- substrate following co-precipitation method. Moreover, the researchers also described that, to achieve single metal atoms distributed over the porous support less material loading is required such that homogeneously distributed Pt atoms can be detected on FeO*x* substrate with a Pt loading of 0.17 wt%, while only Pt atoms, 2D Pt bundles with $\leqslant$ 10 Pt particles and 3D Pt clusters $\leqslant$ 1 nm can be detected with a Pt loading of 2.5 wt% [53]. Another research group, Lin and co-workers mentioned that like the effect of loading, temperature for reduction can also change the shape of Pt on FeO*x* support in co-precipitation. Using the Pt loading about 0.08 wt% and reduction temperature of 200 °C, all Pt atoms on FeO*x* were distributed in the arrangement of only single atoms and there was no formation of cluster particles, agglomerated particles and NPs noticed. The authors observed the agglomeration of single atoms with several Pt atoms or randomly distributed atoms by increasing the reducing temperatures to 250 °C with constant Pt quantity [54].

Overall, co-precipitation is an easy, fast, and cost-effective technique to synthesize SACs. To improve the efficiency, further modification of the parameters is needed to enhance the deposition of more and more single atoms on the suitable substrate. Furthermore, the utilization of co-precipitation method to manufacture metal SACs can lead to the difficulties like metal atoms situated on the boundary areas of support material aggregates which is restricted on the obtainability of precise porous substrates and the complete elimination of inactive metal precursor ligands throughout the post action [54]. Apart from the above discussed synthesis protocols for SACs, there are several other methods summarized in table.1.

Table 1. Represents the different methods utilised for the synthesis of SACs.

Entry	Methods	SACs	References
1.	Mass-selected soft landing	Pt/MgO films	[55]
2.	Ion implantation	$Au/Al_3O_3^+$, $Al_3O_4^+$, $Al_3O_5^+$	[56]
3.	Wet-impregnation method	Pt_1 /FeO*x*	[12]
4.	Strong electrostatic adsorption	Pd, Cu, Co, Ru, Ni/ silica	[57]

5.	Combustion synthesis	Pt/Rh/Pd/Au/Ag/Cu doped into CeO_2, TiO_2, Al_2O_3, and ZnO	[58]
6.	Pyrolysis	Ni/MOF	[59]
7.	High temperature vapor transport	Pt/CeO_2	[60]
8.	Pyrolysis	Fe and Co/ ZIF-8	[61]
9.	Pyrolysis	Mn/ZIF-8	[62]
10.	Modular synthetic approach	Co_1/MOF	[63]
11.	High temperature atom trapping	Nb_1/Graphene	[64]
12.	Galvanic replacement	Pt/MoS_2	[65]
13.	Photochemical route	Pd/TiO_2	[18]

1.3 Other synthesis methods of SACs

There are several synthesis approaches for the preparation of SACs with specific reaction pathway mentioned in the Table 1. Where pyrolysis is one of the most essential procedures for fabricating doped carbon material since it allows the fabrication of single atoms. To generate stabilized SACs, the technique usually includes heating at a high temperature. Li et al. developed a highly reactive and stable isolated single-atom Fe/N-doped porous carbon (ISA Fe/CN) catalyst with Fe loadings up to 2.16 wt % [65]. Initially, $Fe(acac)_3$@ZIF-8 molecular-scale was enclosed by gathering Zn^{2+}, 2-methylimidazole and $Fe(acac)_3$ molecules. After subjecting pyrolysis at 900 °C under Ar atmosphere, ZIF-8 was transferred to N-doped porous carbon, and $Fe(acac)_3$ reduced by the carbonization of organic linkers, thereby directed the formation of Fe single atoms. Likewise, single Ni atoms were created via ionic exchange between Zn nodes and adsorbed Ni ions within ZIF-8 cavities, followed by pyrolysis at 1000 °C [66]. Moreover, wet-chemical synthesis is a superficial technique that act efficiently for the

preparation of SACs. There are some wet-chemical synthetic methods rather than impregnation and co-precipitation. Galvanic replacement processes another wet chemical strategy that is employed for the synthesis of SACs. For example, Li et al. [65] prepared single Pt atoms on MoS_2 where the succeeding reaction, Pt atoms replaced Mo atoms in the MoS_2 nanosheets. Overall, the reaction conditions must be accurately controlled during wet-chemical synthesis to achieve SACs, wherein atomically distributed separation, and isolation of precursors on substrates are critical for the creation of single atoms. To protect as-formed single atoms from migration and aggregation, metal precursors should be reduced at comparatively moderate reaction rates.

Further, ion exchange and strong electrostatic adsorption phenomenon are the two most synthetic tools of wet impregnation method. Where ion exchange can be performed over the neutrally charged porous substrate and selecting an labile ligand species. Initially the metal species are distributed on to the porous substrate. In the next step the ligand species are removed via ion exchange mechanism forming SACs grafted onto the neighbouring O-vacancy sites of the substrate. In case of electrostatic method, the change in the surface charge and metal atoms will undergo electrostatic adsorption mechanism for the fabrication of SACs [57]. Combustion synthesis method was an effective discovery by Bera et al. An aqueous solution of stoichiometric mixture of aluminium nitrate and urea boils, and burns at 1500 °C, providing high surface area R-alumina. The authors further investigated by dispersing the metal atoms containing 1% $PdCl_2$ or H_2PtCl_6. The combustion of this combination resulted in Pd or Pt metals of 4-7 nm size scattered on R-alumina [67]. Unless these mobile atoms can be confined, high temperatures are detrimental to catalyst function. Jones and workers employed ceria particles with similar surface areas, but distinct exposed surface facets. Ref The Pt transferred to the ceria and was restricted when united with a Pt /Al_2O_3 catalyst and aged in air at 800 °C [60]. Modular synthetic approach involves the incorporation of coordinatively unsaturated single atoms into a porous support to form atomically dispersed SACs [63].

2. Large-scale Production of SACs

In spite of high activity, SACs metal loading is often kept less to hinder sintering [68]. This restriction severely limits overall catalytic effectiveness and practical applications. In general, the competition between the distribution of atoms and agglomeration is based upon metal-metal and metal-support interaction [69]. Hence, for the large-scale production of SACs, an

appropriate substrate with strong metal-support interactions is required. To accomplish feasible distribution of metal atoms on suitable supports, mainly two ways are used such as mass-selected soft-landing, and wet-chemistry methods [70]. Physical methods such as ALD, can manufacture SACs because in this method, the size of the metal species can be perfectly controlled. By using the mass-selected molecules or atom beams to carefully handle the surface assembly of the support via ultrahigh vacuum surface science operations. Physical approaches, on the other hand, are impractical for large scale synthesis of SACs due to their high cost and limited yield. The fundamental difficulty with wet-chemistry approaches is anchoring metal species onto a substrate via a chemical reaction while avoiding aggregation during post treatment operation. The yield of SACs by wet-chemical procedures is limited because of the less and lack of anchoring sites on support. For example, the highest loading of single Pt atoms anchored to the surface of FeOx is less than 2.0 wt% even though the coprecipitation temperature and pH are precisely controlled [12]. However pyrolysis is considered as the effective synthesis strategy for manufacturing SACs in large quantity [22]. Also, it has noticed that atoms or molecules containing a lone pair of electrons, such as sulphur (S), oxygen (O), and nitrogen (N) have a strong interaction ability with metal atoms and performed as an effective stabilising site for SACs. Thus, the important factors responsible for large scale production of SACs are the construction of anchoring sites and spatial confinement of atoms [71].

There are several literatures which established the large-scale production of SACs mainly containing N-anchoring sites by following pyrolysis synthesis method. For example, Han et al. prepared Mo SAC on nitrogen doped porous carbon by taking ammonium molybdate ($(NH_4)_6Mo_7O_{24}$) with glucose and hydroxylamine hydrochloride [72]. The mixtures were mixed with water and ethanol and allowed to stir for 16 h under 70 °C until the evaporation of solvents. The precursor powder was transferred to a crucible and heated at 650 °C in an argon (Ar) environment for 4 h providing Mo SACs of 9.54 weight % metal loading. Further, Li et al. mixed a nitrogen-free Cu MOF, (Cu(BTC) $(H_2O)_3$) with dicyandiamide (DCD) to prepare Cu SACs of 20.9 wt % metal loading [73]. The reactants were subjected for thermal treatment at 800 °C in an Ar environment for 3 h. The unreacted residues were then filtered using oxygen saturated 5 % hydrochloric acid (HCl) to yield Cu SACs. It has observed that during the pyrolysis step, the M-N cooperation between metal precursors and N-contained precursors serves to stabilise the distribution of single atoms. By dissolving N-contained compounds instead of using gaseous ammonia, N can be doped into carbon compounds. Because of high

N content (60 wt %), g-C_3N_4 is essential in the large-scale synthesis of SACs. Different N-rich precursors, including melamine, urea, DCD, and thiourea can be thermally polymerized in situ to produce this material. For example, Zhao et al. used a multi-step pyrolysis protocol to prepare SACs on N-doped CNTs [22, 74]. Due to the weak van der Waal's force, $Ni(acac)_2$ was clearly distributed in DCD under normal synthesis procedure, and the mixture was further agitated for 10 h before drying at 70 °C. After then Ni-g-C_3N_4 was produced in situ by melem condensation at 650 °C in the multi-step pyrolysis method. By trapping Ni atoms in the cavity of g-C_3N_4, the formation of Ni- g-C_3N_4 hampered the sintering of Ni atoms. The authors able to maximize the Ni loading upto 20 wt %. Finally, Ni SACs with a Ni-N_4 structure were produced at temperatures ranging from 700 to 900 °C. Further, by pyrolyzing ZIF-8, Ni SACs with 5.44 wt % Ni loading was obtained [75]. Similarly, Wu et al. synthesized Co-SACs on ZIF-67 organic framework having 15.3 wt % of Co loading [76] by following pyrolysis method.

S-contained materials are also used for large-scale synthesis of SACs, in addition to N-contained substrates. For example, Choi et al. synthesized Pt SACs having 5 wt % of metal loading with S-doped zeolite templated carbon (ZTC) by chemical vapour deposition (CVD) method, where the S-density was 17 wt % [40]. In a typical synthesis of acetylene/H_2S in NaX zeolite subjected for CVD process under H_2S/He or only He circumstances at 800 °C and further HCl/HF solution was used to remove the remaining zeolite. Moreover, Wang et al. used pyrolysis technique to form mesoporous S-doped carbons supported SACs with high yield [77]. The huge surface area and high S content provides more crowded anchoring sites for metal atoms to be secure via strong chemical M-S interactions. The authors prepared Ru, Rh, Pd, Ir, and Pt SACs with high metal loading up to 10 wt % using the sulfur-tethering strategy. The synthesized SACs exhibited 30 and 20-fold more reactivity for formic acid oxidation and quinoline hydrogenation than the commercial Pt/C and Ir/C catalysts. The peculiar structure of meso S-C can effectively shield metal atoms agglomeration during the synthesis due to the strong M-S co-ordination. Other than this, Li et al. established Pt SACs having metal content upto 7.5 wt % decorated on the MoS_2 nanosheet [65]. As discussed earlier the Mo atoms were replaced by the metal atoms. It has observed that compared to O and N-doped anchoring sites, S-doped anchoring sites are more strongly bonded to Pt atoms [7, 78]. The use of highly toxic H_2S and HF during the reaction process is the major downside of using S-doped substrates. The production of high metal loading SACs on a large scale is limited because to the several processes required to create S-doped substrates. Moreover, to form a high value of MoS_2

nanosheet a precise working condition is necessary which limits the low cost and high amount SACs manufacturing.

Furthermore, O-anchoring sites similar to N and S can be employed to form SACs in large-scale. Metal oxides are suitable for electrochemical applications, because of their good conductivity. For example, Kim et al. generated Pt SACs of 8 wt % metal loading on antimony doped tin oxide (ATO) [79]. Pt SACs were prepared using an incipient wet impregnation synthesis protocol and then reduced at 400 °C in a 10 % H_2 atmosphere. It was observed that the synthesis mechanism changes with the alteration in the reduction temperature. When the reduction temperature was 100 °C, Pt NPs were formed and with increasing the temperature to 400 °C, Pt SACs were found. Interestingly, the catalytic action of both Pt SACs and Pt NPs were different for formic acid oxidation process and ORR. Pt NPs endured an indirect path for formic acid oxidation and 4e reaction mechanism for ORR, whereas Pt SACs took a direct path in formic acid oxidation and selected the 2e path for ORR. As it is clear that the oxygen containing groups are more freely distributed on the carbon material surface, Ir SACs were prepared on reduced graphene oxide aerogel (rGA) of 14.8 wt % of Ir content [21]. In anhydrous toluene, $Ir(CO)_2(acac)$ reacts with O-containing groups on a reduced graphene aerogel (rGA) carried out in an air-only environment. Because rGA has a large surface area and a high density of sites for attaching Ir species, it has a high metal loading and also rGA is a good electron donor compared to other metal oxides.

3. Stability of SACs

The activity of the metal atoms increases with the increase in the surface free energy and the metal sites become energetic for the chemical interactions between support and adsorbate. This accounts the size effects of metal nanocatalysts. In case of SACs, the surface free energy is comparatively high due to extremely active valence electrons, quantum confinement of electrons, and the sparse quantum level of metal atoms [70]. This results to form chemical interactions with the support to remain stable which can be geometric/position effect and electronic effect. Another factor that is necessary for the stability of SACs is the metal-support interaction which are discussed one by one in this section.

In case of the interaction like geometric or position effect, the metal atoms are associated to the anchoring sites for forming M-O-cation (support) or resides within the place of cations in case of oxide supports [80, 81]. For example, Au SACs on (111) surface of the single crystal

magnetite revealed that Au metal atoms were attached to uncapped O anchoring sites which Fe tetrahedral ions would occupy in bulk iron oxide crystal [80]. Several reports indicated that the atomically distributed metal atoms on γ-Al_2O_3 supports were formed O-Al bonding contributions in single-atom metals [82, 83]. Huang et al. established that the individual Ag chains can be produced in the channels of a hollandite-type manganese oxide support with oxygen channels that have lone-pair of electrons and an appropriate diameter for Ag-O-Mn bonding [84]. The position of single atoms in SACs with metals as support is determined by the chemical potential of the metal atoms. For instance, Zhang et al. investigated that Au stabilised at the corner position of the Pd due to the higher chemical potential ofAu compared to Pd [85]. SACs occupied all active metal atoms due to the simple geometric impact of such single atom positions.

Another bonding effect is generated due to the location and chemical interaction of metal and support which is known as the electronic effect. These effects not only established the stability of SACs but also differentiate SACs from the metal NPs. According to their coordinated surroundings, SACs electrical structures are substantially more volatile. In fact, the coordination with the support material is highly significant that discussing a single metal atom without the support is insufficient. Due to differing chemical potentials, metal atoms connect with open sites of the supports, causing charge transfer between them. Hence, the anchored metal atoms generally contain some charge which is confirmed by various techniques [86, 87]. The electron transfer between single-atom centres and the supports also affects the electronic characteristics of single atoms on metal or graphene. Pt single atoms on graphene was shown high vacant 5d densities of states, similar to metal atoms fabricated on the oxide surfaces [47, 85].

One of most important factor is the interaction between metal and support which inevitably affect the stability of SACs. Generally, it was observed that different single metal atoms can alter the properties of the support material in several ways. For example, Wang et al. noticed that doping lanthanum (La) on α-Al_2O_3 act as single atom prevent the degradation of dyes [82]. Moreover, single metal atoms were detected to assist the reduction of supports for noble metals on reducible supports such as Pt/FeOx and Ir/CeO_2 [12, 32]. Hence, a strong metal-support interaction is necessary for the stability of SACs. Though, there are variety of supports available for the synthesis of SACs, recently oxides were the most widely used substrate. Oxides offer several benefits over alternative supports for the stability of SACs due to their high specific surface areas, abundant oxygen vacancies, and surface OH groups. Fe oxides are

common 3d-metal-based substrate that are utilised to keep single precious metal atoms stable. But due to the redox activity of Fe, the oxide can be formed in multiple phases based on the reaction circumstances. Under oxidising conditions, haematite (α- Fe_2O_3) and maghemite (γ-Fe_2O_3) can be prevailed, whereas under reducing conditions, magnetite (Fe_3O_4) and wüstite (FeO) can generate [70]. Because the composition of Fe oxides is unknown, pinpointing the precise positioning of precious metal atoms on Fe oxide supports is difficult. CeO_2 is a significant 4f oxide that can be reduced to stable single metal atoms, either by substitution at a Ce site or by attaching to the surface O or N. Metal/CeO_2 SACs are predicted to be stable and helpful for many of applications such as CO oxidation, the WGS reaction, and the CH_3OH stream reforming etc are all examples of chemical reactions. The shape and size of the surface influence the stability of single metal atoms on CeO_2. To examine the behaviour of single Pt SAC stabilisation on different faces of nano CeO_2, the authors donated bulk CeO_2 as a cuboctahedral $Ce_{40}O_{80}$ nanoparticle [88]. It was seen that Pt atoms favourably interacted on the polar facets by donating $1e^-$ to every two neighbouring Ce^{4+} cations ($Pt \rightarrow Pt^{2+}$, $2Ce^{4+} \rightarrow 2Ce^{3+}$), generating a PtO_4 core with a square-planar structure in which Pt^{2+} ($5d^8$) is stabilised according to the calculations. Further, simulation revealed that a single Pd or Ni atom can likewise be accommodated in an O_4 metal binding site [89]. The polar CeO_2 (100) surface is less stable than the CeO_2 (111) surface, which could explain why metals bond strongly to the former. However powdered CeO_2 can be used as a support for the formation of SACs instead of nano or single-crystal CeO_2. In industrial catalysis, Al_2O_3 is one of the most commonly utilised metal oxide supports for precious metals. This p-block oxide has favourable structural abilities and firmly binds noble metals, allowing SACs to have outstanding mechanical and thermal stability. Al_2O_3 has a thermal stability benefit over reducible oxides as revealed by current results which may open different synthetic methods to thermally stable SACs [90, 91]. Despite the fact that, Al^{3+} is redox inactive under several conditions. Al_2O_3-supported SACs have received less attention than the above-mentioned reducible metal oxides. The charge transfer between potential single metal sites and Al_2O_3 is limited due to the low reduction potential, providing a driving factor for single metal centres to undergo oxidation and bind oxos rather than remaining in a low valent state and experiencing sintering [27].

Moreover, bonding between metal atoms and the support has a stabilising effect that is not limited to materials with oxo ligands. Other donor atoms can also be useful, especially when it comes to carbon-rich supports. For example, Bulushev et al. observed that N atom in carbon-rich support not only securely anchor individual metal centres but also change the carbon's

electrical characteristics [92]. Metal sites on N-doped carbon materials can have higher activity and selectivity than metals placed on undoped supports. According to DFT calculation for these materials, each single atom is firmly coordinated to two pyridinic N atoms at the graphitic sheet's edge with the bond strength observed in the order of Ru > Pt > Pd.

5 Catalytic application of SACs

5.1 Electrocatalytic Applications of SACs

Noble metal and transition metal based electrocatalysts for various energy applications are well known [93]. However, it still remains a great challenge to build an electrocatalyst with high efficiency, durable and economically stable, displaying greater performance in reactivity and mainly showing the importance in development of electrochemical energy conversion technologies. Fig. 6 shows the schematic representation of some key importance of SACs in electrochemical applications such as HER, OER, ORR, methanol/ethanol/formic acid oxidation and other electrocatalytic applications like zinc-ion battery, CO_2 reduction, N_2 reduction, etc [90, 94].

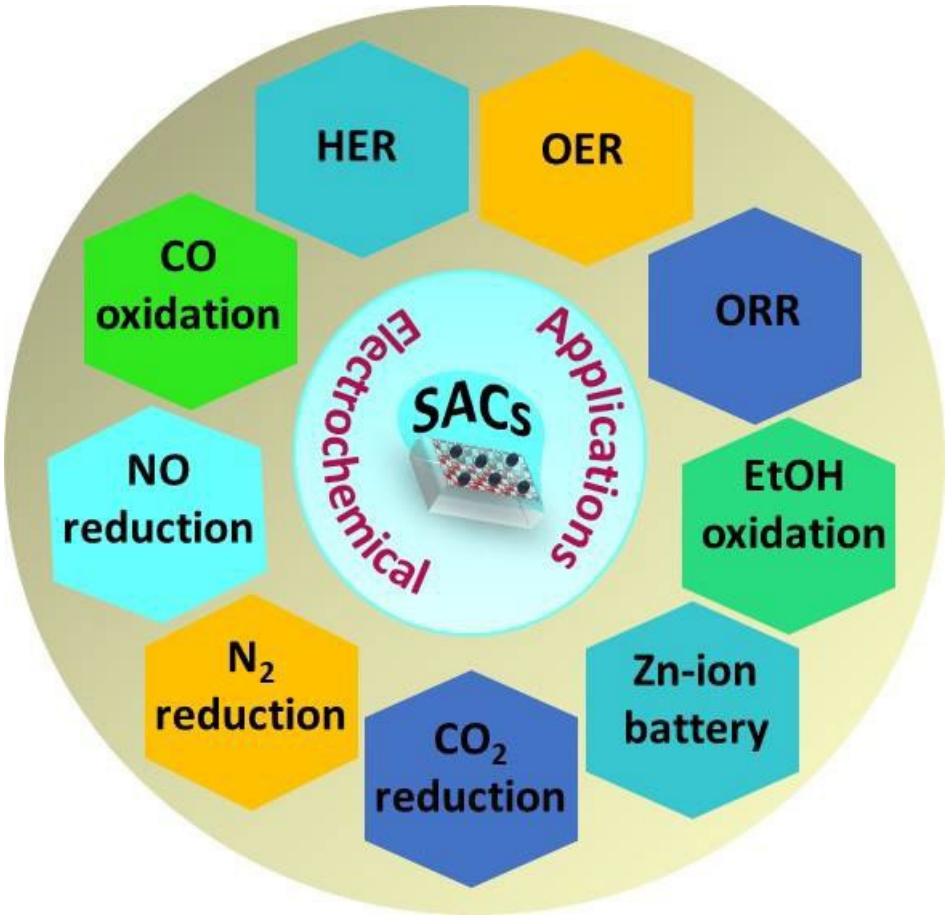

Figure 6. Schematic representation of several key electrochemical applications of SACs.

5.1.1 Hydrogen evolution reaction (HER)

Electrochemical water splitting, also known as HER ($2H + 2e \rightarrow H_2$) provides a reliable explanation about H_2 production for clean and inexhaustible energy systems. Pt based electrocatalytic applications for HER are well known and most effective [95, 96]. However, Pt is an expensive rare earth noble metal and because of the less availability of Pt, it is superior to design an inexpensive and stable catalyst for hydrogen economy. After several trials, a relevant nonprecious sulphide-based material [97] and C_3N_4 [98] materials came into consideration, even after several trials, it was noticed that the replacement of Pt atoms as its present form is not suitable for industrial use [99, 100]. This difficulty was later solved by preparing metal clusters or SACs on various supports. When the size of the Pt NPs was reduced to single atoms, it could reduce the use of metal atoms and increase the atomic utilisation efficiency and enhance the electrocatalytic properties [101]. Cheng and co-workers achieved the production of single Pt atoms fabricated on nitrogen fixed graphene nanosheets by following the ALD technique for HER. The size and distribution of catalyst was controlled by specifying the number of ALD cycles. This resulted in the utilisation of all metal atoms for HER, and SACs showed better performances compared to only Pt NP [102].

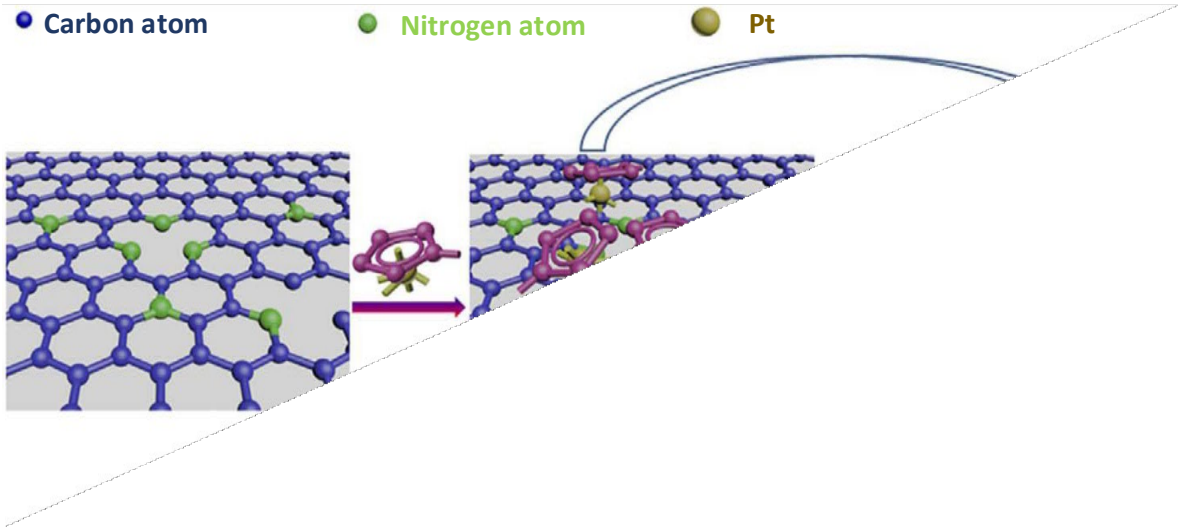

Figure 7. Schematic representation of the Pt ALD process on NGNs. Reproduced from Ref. [102] by permission of Springer Nature Communication.

The succeeding reaction paths were established using ALD process as shown in Fig. 7. This figure represents the process of formation of the single Pt catalyst fabricated NGNs. As revealed, through the ALD procedure, the metal atom precursor first interacts with the NGNs

inclined by the N-dopant. Chemical bonding held among the metal-support resulted a solid contact [64]. To know the shape of the synthesized ALD Pt on NGNs with 50 and 100 ALD cycles, annular dark field (ADF) imaging with aberration corrected scanning transmission electron microscopy (STEM) analysis was performed shown in Fig. 8 (a-d).

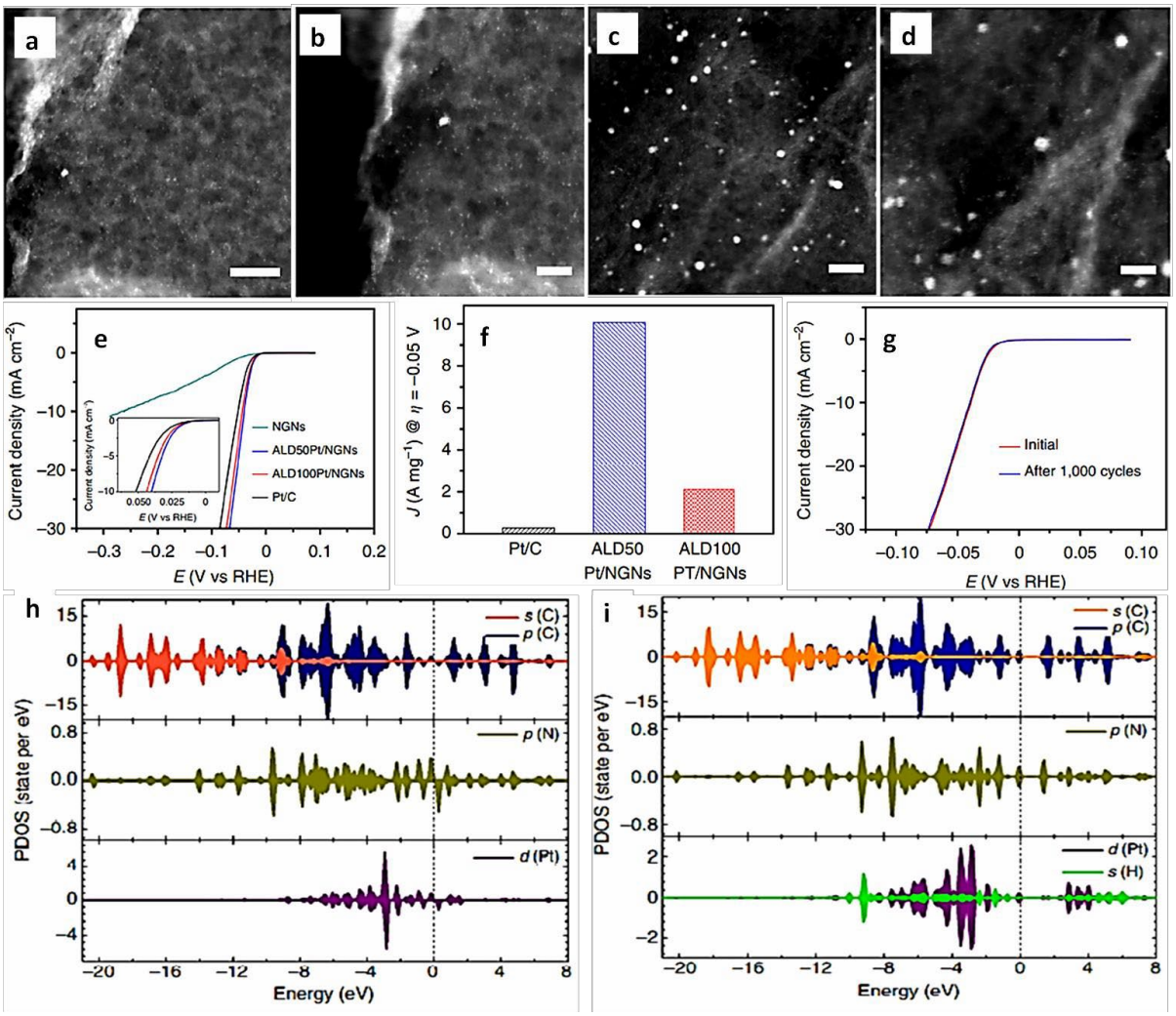

Figure 8. (a, b, c, d) Depicts the ADF STEM images of ALD Pt/NGNs after 50 and 100 ALD process (Where (a, c) 10 nm scale bars and (b, d) 5 nm scale bars). The HER polarization curves for ALDPt/NGNs and Pt/C catalysts were achieved by LSV where the inset demonstrates the inflamed arcs at the onset potential province of the HER for other catalysts. (f) represents the mass activity at 0.05V of the ALDPt/NGNs and the Pt/C catalysts for the HER. (g) The polarization curves at initial stage and after 1000 cyclic voltammetry sweeps which signifies the robustness of the ALD50Pt/NGNs. (h, i) is the electronic arrangement of a Pt atom before and after hydrogen adsorption. Partial density of states (PDOS) of (h) non-H and (i) two H atoms adsorbed on a single Pt atom of ALDPt/NGNs. Reproduced from Ref. [102] by permission of Springer Nature Communication.

The linear sweep voltammetry (LSV) analysis was conducted to observe the HER activity of the ALDPt/NGNs with 50 and 100 cycles. The voltametric study revealed poor HER activity for NGNs without Pt as shown in Fig. 8(e). However, significantly higher catalytic activity was observed for the ALDPt/NGN compared to the Pt/C catalysts. Also, the HER performance of the ALDPt/NGNs was reduced with rising the number of ALD cycles due to the development of clusters after 100 ALD cycles. At 29 mV dec^{-1}, a reduced Tafel slope was accomplished for the ALDPt/NGNs catalysts than for the Pt/C catalysts using the same conditions. Specific activity for individual catalysts was determined from the polarisation curves by normalising the current per the overall area of the electrode. Additionally, controlled to the Pt loading shown in Fig. 8 (f), the action of the HER for the ALD50Pt/NGNs catalysts was 10.1 A mg^{-1} having an overpotential of 0.05 V. It was observed that the ALD50Pt/NGNs catalyst displayed 7.8 times better mass activity compared to ALD100Pt/NGNs compound (2.12 A mg^{-1}) and 37.4 times larger than the Pt/C catalyst (0.27 A mg^{-1}). Fig. 8 (g) unveiled the polarization curve for ALD50Pt/NGNs sample after 1000 cycles and confirmed the retention of similar performance to the initial with only 4% loss in the current density having the same overpotential of 0.05 V. To understand the working mechanism of the catalyst, the authors performed the mechanistical study as shown in Fig. 8 (h, i). It was noticed that Pt and N-doped graphene coordinate with chemical bonding interaction which directed the exceptional charge transfer phenomenon among the single Pt atoms related to the Pt NPs. The distinct 5d-orbitals of the Pt molecules were assorted with the N-2p orbitals at the Fermi level. The Pt atoms situating on N-doped graphene comprise of empty 5d orbitals as shown in Fig. 8 (i), Proceeding with H chemisorption, the 5d empty spaces of the single Pt atom interrelated strongly with the empty 1s orbitals of the H atoms, finally H_2 was generated by electron pairing [102].

Similarly, Qiu and co-workers synthesized single-atom Ni catalysts attached to the nanoporous graphene (np-G) support for HER performance [103]. The CVD technique was used to synthesize the SAC for HER application. Figure 9 (a) represents the FESEM image of np-Ni over an impermeable graphene layer. To form the desired np-G with doped Ni, the sample was allowed for chemical exfoliation by liquifying the np-Ni patterns in a 2.0 M HCl solution.

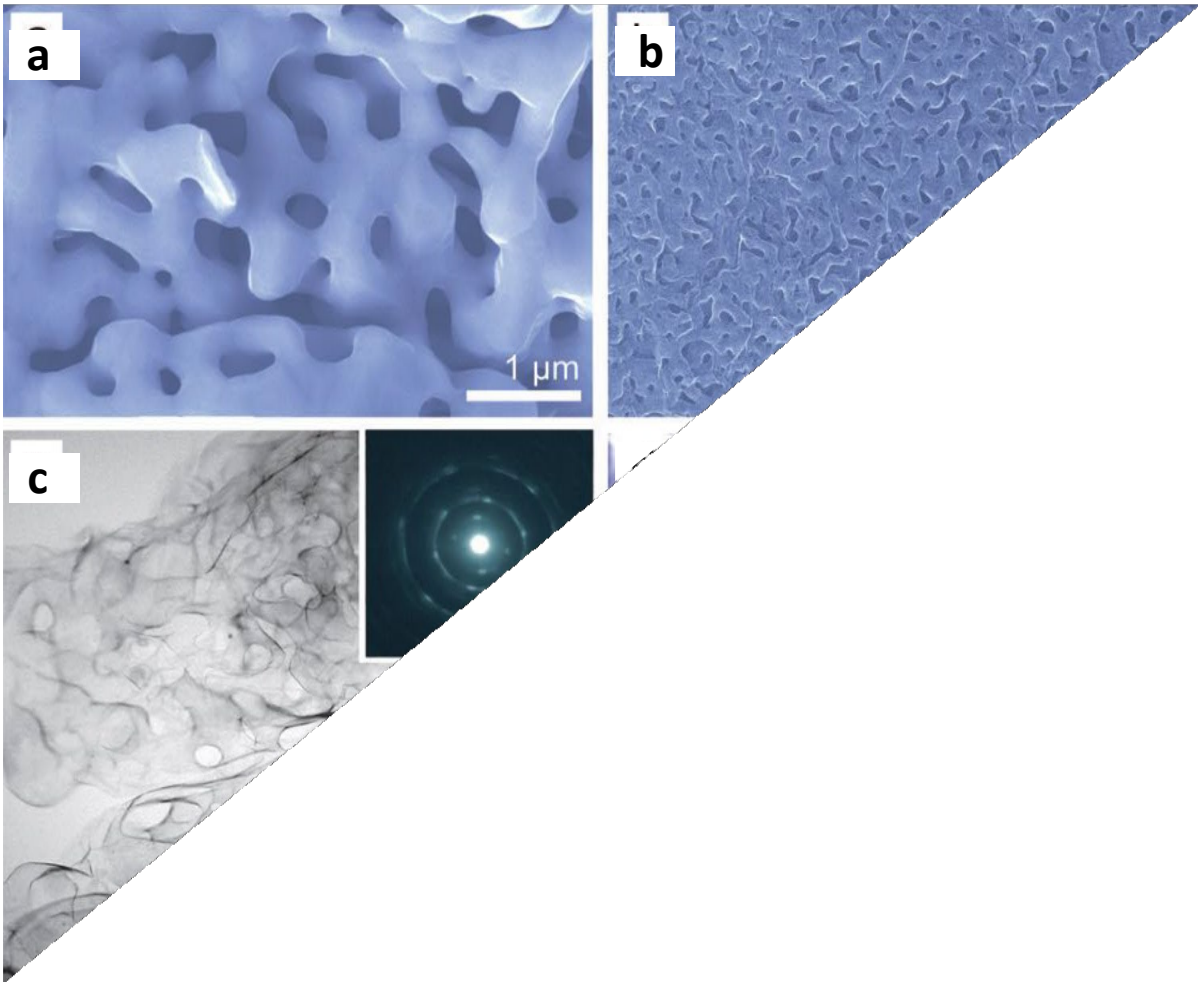

Figure 9. (a) FESEM picture of the synthesized np-Ni/graphene composite, (b) After six hours of Ni suspension, SEM micrograph of Ni-doped np-G, (c) TEM image of Ni-doped np-G. Inset of the SAED pattern, and (d) HAADF-STEM picture of Ni-doped graphene. Inset: In an enlarged HAADF-STEM image marked in red circle and white lines, a positioned Ni atom (bright orange spot) occupies a carbon site in the graphene lattice. Reproduced from Ref. [103] by permission of WILEY-VCH.

After finishing the np-Ni suspension, the nanoporous shape of the material is mentioned in Fig. 9 (b). A bright-field TEM image was captured, revealing the complex 3D shape of np-G as shown in Fig. 9 (c), confirmed the full suspension of the Ni templates. Inset of Fig. 9 (c) showed that the np-G sample had several lattice alignments, which are related to the unintentional movement of the interrelated graphene sheets in the 3D arrangements. Figure 9 (d) represents the STEM image of Ni-doped graphene's structural arrangement, as captured by a high-angle annular dark field (HAADF). The catalytic behaviour of the Ni-doped graphene was initially studied in 0.5M H_2SO_4 solution in a three-electrode system. As revealed in Fig. 10 (a), samples

with lesser Ni suspension times (3–5 h) showed a significant increase in the current response, indicating the huge quantity of remaining metallic Ni(0). A noticeable current comeback was noticed between 0 and 0.1 V, due to the distribution of additional Ni and henceforth, unsatisfactory electrochemical solidity. Subsequently, when 2.0 M HCl solution was taken for Ni dissolution for six hours, the Ni as a dopant became more electrochemically stable. The compared HER activity of the catalyst is shown in the polarisation curve of Fig. 10 (a) and it confirmed that the HER activity was significantly reduced when Ni content is very low (0.38 %, 9 h dissolution). These findings suggest that Ni dopant has an important role in exhibiting HER activity. The Ni-doped graphene material revealed an overpotential substantially lesser than or like the best values obtained with Pt-free uniform catalysis.

The Tafel equation is used to fit the linear parts of the Tafel plots: $\eta = b \log(j)+a$, where j represents the current density and b signifies the Tafel slope. At 6 h dissolution, the Tafel slope of Ni-doped graphene was found to be 45 $mVdec^{-1}$, as shown in Fig. 10 (b). However, Fig.10 (c) showed an evaluation of the Tafel hills and overpotentials of Ni-doped graphene. Substitutional Ni-doping appears to transform graphene's chemical activity from unreacted to the most effective HER catalysis. After 120 h of operating at a continual overpotential of 150 mV, Ni-doped graphene demonstrated exceptional HER activity, with approximately 90% of the preliminary action retained as shown in Fig. 10 (d). The catalyst showed minor cathodic current reduction after 1000 cycles. In acidic solutions, the HER reaction mechanism can be defined as a three-step procedure involving 1) initial H^+ and e^- production, 2) midway H* adsorption, and 3) ultimate ½ H^2 production [104-106]. The Gibb's free energy of a suitable catalyst has H* adsorption, [ΔG_{H^*}]. To further understand, why single-atomic Ni-doped graphene has such high catalytic activity, the structural characteristics of Gibb's free energy image of graphene- Ni catalysts in three different conformations, Ni-dopants can exist as 1) interstitial atoms in a material, 2) replaceable dopants that reside in c sites in the graphene lattice's location, and 3) attaching atoms on defect spots. These findings show that single Ni atoms residing in graphene carbon sites were the most effective HER catalysts. Hence, perform a key character in the remarkable HER actions. Furthermore, chemical interaction amongst the Ni dopants and the carbon around the Ni species appears to stabilise the Ni species in acidic conditions. Due to the interaction between the substituted single atomic Ni dopants and the adjacent C atoms, the Ni-doped graphene exhibits outstanding HER catalysis and was extremely stable. The suitable structural representation and the free energy diagram is shown in Fig. 10 (e, f) respectively.

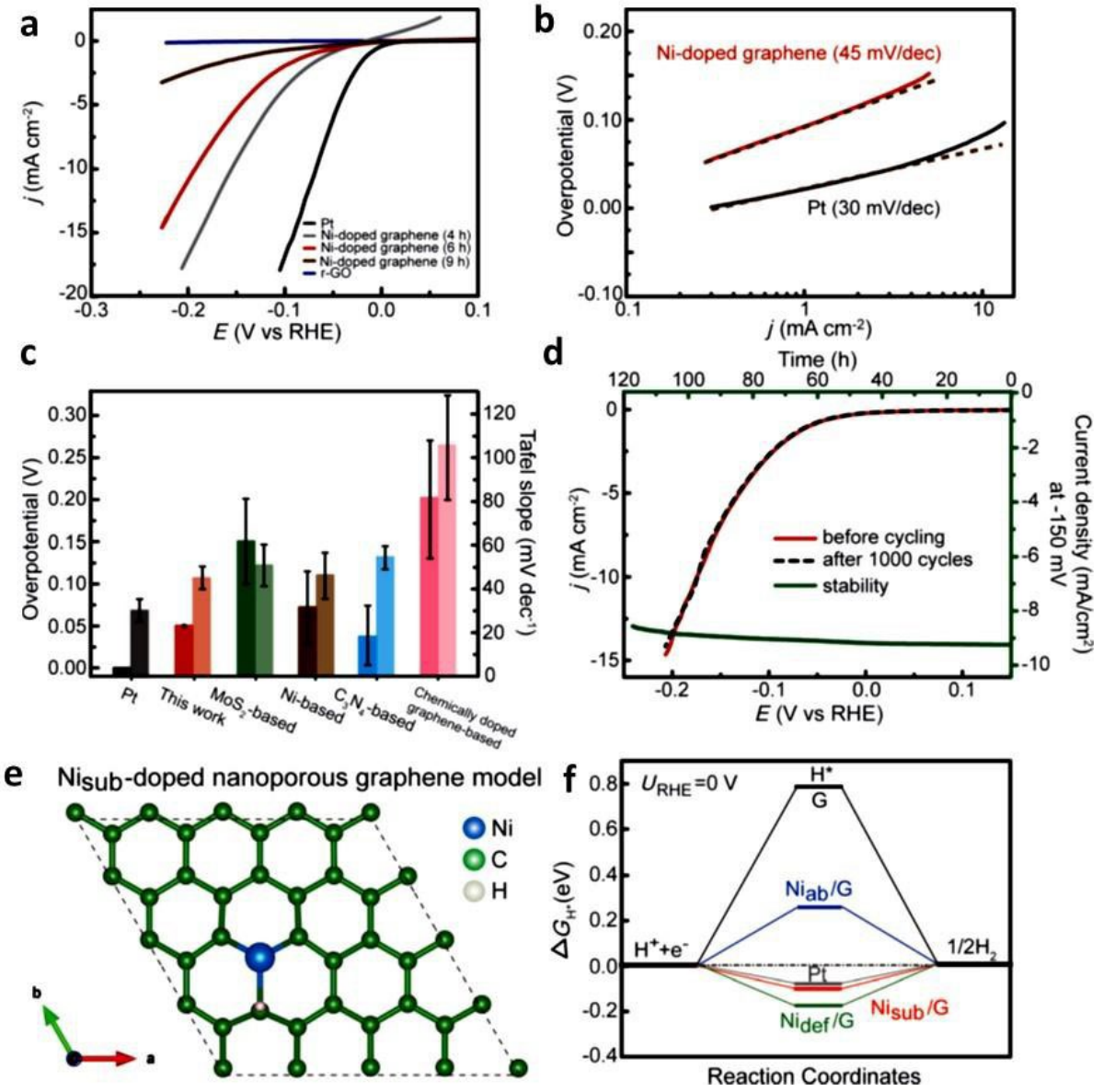

Figure 10. (a) Polarization curves of the synthesized material with different Ni mixing times compared with Pt, (b) Ni-doped graphene and Pt-doped graphene Tafel plots (both at 6 h dissolution), (c) Studies of the overpotential (left) and Tafel slope (right) of several HER catalysts in acidic medium, (d) Cycling stability tests (red line: Ni-doped graphene (6 h dissolution); black dashed line: after 1000 cycles) and (green line) durability of Ni-doped graphene, and (e) For a Pt catalyst and Ni-doped graphene (Niab/G, Nisub/G, and Nidef/G) trials, hydrogen adsorption positions and arrangement of the Nisub/G model with DGH*=0.10 eV (left) and calculated Gibbs free energy of the HER at equilibrium potential (right), (f) The free energies for hydrogen adsorption on pristine graphene and Pt metal, with DGH*=0.79 and 0.09 eV, correspondingly, are designed for comparison. Reproduced from Ref. [103] by permission of WILEY-VCH.

Apart from using metal atoms on the graphene-based support, sulphide-based supports such as MoS_2 with a cost-effective single atom can be proposed as a possible substitute for Pt-based catalysts for HER. For example, Wang et al. established an innovative way of synthesizing single metal Ni atoms on MoS_2 [107]. The authors confirmed the rise in the HER action of the catalyst in case of alkaline as well as acidic conditions. The synthesis protocol includes the hydrothermal method to form MoS_2 nanosheets on carbon cloth and following the decoration of solo Ni atoms by wet-impregnation and calcination method. It was established that the synthesized MoS_2 showed a uniform distribution of the nanosheet array on the carbon cloth substrate, which indicates that the geometry and combined behaviour of the MoS_2 nanosheets on Ni-decorating. The optimization for HER performance was initially estimated in a 1 M KOH solution due to the exceptional geometrical structures of Ni_{SA}-MoS_2/CC. For a better evaluation study, the HER activity of Ni/CC, MoS_2/CC and Nic-MoS_2/CC were examined by following the same reaction parameters. Initially the LSVs of the above-mentioned catalysts were taken in 1 M KOH. It was confirmed that the HER performance of MoS_2 was improved after Ni distribution in the form of gathered or distributed atoms. It can be due to the collaborative result of Ni on the support material.

The activity of HER has further performed in 0.5 M H_2SO_4 electrolyte. It acquired an overpotential of 110 mV to attain a current density of 10 $mAcm^{-2}$, whereas for Nic-MoS_2/CC and for simple MoS_2/CC the overpotential was 157 mV and 186 mV. However, Ni_{SA}-MoS_2/CC exhibited a Tafel slope of 74 mV $decade^{-1}$ which was lesser in comparison to Nic-MoS_2/CC (119 mV·decade-1) and the bare MoS_2 showed 130 mV $decade^{-1}$, representing the greater HER performance of single atom catalyst in acidic condition. After the HER study, the stability of Ni_{SA}-MoS_2/CC was carried out and a slight decrease in activity was observed after 2000 CV cycle. EDS results discovered that Ni atoms in Ni_{SA}-MoS_2/CC still uniformly spread and there is reduce in the loading amount. Whereas Ni clusters present in Nic-MoS_2/CC was immediately disappeared after performing 2000 the CV cycles as mentioned.

5.1.2 Oxygen evolution reaction (OER)

The oxygen evolution reaction (OER) has broadly considered due to its usefulness in the growth of environmentally required energy aids such as HER, batteries, and so on. Due to the OER's inherent slow reaction kinetics, highly effective electrocatalysts are sought to increase energy conversion efficiency. The mechanistic aspect for enormous and robust electrocatalysts for water splitting was established by OER's fundamentally slow kinetics, which include multi

proton-coupled electron-transfer steps [108]. Advanced OER electrocatalysts have also been investigated using nanomaterial containing single atoms. Li and colleagues discovered that the transition metal atoms fabricated on graphitic C_3N_4 could be useful as a novel class of effective OER catalysts based on DFT calculations [109]. As a result, Co/Ni-C_3N_4 electrocatalysts with exceptionally low overpotentials should be capable OER electrocatalysts. Kent and his colleagues synthesized single-atom Co(II)-improved fluoride doped tin oxide (FTO) electrodes. Further, they dipped the FTO in a Co $(ClO_4)_2$ in methanol solution at ambient temperature [110]. Co(II) substituting Sn(IV) in the FTO, and the development of oxygen defect was proved the presence of single-atom Co(II) on FTO. The OER's high-turnover frequency was indicated by the analysis of a steady state current. When the high-surface-area nano FTO electrode was used as a backing material instead of the planar FTO, the current density increased by a factor of 5. Another advantage is that FTO electrodes can be used as the inner electrical sensors to detect O_2 produced in real time. Methodical X-ray absorption studies and direct transmission electron microscopy imaging were performed to recognize a sequence of uniformly distributed metal atoms (for example, Fe, Co, Ni) surrounded by N-doped graphene with a common MN_4C_4 fraction, as stated by Fei and co-workers [111]. The clear structure allows density functional theory to predict MN_4C_4 fractions as the effective OER catalysts with activities that follow the trend as Ni > Co > Fe which is supported by electrochemical experiments. The purpose of atomistical construction and its relationship to catalytic capabilities is a crucial step in rationally designing and synthesising precious and nonprecious SACs with high atom usage efficiency and catalytic activity.

The researchers predicted a four-step OER process involving OH*, O*, OOH*, and O_2* (the symbol signifies the adsorption position). Both the M and C moieties in MN_4C_4 have been explored as plausible absorption places for the intercedes. The metal's amount of d electrons (Nd) in MN_4C_4 halves has a major influence on whether C atoms engage in the OER method. On the other hand, O* and OH* favour to be at the C site, while OOH* prefers to be at the M atom. The presence of metals increases activity to varying degrees: Ni > Co > Fe. The Ni–NHGF catalyst was shown an arrival potential of 1.43 V (mentioned as the potential at 0.5 mA cm^{-2}) and a 10 of 331 mV, which is substantially lower than the Co–NHGF (402 mV) and Fe–NHGF (402 mV) catalysts (488 mV). Tafel plot was used to examine the OER kinetics. Tafel slope of Ni–NHGF was significantly lower (63 mV per decade) than that of Co–NHGF (80 mV per decade) or Fe–NHGF (164 mV per decade). To assess Ni–intrinsic NHGF's activity,

the authors calculated the turnover frequency (TOF), which measures a catalyst's activity on a particular-energetic-site base.

In another report, Talib and co-workers recently reported, the electrocatalytic performance of nineteen different transition metals (TM) (TM = Ti, V, Cr, Mn, Fe, Co, Ni, Zr, Nb, Mo, Ru, Rh, Pd, W, Re, Os, Ir, Pt, and Au) catalyst attached to phosphomolybdic acid (PMA) substrate [112]. It was observed that out of all the SACs, the Co_1/PMA, Pt_1/PMA, and Pd_1/PMA exhibited excellent catalytic activity for OER with designed overpotentials of 0.45, 0.49, and 0.54 V, respectively.

According to the definitive path of OER at pH zero,

$2H_2O \rightarrow 4H + O_2 + 4e^-$

The progress of 4 electron reaction steps for OER are mentioned below,

$H_2O(l) + M_1* \rightarrow M_1OH* + e^- + H^+$

$M_1OH* \rightarrow M_1O* + e^- + H^+$

$H_2O(l) + M_1O* \rightarrow M_1OOH* + e^- + H^+$

$M_1OOH* \rightarrow O_2(g) + e^- + H^+ + M_1*$

Here M_1* denotes the catalyst and energetic adsorption site, liquid and gas phases represented by (l) and (g), and OH*, O*, and OOH* represent the adsorbed mediates on the active species. $\Delta G_a = \Delta G_{OH*}$, $\Delta G_b = \Delta G_{O*} - \Delta G_{OH*}$, $\Delta G_c = \Delta G_{OOH*} - \Delta G_{O*}$, $\Delta G_d = 4.92 - \Delta G_{OOH*}$ are denoted for the variation in the Gibbs free energy throughout the OER process.

It was reported that the morphological arrangement of PMA support permits four different bonding positions to the metal species. Those are basically, two 3-fold hollow sites (3H - O_c and $3HO_{bri}$), one 4-fold hollow site (4H), and a bridge site (B - O_c - O_{bri}) as shown in Fig. 11 (a). The authors confirmed that all the atoms are positioned in a distorted-square planar geometry at the 4H site. According to Fig. 10 (b, c), the higher stability showed higher binding energy to the substrate and vice versa. The trend of binding strength follows the order as: Zr > Ti > Nb > W > V > Mo > Os > Re > Cr > Mn > Fe > Co > Ir > Ni > Ru > Rh > Pt > Pd > Au. Further, for a better understanding about the stronger metal-support interaction, the authors were carried out an outstanding analysis of difference in the charge density with respect to the Bader charge comparison with the subsequent doping of the active metal atoms. The Bader charge analysis is shown in Fig. 11 (b) which signifies the transfer of electrons from the TM

atom to the PMA surface and the electron movement decreases with the increasing the atomic number of active metals.

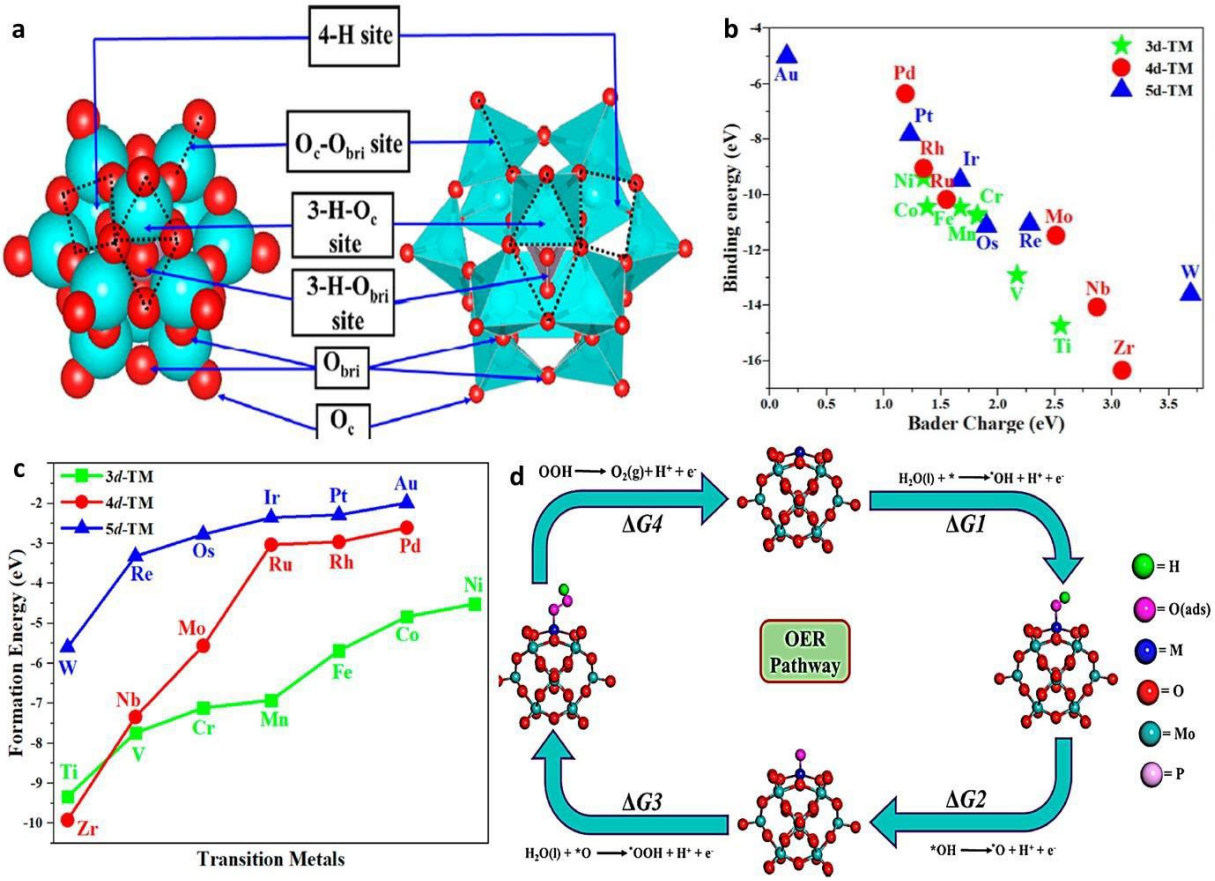

Figure 11. (a) Schematic arrangement of PMA substrate with different possible binding positions, (b) Connection of the calculated binding energy and the Bader charge of all the active metal atoms bonded to the PMA substrate, (c) Plot between the formation energy and TM atoms in eV, and (d) Represents the 4e− OER mechanism on the M_1/PMA catalyst with the enhanced arrangements for intermediates. Reproduced from Ref. [112] by permission of WILEY-VCH.

It was confirmed that the above-mentioned data refers to the formation of chemical bonds between the support PMA and metal atoms. The complete OER reaction was usually described in terms of four major adsorption/5-desorption stages as shown in Fig. 11 (d) on PMA surface. The initial step was completed by dissociating the H_2O into *OH and H^+ fragments. In the second step, the dissociation of *OH forms *O and H^+ species. After this, the generated *O has reacted with another H_2O molecule to generate *OOH and H^+ in the third step. The fourth and final step has completed by generating H^+ and O_2 from *OOH fragment and O_2 fragment has been removed from M_1/PMA substrate. The effective OER analysis was conducted by taking

the series of metals supported on PMA substrate. It was observed that, the Co_1/PMA and Pt_1/PMA catalysts displayed excellent electrocatalytic act for the OER property.

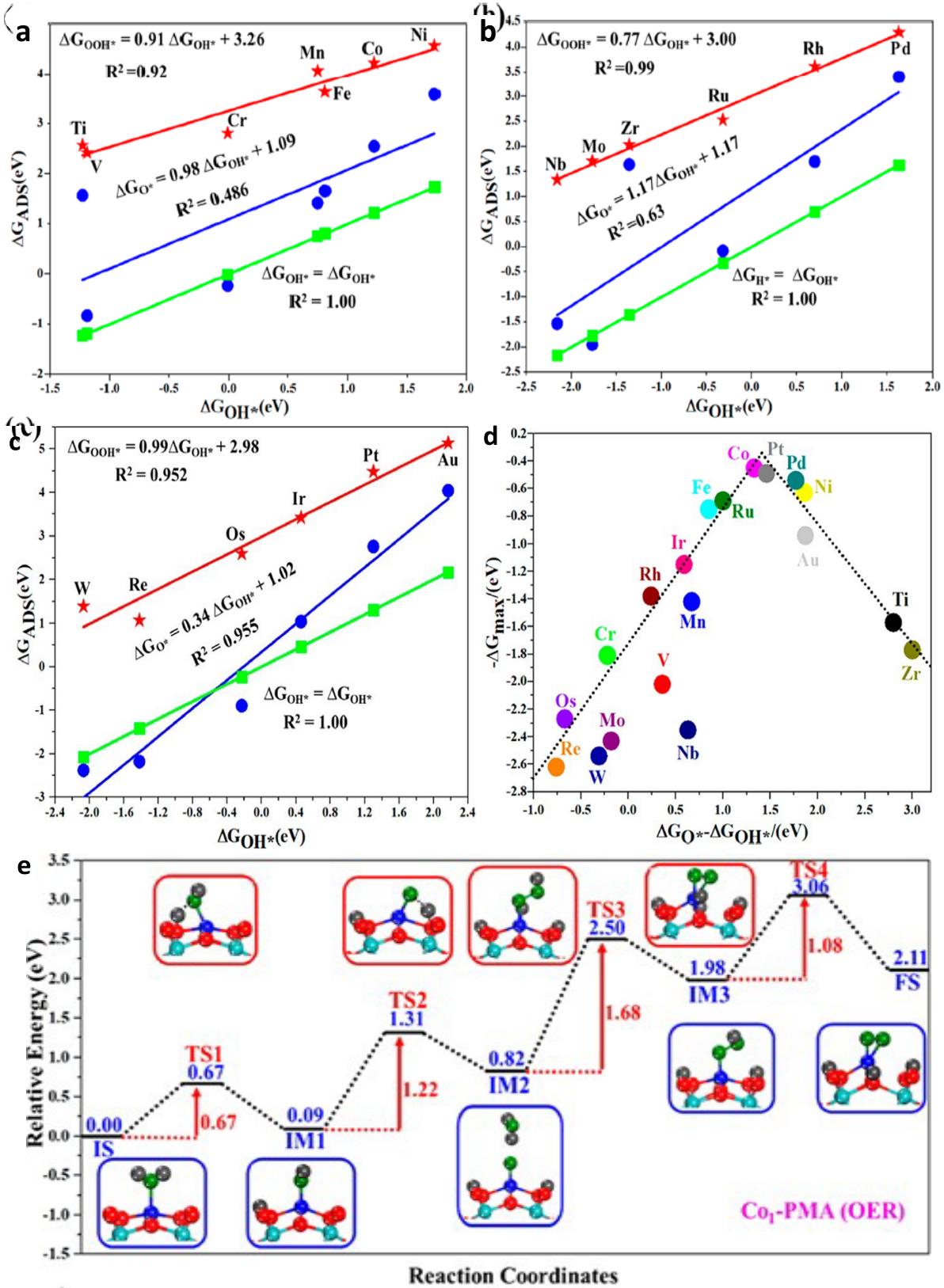

Figure 12. (a-c) Relation between the Gibbs free energy (ΔG) and the oxygenated (ΔGO*, ΔGOH*, and ΔGOOH*) fragments. (d) The maximal potential-limiting ($-\Delta G_{max}$) step is

displayed against the ΔGO* − ΔGOH* step to better understand the OER properties. (e) mechanistical representation of the four consecutive basic paths involved in the OER of Co_1/PMA catalyst. Reproduced from Ref. [112] by permission of WILEY-VCH.

Fig.12 (a-c) shows the connection between the free energy of adsorption and the fragmented intermediates (ΔGO*, ΔGOH*, ΔGOOH*) for the diverse M_1/PMA systems. A link between the adsorption energies GO* and GOH*, on the other hand, appeared to be less likely. As a result, the distinction served as an exceptional signifier for the OER activity. Fig.12 (d) displays a volcano curve relationship between ΔGO*- ΔGOH* and adverse extreme potential limiting phases. Theoretical investigations revealed that among the various M_1/PMA catalysts, the Co_1/PMA and Pt_1/PMA combinations have the lowest values (0.42 and 0.49 V) and are near the maximum of the volcano curve. As a result, Co_1/PMA and Pt_1/PMA could be viable OER electrocatalysts. The Co_1/PMA catalyst's excellent catalytic behaviour for the OER was further supported by the thermodynamic mechanism. Fig. 12 (e) displayed the energy profile diagram for detailed OER pathways. The H_2O molecule is chemically bonded to the 4H site of the Co_1/PMA catalyst through atomic oxygen in the catalytic cycle, with a predicted adsorption energy of -0.58 eV. The adsorbed H_2O was first deprotonated by the breaking of the H-O bond in H_2O to a *OH species, and then a proton passage from H_2O to the neighbouring 4H site O atom, resulting in the [M_1]-O-H…..OH intermediate through the first transition state (TS1) having 0.67 eV energy of activation and an imaginary frequency of 459i cm^{-1}. In the second phase (TS2), the residual *OH radical on the Co_1/PMA undergoes further deprotonation with a subsequent formation of *O, and a proton travels from *OH to one more 4H site O atom via the breakage of an O-H bond. For the deprotonation of *OH→ *O + H* alteration. The formed radical was tightly attached to the Co_1/PMA, as evidenced by the fact that this kinetic energy barrier is much more than the OH* first-step energy barrier. A crucial and most awaited step was the third step (TS3), which started with the creation of an O_2 molecule. The second H_2O molecule contact with the residual metal-oxo species (O*) to give a hydroperoxo (*OOH) species through a TS with a kinetic energy barrier of 1.68 eV. The proton was released from the H_2O molecule and attaches to the nearby 4H site O atom when the O-H bond is broken and leading to the formation of *OOH species. The *OOH fragment was deprotonated in the last phase, resulting in the creation of *OO species by breaking the O-H bond. The activation barrier (TS4, imaginary frequency 1094i cm^{-1}) derived mathematically and found to be 1.08 eV. The first stage was advantageous in terms of both thermodynamics and kinetics. The produced *OO species can then be recovered from the surface, producing an O_2 molecule, and

the catalyst's active site can be reused, allowing another OER cycle to begin. Further, considering the importance of OER, Zeng and co-workers reported the fabrication of Sc, Ti, V, Cr, Mn, Fe, Co, Ni, Cu, Zn, Rh, Pd, Ir, and Pt as the catalytically active metals on nitrogen-doped boron phosphide (N_3-BP) 2D support for the performance of OER [113]. The initial experimental analysis in this literature was highlighted the study of the geometrical, electric, and magnetic assets of the pristine and vacancy-doped BP monolayers (MLs), which was subsequently demonstrated insufficient electrocatalytic action for OER as well as for oxygen reduction reaction. By thoroughly examining the behaviour of each metal atom's activity, it was confirmed that CoN_3-BP, NiN_3-BP, and PtN_3-BP showed better catalytic property for OER. The binding energy of the adsorption material vs the overpotential were used to detect the activity. The authors mentioned several characteristics which made them capable of ORR as well as bifunctional electrocatalysts. Furthermore, the reported findings have shown that the M site's catalytic activity was extremely connected to the electrical structures of its immediate surroundings. More importantly, this study revealed an intrinsic property of highly efficient OER catalysts. It also enlightened the reaction site's spin- and site-precise electrical conditions, as well as the surrounding N atom's parallel spin polarisation.

5.1.3 Oxygen reduction reaction (ORR)

Significant and long-term application of polymer electrolyte membrane fuel cells in cars requires high-reactive active species with minimal Pt feeding for cathode material throughout the ORR in fuel cells. Liu et al. reported a carbon black-reinforced, inexpensive, active, and stable Pt SACs with CO/methanol acceptance for the cathodic ORR [114]. A Pt payload of 0.09 $mg_{Pt}\,cm^2$ and power density of up to 680 $mWcm^2$ at 80 ºC was achieved in agreement with a Pt utilization of 0.13 $g_{Pt}\,kW^{-1}$ in the fuel cell. According to theoretical calculation, the important efficient sites on such Pt SACs were single-pyridinic-N-doped single-Pt atom centres, which are CO/methanol tolerant yet very active for the ORR. Further, Wan and colleagues successfully built single-atom-distributed Co sites with nonplanar organization in N-doped carbon, as evidenced by advanced electron microscopic and X-ray spectroscopy measurements [115]. The ORR performance and efficacy of catalysts were evaluated and compared in detail. CoNC700 provided significantly higher reactivity as shown in Fig.13 (a,b) than cobalt-free catalysts, with a high onset potential (0.960.01 V) and half-wave potential (E1/2, 0.850.01 V). In addition, CoNC700 showed a Tafel slope of 78 mV dec^{-1}, which was somewhat greater than that of Pt/C (73 mV dec^{-1}) as mentioned in Fig. 13 (e). Likewise, catalyst CoNC700 represented in Fig. 13 (c) exhibited a large rise in ORR actions in the acidic medium

due to the insertion of single-atom Co sites as shown in Fig. 13 (c, d) and a small Tafel slope of 72 mV dec^{-1}, nearly alike to that of Pt/C (70 mV dec^{-1}) represented in Fig. 13 (f). SAC with planar Co-N site was substantially lower activity.

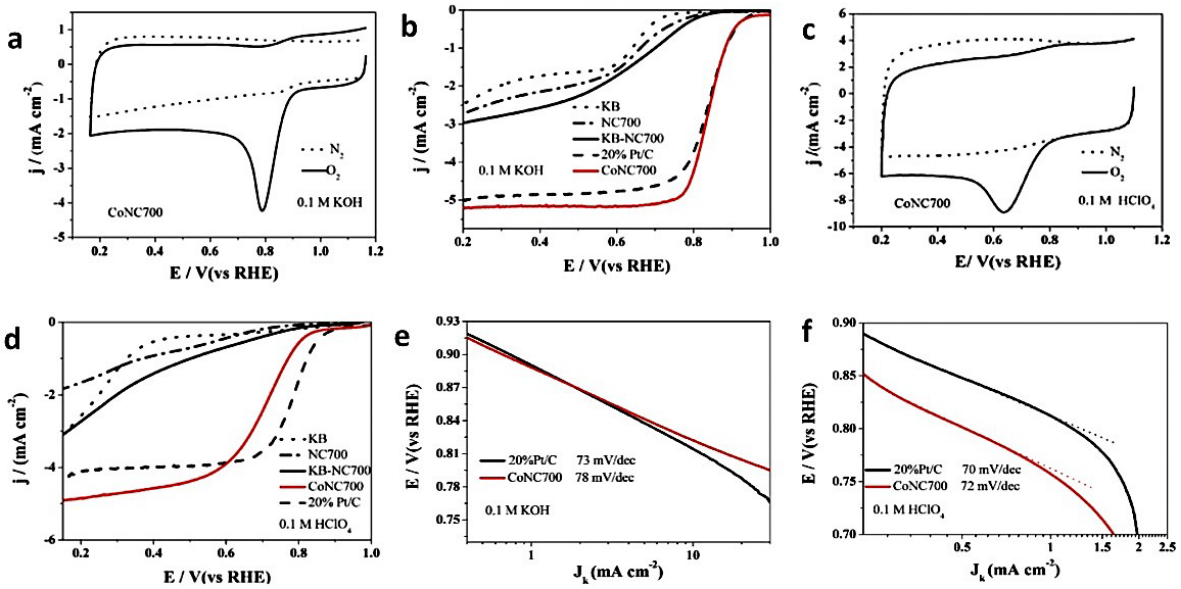

Figure 13. (a) Cyclic voltammograms of CoNC700 at a scan rate of 5 mVS^{-1} in 0.1 m KOH, (b) CoNC700, and Pt/C in 0.1 M KOH. (c) 0.1 M $HClO_4$ saturated with N_2 or O_2 LSVs at 5 mVS^{-1} of KB, NC700, KB-NC700, (d) 0.1 m $HClO_4$ saturated with oxygen at the speed of 1600 rpm, Tafel slopes of CoNC700 and Pt/C catalysts in (e) 0.1 M KOH, and (f) 0.1 M $HClO_4$. Reproduced from Ref. [115] by permission of WILEY-VCH.

In situ chemical ion probing was used to investigate the connections between single-atom Co-sites and adsorbates. A half-wave potential shift of roughly 150 mV in the negative direction. The action of CoNC700 in an acidic media has been demonstrated in Fig. 14 (a), illustrating the importance of Co-comprising catalytic materials spots in an acidic environment. The same activities in 0.1 M KOH, on the other hand, only bring about minor activity degradation, as shown in Fig. 14 (b). Further, pyridinic-N doping might function as the major catalytic positions in the alkaline medium deprived of being contaminated by SCN ions, resulting in nearly undegraded ORR activity even if SCN ions were present in the active sites for Co were completely blocked as shown in Fig. 14 (c). Co L-edge NEXAFS was performed before and after ORR catalysis to gain a well knowledge of Co–adsorbate interactions in various situations. It was mentioned that the two tiny satellite peaks may have appeared for CoNC700- cycled at roughly 784.5 and 799.5 eV, respectively mentioned in Fig. 14 (c, d). These two satellite peaks substantially stable in the Co L-edge NEXAFS of CoNC700-cycled after

finishing the ORR in acidic media shown in 14 (c). Adsorbate ligands efficiently and easily adsorbed on single-atom Co sites with more vacant 3d orbitals.

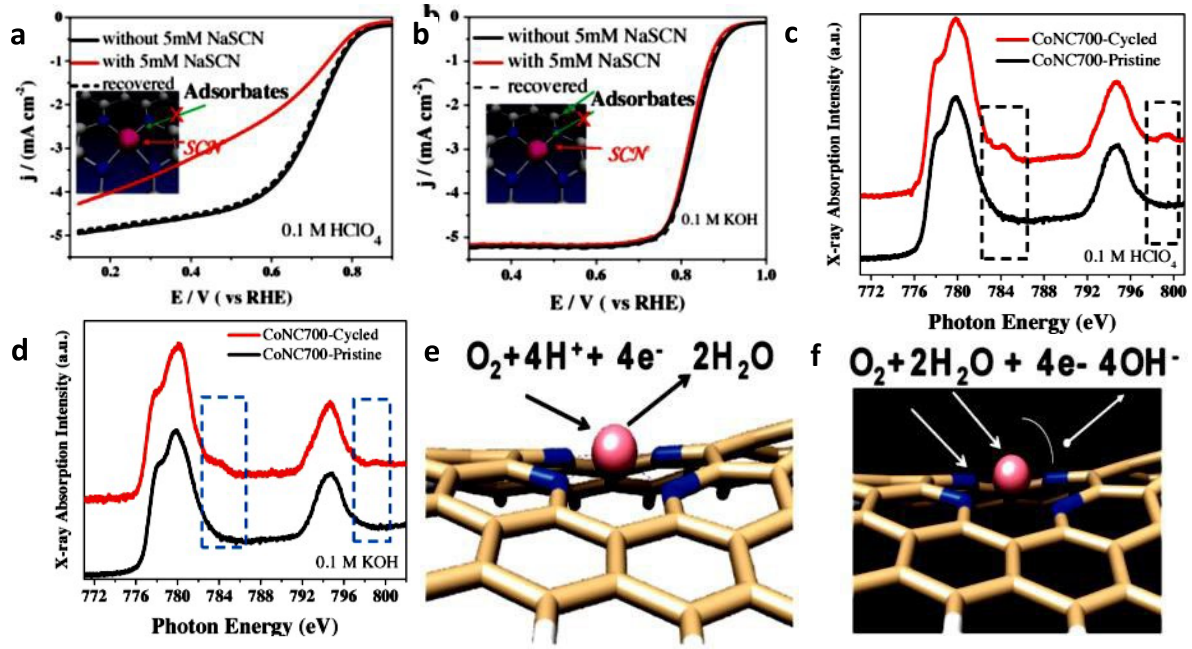

Figure 14. (a) In acidic, and (b) alkaline media, probing the primary catalytic sites in single-atom dispersion catalysts. Co L-edge NEXAFSs of pristine catalyst CoNC700 and cycled CoNC700 in (c) alkaline, and (d) acidic media, respectively; LSV curves of catalyst CoNC700 with/without 5 mM NaSCN in acidic and alkaline media. Several overriding catalytic paths are depicted schematically in (e) acid and (f) base. Reproduced from Ref. [115] by permission of WILEY-VCH.

The metal-to-ligand and ligand-to-metal charge transfer amid Co spots and adsorbates was substantially weaker in alkaline media under the similar circumstances shown in Fig. 14 (d). In addition to the Co sites, the above-mentioned adsorbates can be absorbed by some type of doped N-species in alkaline media, catalysing the ORR. As a result, compared to acidic media, Co sites showed a lower important role in ORR in alkaline media. In this study, the authors directed evidence for Co–adsorbate relations and Co -comprising sites in SAC. Because the as-prepared SAC contained Co -containing and pH-dependent ORR catalytic sites, it exhibited moderate-dependent ORR catalytic characteristics. ORR positively occurred on single-atom scattered Co sites with strong contact with adsorbates in acidic media, but active ORR catalysis in basic media may be obtained for single-atom Co places or pyridinic-N doping shown in Fig. 14 (e, f).

5.1.4 Methanol, ethanol, or formic acid oxidation

The indirect pathway of the methanol oxidation process (MOR), which results in the generation of CO, is widely recognised. To understand the consequence of scope of Pt atom on the electrochemical MOR activity, Kim and co-workers prepared size-measured Pt catalyst fabricated on CNTs [116]. Pt atoms remained on thiolated multiwalled CNTs (Pt-SMWNTs) can be easily formed by reducing a Pt precursor adsorbed on thiolated MWNTs (S-MWNTs). The formation of Pt clusters of various sizes was triggered by further heating at various temperatures. The resulted Pt- S-MWNTs by single Pt atoms was verified by XANES. For the MOR, several nanomaterials were utilised as electrocatalysts. The electrocatalytic activity of the MOR was observed to rise with a decrease in the size of the Pt catalyst. On the other hand, the generated Pt-S-MWNTs containing single Pt atoms, displayed that the MOR couldn't proceed, confirming that only Pt atoms are not advantageous for the MOR through either the indirect or direct methods. Sun et al. produced Pt/ graphene with varied particle sizes, beginning from a single atom using ALD technique [47]. The number of vacancies and defects in graphene was crucial for the single atoms to remain stable. After 50 ALD cycles, the coexistence of Pt single atoms, clusters, and tiny NPs was detected. The cluster/NP size increased when the ALD cycles increased (100 and 150 ALD). Relating to the current density and onset potential, Pt/graphene after 50 cycles was shown the best MOR activity. Zhang et al performed MOR using Pt_1/RuO_2, the catalyst was prepared by following an impregnation- adsorption approach [117]. It was confirmed that Pt_1/RuO_2 exhibited good performance for MOR compared to the commercial Pt/C which is 6766 vs. 441 mA mg_{pt}^{-1} respectively. The ethanol oxidation reaction (EOR) is complicated as there are two separate adsorption facilitates with one or two carbon atoms [118]. Weber and colleagues studied the size-relevant electrocatalytic performance in the EOR at Pt_n/ITO (n=1 to 14) after depositing mass-selected Pt_{n+} on ITO [119]. The electrocatalytic activity of the OER was shown to vary randomly, with Pt_4/ITO and Pt_{10}/ITO providing the finest EOR results. Pt_1/ITO electrocatalysts with separated Pt atoms were ineffective for EOR. The EOR activity was likewise said to be anticorrelated with Pt 4d binding as reported.

Formic acid fuel cells are considered the most viable and suitable energy-conversion strategies. The attempts to produce an efficient catalysts for the formic acid oxidation reaction (FAOR) have continued from a long time. The electrocatalytic FAOR is widely known to use a dual route mechanism. The direct method ($HCOOH \rightarrow 2H^+ + CO_2 + 2e^-$) includes a direct oxidation to CO_2 deprived of producing CO as a chemical intermediary, whereas the indirect pathway

outcomes in the creation of surface contaminating species of CO_{ads} ($HCOOH \rightarrow H_2O^+ + CO_{ads}$) [120]. As it is clear that exploring novel formic acid oxidation catalysts with ultra-high mass activity and CO resistance is critical to overcome the criteria of possible applications. In this regard, recently, Xiong et al. synthesized atomically dispersed Rh on N-doped carbon (SA-Rh/CN) for FAOR [121]. After several thorough testing, it was confirmed that SA-Rh/CN provided considerably improved resistance to CO poisoning and that Rh atoms in SA-Rh/CN shield sintering, ensuing high catalytic stability. Further, the CO resistance was confirmed by performing two separate reactions which confirmed that SA-Rh/CN can hinder the dehydration of formic acid, eliminating CO poisoning. To understand the mechanism of FAOR on SA-Rh/CN and its superior CO tolerance, DFT calculation was performed. It was found that on SA-Rh/CN, the formate approach is preferable. The high barrier to producing CO together with the highly unfavourable binding with CO contribute to its CO tolerance. Li et al. devised an universal host–guest technique for producing a variety of SACs on nitrogen-doped carbon (M1/CN, M = Pt, Ir, Pd, Ru, Mo, Ga, Cu, Ni, Mn) [122]. It was observed that Ir_1/CN showed good performance for FAOR compared to SACs. Moreover, the reactivity of Ir_1/CN was 16 and 19 times higher compared to commercial Pd/C and Pt/C, respectively.

5.1.5 Other electrocatalytic activities of SACs

The necessity for developing a suitable and adequate catalyst for high-performance electrochemical devices like rechargeable Zn–air batteries is increasing. Recently, SACs are being investigated for several electrocatalysis applications. In this view, Li and co-workers described a suitable method to build a single-atom Co–N_x–C electrocatalyst for HER, OER and Zn–air battery applications [123]. A hybrid of Co-coordinated framework porphyrin with graphene (called Co-G@POF) was developed as the pyrolysis precursor. The Co-coordinated framework porphyrin (Co-POF) was chosen because of its analogous chemical structure, which is Co–N_x–C. A facile one-pot synthesis protocol was followed to get high yield and output. Graphene (G) was used as a template for the morphological framework of porphyrin during stacking. Co-POC, a pyrolyzed product generated from Co-G@POF, was the necessary single-atom Co–N_x–C structures, as evidenced by extensive characterizations. With a narrow overpotential gap of 0.87 V, comparable to noble-metal-based electrocatalysts, quick kinetics with reduced Tafel slopes, and long-term durability, the Co-POC electrocatalyst exhibited good bifunctional oxygen electrocatalytic activity. As a result, rechargeable Zn–air batteries with the Co–POC cathode contained higher power density, better rate performance, and cycling stability for over 200 cycles at 2.0 mA cm^2 than noble metal-based cathodes. Co-G@POF is a covalently

bound Co-coordinated porphyrin connected into a hybridised 2D structure on the surface of G produced via π-π intermolecular interactions.

To combat the increasing CO_2 concentration in the surrounding, electrochemical CO_2 reduction reaction (CO_2RR) is necessary. There are variety of different products can be obtained after the CO_2RR such as CO, formic acid, hydrocarbons including methane, ethane and alcohols like methanol, ethanol etc. These gases further can be utilized in fuels or suitable fit for the vehicles and industries. Zheng and workers described a simple technique of abundant Ni SACs using commercial carbon black in a gas-phase electrocatalytic reactor in a suitable ambience. As a result, the single-atomic spots work exceptionally well in converting CO_2 to CO with current density exceeding 100 mA cm^2 and approximately 100% selectivity for CO. However, the HER was roughly 1% in favour. The total current in one unit cell may readily rise to more than 8 A while retaining restricted CO evolution with a production rate of 3.34 L hr^{-1} per unit cell by climbing up the electrode to a 10 3 10-cm^2 modular cell [124]. Similarly, Sheng et al. performed the electrochemical CO_2RR by taking in Fe-N-C SACs and proposed the reaction mechanism shown in Fig. 15 (a) and CO_2 reduced to CO involves the steps such as [125],

$$CO_2 + * + H^+ + e^- \rightarrow *\text{COOH} \quad (1)$$

$$CO_2 + * + e^- \rightarrow *CO^-_2 \quad (1b)$$

$$*CO^-_2 + H^+ \rightarrow *\text{COOH} \quad (1c)$$

$$*\text{COOH} + H^+ + e^- \rightarrow *\text{CO} + H_2O \quad (2)$$

$$*CO \rightarrow CO + * \quad (3)$$

Where $*$ denotes the active sites of the SAC surface.

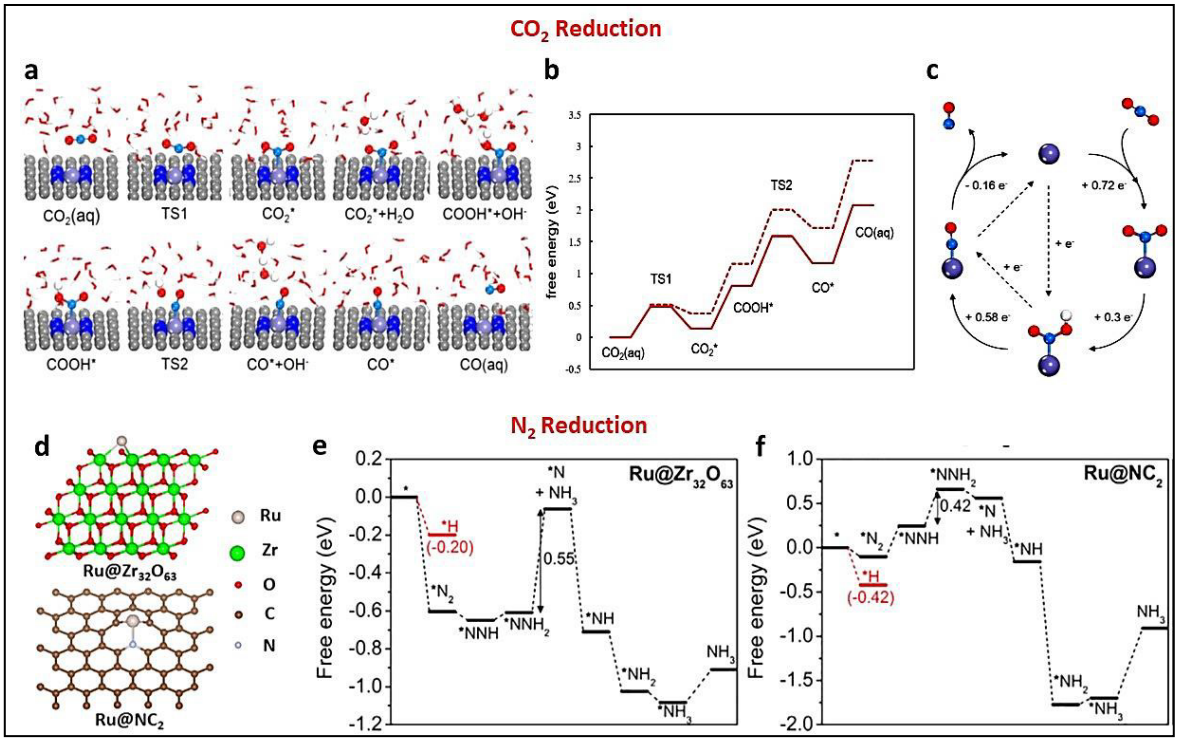

Figure 15. (a) Structural illustration of electroreduction of CO_2 to CO, counting CO_2 adsorption, COOH* intermediate generation, CO* production and CO* desorption and CO formation. (b) Energy profiles diagram of CO_2RR to CO. (c) mechanistic aspects for CO production considering the electron transfer in every elementary phases. Reproduced from Ref. [125] by permission of Elsevier. (d) Calculation models for $Ru@Zr_{32}O_{63}$ and Ru/NC_2. Free-energy diagram for NRR on (e) $Ru@Zr_{32}O_{63}$ and (f) on $Ru@NC_2$. Reproduced from Ref. [103] by permission of Cellpress .

The electrochemical conversion of CO_2 to CO can be completed in two mechanistic path such as coupled proton-electron pathway and proton decoupled electron pathway. However, proton-electron coupled pathway is broadly followed, where the electron transfer from CO_2 provides *COOH. Further, the *COOH intermediate undergoes proton-electron transfer and forms *CO, and the weakly bonded *CO then dissociates to form the CO. In case of proton decoupled pathway, the formation of hydroxyl intermediate *COOH forms in two steps i) CO_2 adsorption via one electron transfer to form CO^{-}_{2}as shown in equation 1(b) and further by protonation process CO^{-}_{2} generates *COOH equation 1(c) and finally proceeds to form CO product. Yang et al. synthesized Ni (I) SAC anchored on N-doped graphene matrix for electrocatalytic CO_2RR and showed excellent reduction ability and stability [126]. The authors observed the delocalization of the unpaired electron in Ni $3d_{xz\text{-}yz}$ orbital which attributed to the rapid charge transfer from the metal atom to the substrate 2p-orbital. As a result of which the energy barrier

for CO_2RR was reduced fastening the product formation. A variety of Ni_{SA}-N_x-C SACs prepared by Gong et al. for the CO_2RR to form CO product [127]. It followed host-guest co-operative strategy for the formation of SACs by taking polypyrrole (PPy) into bimetallic MOF. It was illustrated that by incorporating Mg^{2+} in MgNi-MOF-27, extended the spatial distance of the neighbouring Ni atoms and PPy acted as the stabilizing agent for the individual Ni atoms during the synthesis. Further, different N-coordination number of Ni SACs was found with altering the pyrolysis temperature. Pointedly, it was confirmed that the NiSA-N_2-C catalyst accomplished highest CO Faradic efficiency upto 98 % and 1622 h^{-1} turn over frequency compared to NiSA-N_3-C and NiSA-N_4-C catalysts. The reason was confirmed from theoretical calculation which stated that due to the low co-ordination number of metal atoms in NiSA-N_2-C, it become more feasible for the generation of *COOH intermediate. Therefore, responsible for superior CO_2 reduction ability. There are many other reports which established for the CO_2RR in the presence of different SACs [128-131].

Ammonia (NH_3) is an important chemical material for manufacturing fertilizers and other products. Apart from using the old Haber-Bosch process for NH_3 production, it is more feasible to follow the N_2 conversion to NH_3 by electrochemical reduction pathway. Different SACs catalysed nitrogen reduction reaction (NRR) to ammonia are widely reported. Wang et.al produced Au_1/C_3N_4 SAC for NH_3 production under ambient conditions [132]. Qin et al. also reported Au SAC supported on N-doped porous carbon for NRR and exhibited outstanding NH_3 production [133]. In another report, it was seen that Ru SAC on N-doped carbon showed enhanced NRR [134]. Geng et al. confirmed that the catalyst facilitates the adsorption of N_2 and the ΔG for dissociating N_2 on Ru-N-C SAC was lower than Ru (101), which subsequently enhance the NRR activity. Similarly, Tao et al. synthesized Ru@ZrO_2/NC SAC by annealing UiO-66 containing Ru [135]. The structural model of Ru@$Zr_{32}O_{63}$ and Ru/NC_2 are shown in Fig. 15 (d) and as demonstrated in Fig. 15 (e, f) The increased NRR performance of Ru@ZrO_2/NC was due to a lower ΔG for the energy-consuming stage in electrochemical NRR (*NNH production on Ru SAC) compared to Ru (0001). Moreover, there are several non-noble metal-based transition metal SACs which plays critical role in NRR.For instance Zhao et al. compared the NRR performance between the metal catalysts such as Zn. Mo, Rh, Pd, Ag etc. and observed that Mo SAC showed enhanced N_2 reduction over other transition metal atom SACs [136]. There are some reports which established the better N_2 reduction ability of Mo SACs compared to costly catalyst [137, 138].

Various NOx air pollutants are generated due to fossil fuel burning. Out of which NO is the major air impurity released from the automobile and industry sources. Among the technologies used after combustion, selective catalytic reduction is thought to be the best method for reducing NO emissions because of its superior NO removal performance and it is quite easy to remove. Installation of equipment that is simple to use and has a low operating cost and so on. Previously, Pt based metal nanocatalysts were used to reduce NO, but due to the cost and the availability issue of Pt, SACs are considered to be the better substituent instead of Pt based metal nanocatalysts [139]. For example, Lin et al. synthesized FeOx supported Pt SAC for NO reduction to N_2 and it is confirmed that Pt SAC showed substantially higher selectivity compared to Pt nanocatalyst [54]. A co-precipitation method was followed for the preparation of Pt-SAC of 0.06 wt % Pt loading and further by following a suitable approach, Pt-Nano catalyst with 1.22 wt % of metal loading was prepared for the comparison study. The reduction of NO to N_2 was carried out in the presence of H_2. The electrochemical study was confirmed the superior activity of Pt-SAC over Pt nanocatalyst. This improved performance was due to the presence of more oxygen vacancies on the Pt-SAC, as well as stronger NO adsorption and simpler dissociation of the N–O link. The authors confirmed that Pt SACs enabled the dissociation of NO to $N_{(ad)}$ and $O_{(ad)}$, later the oxygen vacancies can absorb the $O_{(ad)}$ and endorsed the formation of N_2 by NO reduction. In another report, Wu et al. performed the reduction of NO in presence of Cu SAC fabricated on the spinel structure of $MgAl_2O_4$. Cu_1-$MgAl_2O_4$ is reported to have substantially higher catalytic activity for NO reduction by CO compared to 1.0 wt % Pt/CeO_2 [140]. Apart from this, there are several other reports have been published for the NO reduction to N_2 in terms of good catalytic activity and N_2-selectivity [141, 142].

CO is prevalent in both car and stationary exhaust systems, and catalytic oxidation is one of the more efficient methods for removing CO and purify the air. There are many reports for the catalytic oxidation of CO, such as Pt SACs on CeO_2 support shows great impact on CO oxidation [143-145]. Jones et al. performed CO oxidation by taking Pt SAC supported on different active facets of CeO_2 [60]. The authors observed that polyhedral ceria and nanorods were most suitable than ceria nanocubes for Pt binding. Zhao and co-workers synthesized Au_1/CeO_2 SAC for CO oxidation and compared its activity with Au NPs in presence of H_2O [146]. It was observed that the CO oxidation intensely endorsed in case of Au SAC in presence of H_2O, and the reaction progress is slower in case of NPs. To further understand the active-site geometry dependent H_2O boosting effect and the underlying processes that distinguish

Au_1/CeO_2 SAC from CeO_2-supported Au NP catalysts, DFT calculation was performed. The Mars-van-Krevelen (MvK) mechanism governs CO oxidation on ceria-supported metal NP catalyst in general [147].

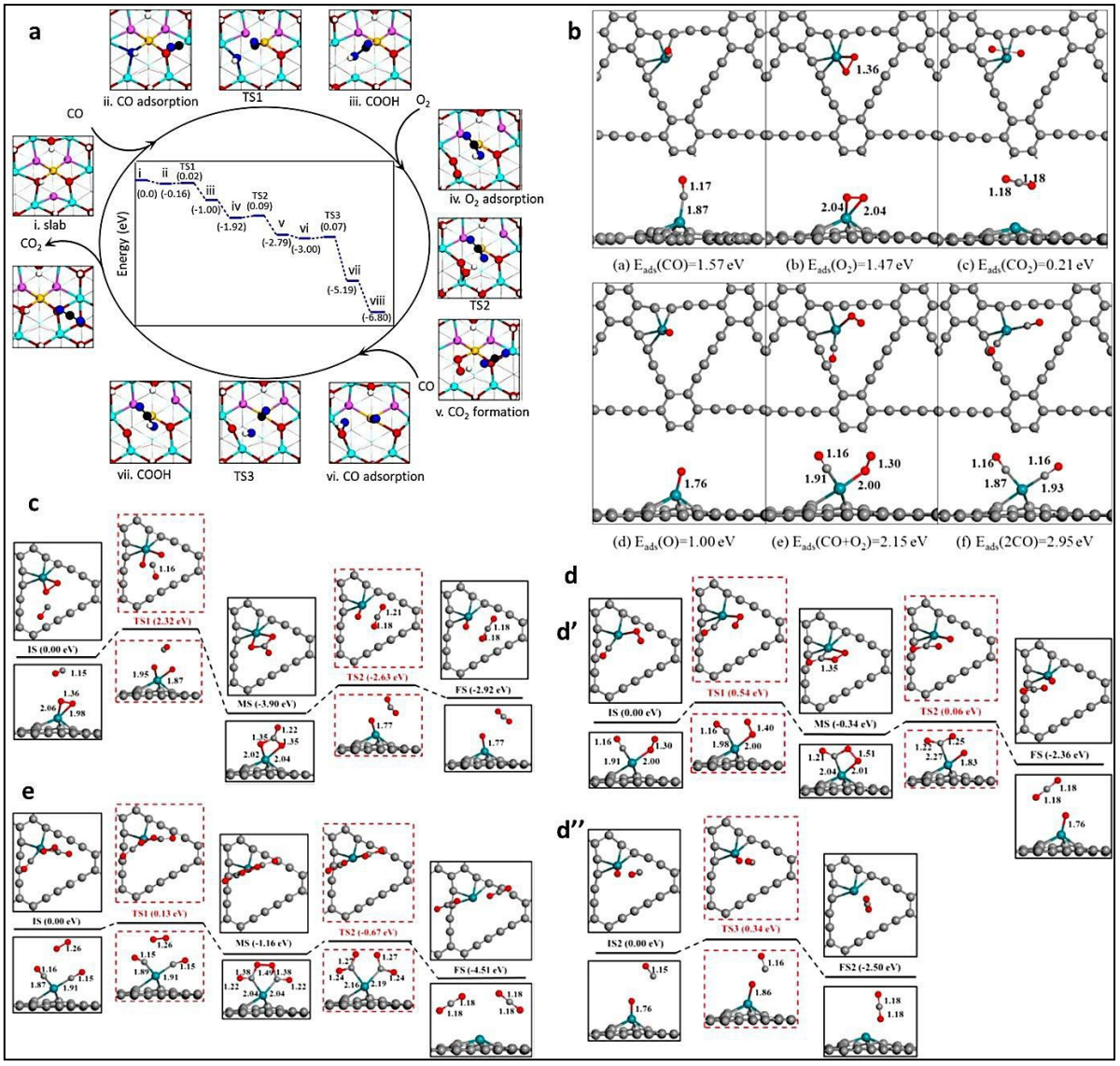

Figure. 16 (a) Mechanism for CO oxidation on the Au_1/CeO_2 (111), the inset displays the energy profile and elementary phases. Reproduced from Ref. [146] by permission of Nature communication. (b) Structural model of the configuration of all molecules adsorbed on Rh-GDY. (c) ER mechanism for CO oxidation catalyzed by Rh-GDY. (d) (d') and (d'') LH mechanism for CO oxidation in presence of Rh-GDY. (e) CO oxidation energy profile diagram of TER mechanism. All bond lengths are specified in Å. Reproduced from Ref. [148] by permission of Elsevier.

The energy profile diagram of Au_1/CeO_2 catalysed CO oxidation and detailed structure is described in Fig. 16 (a). The OH-groups on the surface over Au_1/CeO_2 might participate in the

reaction more easily and MvK was greatly suppressed by the formation of H_2O process. Xu et al. designed Rh single atom anchored on graphdiyne nanosheet (Rh-GDY) for CO oxidation in presence of O_2 [148]. The Rh atom was discovered to be stable and isolated as a single metal atom bound to the carbon atom in the GDY. The most stable configuration bound to the catalyst surface is mentioned in Fig. 16 (b). As mentioned in Fig. 16 (c, d, and e), there are general pathways followed for CO oxidation such as Eley-Rideal (ER), the Langmuir–Hinshelwood (LH) and Trimolecular Eley–Rideal (TER) mechanism. However, LH and TER paths can be more desirable because of their rate-determining stages have a low reaction barrier as shown in Fig. 16 d, and e, respectively. Additionally, based on their rection rate constants under several temperatures, LH mechanism may preferably follow over TER mechanism. There are several other examples of SAC catalysed CO oxidation observed, such as Pd–CeO_2 [149] Pt/Al_2O_3 [15], Au/FeOx [150], Pd/CeO_2 [151], Ir/Fe(OH)x [32], Ag/MnOx [152], Pt/graphene [47].

5.2 Photocatalytic application of SACs

Due to the increasing of light-harvesting, charge transfer dynamics, and surface reactions of a photocatalytic system, SACs have probably become the most active study direction in photocatalysis. A catalytically active site and a light-harvesting unit are the two main factors responsible for a conventional photocatalytic system. The metal single-atom and its support generally serve as the catalytically active site and the metal light-harvesting unit, respectively, in photocatalysis. As a result, the charge-transfer dynamics during photocatalytic reaction are directly related to the metal-support interaction, which fundamentally defines the overall activity of the photocatalytic system. The initial step in photocatalysis is light harvesting, which involves determining a photocatalytic system's ability to absorb incident photons and produce enough electron hole pairs for succeeding catalytic reactions [153]. To obtain high photocatalytic performance, charge separation and transmission of photogenerated electrons and holes at the metal semiconductor contact is critical [154, 155]. Based on this mechanism, photocatalytic reactions like H_2 production, CO_2 reduction and N_2 fixation are performed.

Until now, production of hydrogen with an affordable, efficient scheme driven by light has been a significant hurdle. Photocatalytic production of hydrogen by splitting the water has been projected to be a viable option for ensuring long-term environmental sustainability for the supply of energy [156]. The most significant challenge is to improve the photocatalytic performance even more. SACs have recently appeared as an innovative technique for

constructing efficient surface-active sites, [157] overcoming classic metal nanoparticle flaws such as limited atom usage and slow charge transfer [97]. Pt SA on a highly stable Al based porphyrinic MOF (Al-TCPP) was prepared by Fang et al. for photocatalytic H_2 production [158]. The structural diagram of Al-TCPP is shown in Fig. 17 (a) which demonstrated that $Al(OH)O_4$ chains were interlinked with the porphyrin linkers to form a 3D microporous network. Further, the Pt single atoms were fabricated into the 3D network by simple reduction shown in Fig. 17 (a). In hydrogen formation, the Al-TCPP-0.1Pt catalyst was shown excellent visible-light photocatalytic efficiency. On a per-Pt-atom basis, the achieved TOF value was 30 times that of Pt NPs (3 nm) stabilised by Al-TCPP as well as all previously reported Pt-MOF composites. The energy profile diagram of H_2 production is shown in Fig. 17 (b). In another report, Jin and workers described a simple method to activate Ni SA on carbon nitride (CN) substrate for photocatalytic H_2 production [159]. Because of its unique N/C-organizing arrangement containing of tri-s-triazine construction, which formed active reactive sites for metal atoms, CN was selected as the effective material for photocatalyst. Large CN was sequentially ultrasonicated for 3 h in $NiCl_2$ solution, then cold-dried to ensure the molecular level distribution of Ni atoms (the required material was designated as CN-xNi^{2+}, where x represents the atomic % of Ni in the solution). Afterwards, the powder was calcined in either H_2, O_2, or H_2 followed by O_2, yielding CN-xNi-H, CN-xNi-O, and CN-xNi-HO photocatalysts, respectively. Bulky CN has also been calcined in H_2 or O_2 at 350 °C as standard samples, designated as CN-O and CN-H, correspondingly. The authors discovered that the photocatalytic performance of the synthesised SAC material was increased by 30 times. The 3d orbitals of partly oxidised Ni single atom sites were discovered to be loaded with half-filled d-electrons that are prepared to be stimulated by radiation. There are several reported literatures that enables the property of the SACs towards photocatalytic H_2 production [160-163].

Recently, photocatalytic CO_2 reduction has gained a lot of interest as a way to reduce CO_2 levels in the air by completing the carbon cycle and producing lucrative solar fuels like methane, methanol, and ethanol [164, 165]. Single-atom photocatalysts have discovered to be one of the promising materials for attaining practical application in the pursuit for a viable photocatalytic system for CO_2 reduction amidst of several research. For instance, Huang et al. performed the synthesis of single Co^{2+} sites on C_3N_4 substrate by a simple deposition method and demonstrated excellent activity and product selectivity toward CO formation [166]. As the presence of the Co single-atoms could greatly enhance the charge carrier utilisation efficiency and enhance the number of reactive sites on the surface of the SAC, the photocatalytic act of

the Co^{2+}/g-C_3N_4 slowly enhanced with the Co loading up to 0.016 mol/mg. Further, the performance of the Co^{2+}/g-C_3N_4 was decreased with increasing the Co loading due to the formation of CoOx. Similarly, Jun et al. thoroughly explored the performance of Co single-atoms on the 2D layered Bi_3O_4Br in the photocatalytic CO_2 reduction activity [167]. The charge transfer, carrier separation, CO_2 adsorption, and activation are all favoured by the Co SAC in Bi_3O_4Br. It can lower the CO_2 activation energy barrier by stabilising COOH* intermediates and altering the rate-limiting step from COOH* formation to CO* desorption. The efficiency of the synthesized SACs was confirmed by performing the light-driven CO_2 reduction with a selective CO production, which was roughly 4 and 32 times greater than atomic layer Bi_3O_4Br and bulk Bi_3O_4Br, respectively. According to the report, the photocatalytic CO_2 reduction can be followed as,

$$CO_2(g) \rightarrow CO_2$$

$$H_2O \rightarrow H^+ + OH^-$$

$$CO_2 * + e^- \rightarrow CO_2^{\cdot -} *$$

$$CO_2^{\cdot -} * + H^+ \rightarrow COOH^*$$

$$COOH^* + H^+ + e^- \rightarrow CO^* + H_2O$$

$$CO^* \rightarrow CO$$

Where " $*$ " signifies the adsorption site on the catalyst surface.

To explore the catalytic performance the DFT calculation was performed by the authors and the theoretical model or structural illustration of CO formation is shown in Fig. 17 (c) and Fig. 17 (d) showed the electronic state of CO_2 reduction. Based on SAC, there are many reports published on photocatalytic CO_2 reduction [63, 168].

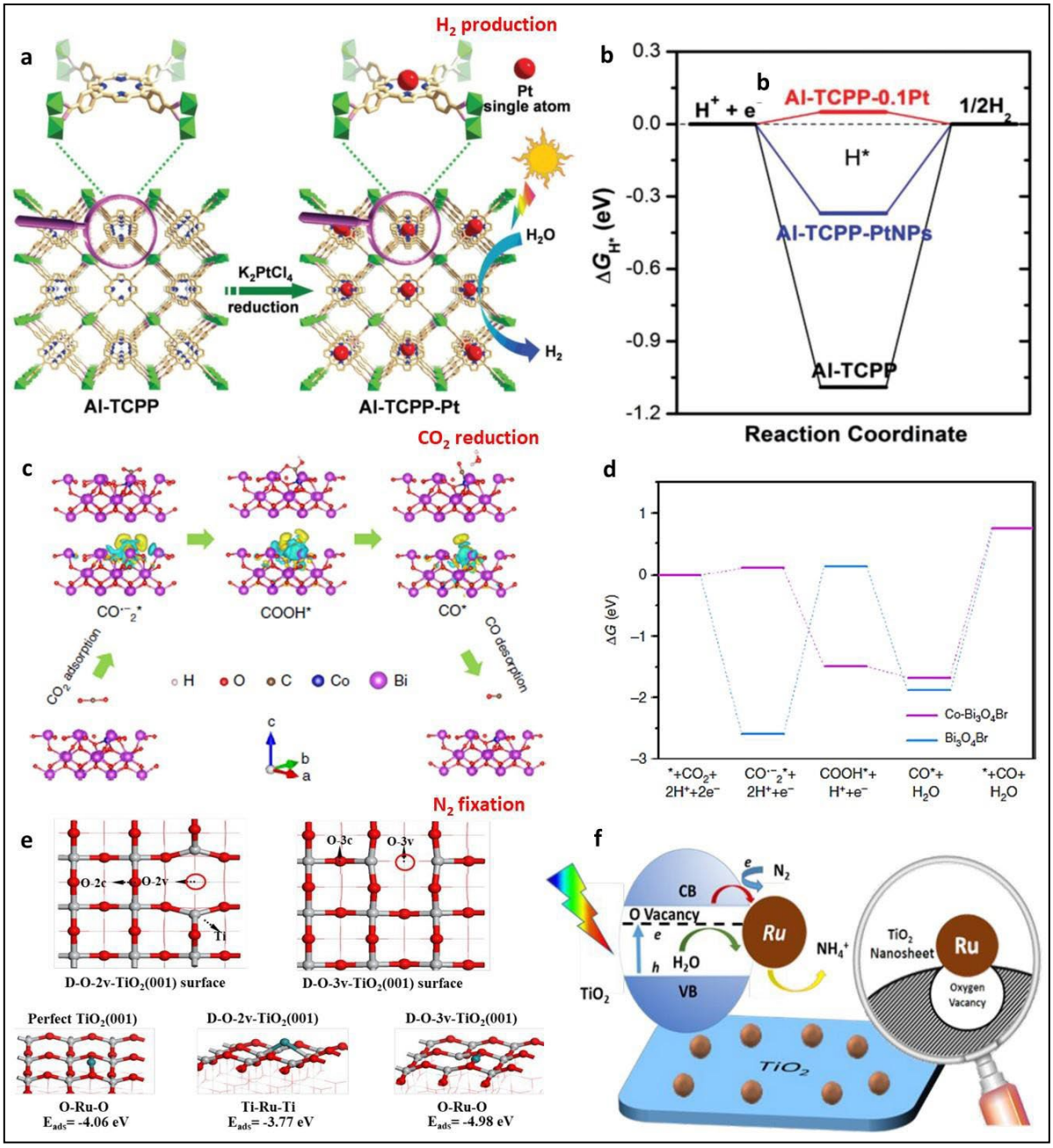

Figure 17. (a) Schematic illustration for synthesis of Al-TCPP-Pt for photocatalytic H_2 production, (b) Free energy diagram for photocatalytic H_2 production, Reproduced from Ref. [158] by permission of WILEY-VCH, (c) Theoretical study and diagram of CO_2 photoreduction mechanism on the Co–Bi_3O_4Br, (d) Free energy diagrams of CO_2 photoreduction to CO for the Bi_3O_4Br and Co–Bi_3O_4Br. Reproduced from Ref. [167] by permission of Springer Nature Communications. (e) The possible structure of the $TiO_2(001)$ surface (upper-layer) and the most stable binding states and their comparative adsorption energies of Ru atomic sites supported on the perfect, O-2v, and O-3v defective surfaces (bottom-layer), (f) Mechanism of N_2 fixation of Ru/ TiO_2 SACs. Reproduced from Ref. [169] by permission of American Chemical Society.

Production of NH_3 is an important reaction since it is one of the most essential source for living beings to sustain the life cycle. However, photocatalytic reduction of N_2 to NH_3 under normal reaction condition represents a suitable method for substituting Haber-Bosch process. Yet, the real-world application of such procedure was restricted due to low productivity and unsuitable mechanism. To address these drawbacks, SACs can be a workable solution because it not only improves the generation of charge carrier but also offers numeral surface-active sites for adsorption and activation of the N_2 molecules. Cleavage of the N-N triple bond of N_2 is widely known to be a difficult problem for photocatalytic dinitrogen fixation. As a result, the defect was always presented onto semiconductors as a dinitrogen activation point on the surface, lowering their bonding strength in order to hasten the dinitrogen reaction to form HH_3 following a typical conversion process. For example, Liu et al. described the formation of Ru SAC fabricated onto the TiO_2 nanosheets [169]. It was concluded that the Ru SAC significantly enhanced the photoreduction of N_2 to NH_3 with a high rate. Further, the DFT study was performed to confirm the stability of Ru atoms on TiO_2 substrate. All of the results are based on TiO_2(001) surface phenomena that are both perfect and imperfect. From two types of oxygen atoms (two-fold coordinated O-2c and three-fold coordinated O-3c, as indicated in Fig.17 (e), two kinds of oxygen vacancies (D-O-2v and D-O-3v) might be formed. The electron densities of D-O-3v-TiO_2(001) surface move to lower energies compared to the electron densities of Ru_{4d} and O_{2p} over flawless TiO_2 (001) surface, resulting in improved Ru-O interaction. As a result, the Ru-O link is stronger. The photoreduction mechanism of N_2 to NH_3 is shown in Fig. 17(f). Similarly, in another report Guo et al. showed that the Mo single-atoms could be used as N_2 adsorption sites on semiconductors to initiate the photocatalytic NH_3 formation [170]. Beside this, some other photocatalytic application on organic synthesis was performed by using SACs [171-173].

6 SACs for organic transformation

In this section, out of several uses, the main factors discussed are C-C bond forming reactions, C-X heteroatom bond coupling reactions, selective oxidation from alcohol to aldehyde, and selective oxidation from alkane to alcohol.

6.1 C-C bond forming reactions

The scarcity of fuel supplies and the inadequacy of eco-friendly importance not only motivate individuals to seek out innovative and clean energy sources, but they also provide a promising need to keep the source of fuel regular and consistent. In the future, bulk chemical raw materials

will be needed in order to fulfil the demands of mankind . Owing to its direct use of functionalizing materials and lengthening carbon chains, the C-C bond forming reaction stands out from other types of chemical synthesis processes, making it crucial in upgrading methane [174-177].

Figure 18. Shows two hydroformylation reaction routes, each giving a linear and branched product. Reproduced from Ref. [176] by permission of Springer Nature Communication.

With association to costly and difficult-to-separate homogeneous catalysts, SAC provides suitable contact for industrialization due to its heterogeneous catalytic mode. Tang et al. also stated that Rh_1O_5@ZSM-5 may convert methane to acetic acid [178]. Wang et al. investigated propene hydroformylation in great depth, both experimentally and conceptually [176]. The authors provide a method that can be used to improve our knowledge of both reaction and catalyst design as shown in Fig. 18. Finally, several complex organic applications like alkene metathesis [176], Sonogashira and Heck [179] and Suzuki, [180, 181] C-C coupled reactions have effectively presented into the SAC system, inspiring people to build a catalytic construction of outdated homogeneous catalysts in a heterogeneous SAC system with a depth consideration of reactions [182].

6.2 C−X Bond Coupling Reactions (X = Si, B, Cl)

The heteroatom catalysing hydrosilylation reaction is important in several ways; it can be used to make aerogels, wetting agent, release coatings, greases/oil/fats, and adhesives along with chemical synthesis. Miura et al. reported the first hydrosilylation SAC, Pd_1Au_5/Nb_2O_5, in 2017 [183]. This SAC has good reactivity and can catalyse not only selective hydrosilylation of essential alkynes, but also hydrosilylation of 1,4-unsaturated ketone. Both the catalytic phenomena exhibit an effective range of applications. Another major C-X bond coupling reaction, hydrochlorination, is critical in the production of vinyl chloride monomer, which is one of the most prevalent and in high demand chemicals. Because the Cl atom is valuable in the replacement reaction, the insertion of Cl atom in an organic fragment will also open more chances for industrialisation towards the manufacturing of intricate designed compounds. Since Cl atom can be easily replaced and beneficial for substitution reaction, which is helpful for more functionalising the catalyst at an engineer scale. Still, the previously reported, Hg- based materials are substituted with Au-based catalysts because Hg-based catalysts are less ecological, inactivation of Au-based catalysts, such as severe over-reduction, creates new challenges for the vinyl chloride sector [183]. Ye et al. reported that Au/CeO_2 SAC with self-renewal characteristics under reaction parameters in 2019 to overcome this challenge [184]. The further reduced Au atoms oxidised by Ce^{4+} from the CeO_2 support during the catalytic cycle, emphasising the utility of metal support contact. Even though this inside oxidation-reduction interaction between energetic atoms and supporter has been described in the past [185].

6.3 Selective Oxidation from Alcohol to Aldehyde

Because of its huge potential for lowering economic costs, careful oxidation of alcohol or dehydrogenation of alcohol to create an aldehyde has widely explored from years. In order to eliminate H atoms from the -OH group and carbon, a slight oxidizing agent (air, peroxides, water, and ethanol) can be used [186]. Similarly, some other reactions, for example, alcohol elimination, which provides alkene, acid produced oxidation, profound C-C bond breakage, harvesting CO and evaporative hydrocarbon. The aldol reaction, which produces ketone, consequence in low yields of required products. Because the reactions that may occur in the reaction scheme cannot be designated physically by merely altering the parameters (temperature or pressure) without the presence of catalyst [187, 188].

The initial stage in the selective oxidation of alcohol is the cleavage of the OH bond. As a result, instead of stable acidic sites, moderate acidic or sturdy basic positions on support are essential. Less alkalinity can also increase back-donation, i.e., the π* bond contact that endorses CO. bond breakage [189]. Single atom catalysis allows for more flexibility in adjusting the acidity of active positions than NP equivalents. For example, on Au/ZnZrOx, the output of the isopropanol dehydrogenation performance is effectively increased, thanks to the Au single atom's lower acidity than that of Zn and Zr [190].

6.4 Selective Oxidation from Alkane to Alcohol

It's even more difficult to prepare alcohol from an alkane. Controlled C-H cleavage appears to be so subtle as a vital phase as it is necessary to decrease the energy wall of the early C-H breakage to acquire high affinity while simultaneously enlarging the energy wall of the deep CH breakage to avoid carbon deposition [191]. Various processes of alkane to alcohol changes were mentioned previously, as opposed to dehydrogenation of alcohol [192-195]. Deng et al. discovered in the FeN_4/GN system that benzene to phenol oxidation proceeds via the E-R mechanism, in which CH activation is substituted by a proton release path of a supported particle [196]. In recent years, researchers have discovered Fe-SA/CN and Cu-SA/HCNS [197], both of which have a structure like FeN_4/GN. Advanced selectivity of ADCs associated to majority metal catalysts that ignore additional oxidation than NP matching part may be due to localised heterogeneousness of electron dispersal on the outward. Where the H atoms are distributed gradually compared to the metal surface and O_2 stimulation is slightly decreased because of the restricted intersection of d and antibonding orbitals [196].

Apart from the uses described above, there are number of other literatures based on several applications using SACs as shown in Table.2.

Table 2. Several applications by taking SACs on different suitable support.

Entry	Support	SAC	Application	Reference
1	Graphdiyne	Pt	HER	[198]
2	S-doped carbon	Fe	ORR OER Metal-air battery	[199, 200]

3	MoS_2	Co, Pt, Ni	Hydrodeoxygenation reaction HER	[201, 202]
4	FeOx	Pt, Ir	CO oxidation reaction Hydrogenation of nitroarenes Water-gas shift	[203-205]
5	MgO	Ni	CO_2 reduction	[206]
6	ZrO_2	Pd	Direct synthesis of indole	[207]
7	MoS_2	Co	Peroxidase-like reaction	[208]
8	Al_2O_3	Pt	Hydrogenation reaction CO oxidation reaction	[209]
9	MoC	Pt	Hydrogenation from water and methanol	[210]
10	ZnO	Rh	Hydroformylation of olefins	[211]
11	N-doped carbon	Sn	CO_2 reduction reaction	[212]
12	Ultrathin g-C_3N_4	Ag and carbon quantum dots	photocatalytic degradation of naproxen	[213]
13	Carbon nitride	Ag	Photocatalytic 1-hexyne hydrogenation	[214]
14	Carbon nitride	Cu	Photocatalytic hydrogen production	[215]
15	g-C_3N_4	Pt	for photocatalytic H_2 evolution or NO oxidation under visible light	[216]

16	g-C_3N_4	Ni, Pd, Pt, Cu, Ag or Au	Photocatalytic HER and OER	[217]
17	g-C_3N_4	Ag	Photocatalytic degradation of bisphenol A	[218]

7. Dual site behaviour of SACs

As it is clearly understood that SACs are designed to bridge the gap between homogeneous and heterogeneous catalysts, the main concern to discuss is the role of the mixed valency state of the single metal atoms in catalysis. Since most of the transition metals have the capacity to be stable in different oxidation states, the reaction conditions would control the electron transfer and electron accepting behaviour. Hence, the issue is to create SACs that allow metal atoms in different valence states to coordinate while limiting leaching and nanoparticle formation. However, there are very few reports published for the dual site behaviour of SACs. For instance, Bakandritsos et al. designed cyanographene (G(CN)-Cu) supported strong coordination of single metal Cu(II) ions somewhat reduced to Cu(I) due to graphene-induced charge transfer [219]. The synthesized 2D mixed-valence SAC employed for the two O_2-mediated reactions such as oxidative coupling of amines and the oxidation of benzylic C-H bonds. A schematic view of the SACs through the characterization of the mixed valency state of catalyst by different techniques is shown in in Fig. 19 (a) The low magnification HRTEM image of the G(CN)-Cu is shown in Fig. 19 (b) and high resolution HRTEM images of the before and after reaction are represented in Fig. 19 (c, d) and Fig. 19 (e, f), respectively. The elemental mapping for C and Cu are shown in Fig. 19 (g, h) and the HR-XPS analysis shown in Fig. 19 (i) achieved the reduction of ≈50% of the Cu(II) ions to Cu(I), the charge transfer phenomena of G(CN)-Cu catalyst is shown in Fig. 19 (j-l) established the stability of the metal atom on the substrate. Further, a possible organic reaction mechanism catalysed by the mixed valency SACs is shown in Fig. 19 (m). Fig. 19 (n) is the spectra drawn for radical formation during the reaction and Fig. 19 (o) represents the EPR spectrum after catalyst turnover. It was confirmed that the synergistic property of Cu(II) and Cu(I) was played a vital part in the reaction progress providing high conversions (up to 98%), selectivities (up to 99%). Through their cooperation with other functional groups of graphene is the established technique opens the door to a large portfolio of additional SACs such as Fe(III)/Fe(II) on carboxy graphene synthesized by the same group.

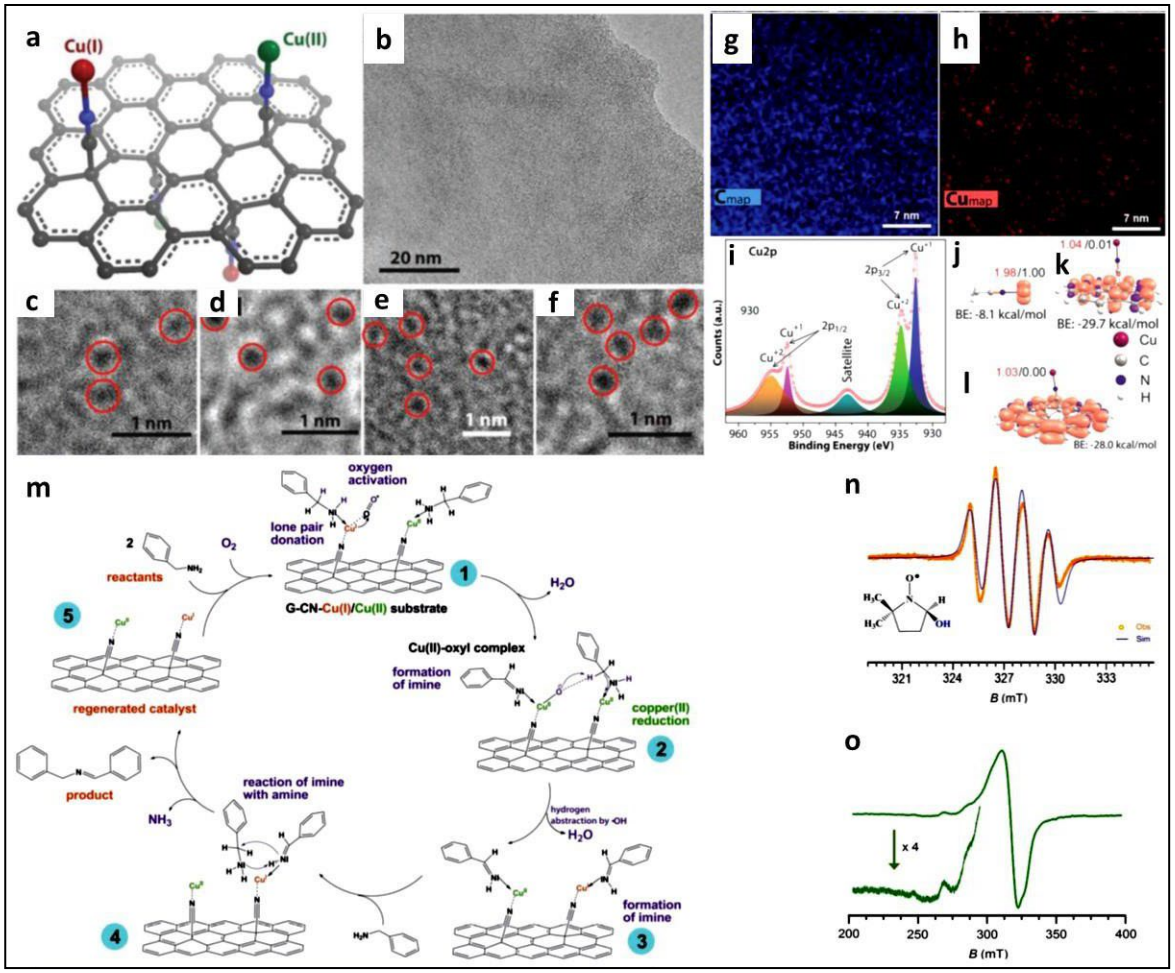

Figure 19. (a) Represents the schematic of mixed-valence copper catalyst. b) HRTEM image of graphene in G(CN)-Cu catalyst. (c–f) High resolution HRTEM images from the catalyst (c, d) before and (e, f) after reaction. (g) EDS elemental mapping of G(CN)-Cu for C and h) Cu. (i) HRXPS G(CN)-Cu catalyst. (j–l) charge transfer mechanism of G(CN)-Cu catalyst. (m) possible mechanism of organic reaction. (n) plot of the •OH radicals formed during the catalytic reaction. (o) X-band EPR spectrum of the G(CN)-Cu catalyst after turnover. Reproduced from Ref. [219] by permission of WILEY-VCH.

From this discussion, we observed that even after having higher co-ordination with substrate, less sintering and outstanding performance, the dual site study of the SACs is remained unexplored. This can lay the way for a new field of 2D coordination chemistry including covalent graphene derivatives having several functional groups such as thiols, carboxyls, or hydroxyls co-ordinating with different metal atoms (e.g., Au, Fe, Ni, Co, Pt, Mn etc.) [220, 221].

8. Bimetallic SACs

SACs that use only a single or a few metal atoms as active sites not only reduce the amount of metal atoms in the catalyst, but also display interesting activity due to their significant proportion of low-coordinated metal atoms which generally function as active sites [222]. As discussed throughout in this review, the only way to improve the atomic efficiency of supported noble metal catalysts is to downsize the usual noble metal NPs to single atoms or an alternative approach is to form bimetallic SAC by incorporating second metal atoms. The synergistic effect of the bimetallic catalyst in catalysis is widely reported, however, it is still remained unexplored that how the effect can serve in case of atomic scale NPs. Based upon this, Fu et al. synthesized a bimetallic Ir_1Mo_1/TiO_2 SAC and performed the chemoselective hydrogenation of 4-nitrostyrene (4-NS) to 4-vinylaniline (4-VA) and it is found that 100% conversion with > 96 % of selectivity [223]. The catalytic efficiency of the synthesized bimetallic SAC was compared with single atom Ir_1/TiO_2 and Mo_1/TiO_2 catalysts. It was noticed that the individual catalyst provided less activity of 38 % selectivity, and 87 % conversion for Ir_1/TiO_2 and no activity for Mo_1/TiO_2 for 4-NS reduction. The EDS mapping characterization as mentioned in Fig. 20 (a) showed that the bimetallic SAC was well distributed on the TiO_2 support and DFT study revealed that both the metal atoms played significant role in hydrogenation reaction. The Ir_1 atomic site was responsible for H_2 activation and Mo_1 site was accountable for 4-NS adsorption by the synergistic effect between the two single atoms providing better activity as compared to SACs. The reaction mechanism is shown in Fig. 20 (b) which expanded the understanding for bimetallic SACs.

Similarly, Kaiser et al. reported Au based bimetallic SACs synthesis on C- support for acetylene hydrochlorination [224]. Several salts were used as an alternative Cl-source for gold dispersion and finally reached to atomic level using H_2PtCl_6 and Fig. 20 (c) provided the structural illustration of the synthesis of Au/Pt-C bimetallic SACs. The synthesized bimetallic SACs exhibit higher stability and prevent agglomeration up to 800 K and exhibited two times increased acetylene hydrochlorination with retention in the activity. From this observation, it can be understand that the Au-Pt single atoms successfully improves the tendency for catalytic process. Feng and co-workers performed electrochemical CO_2RR by taking M@Cu(211) bimetallic SACs [225].

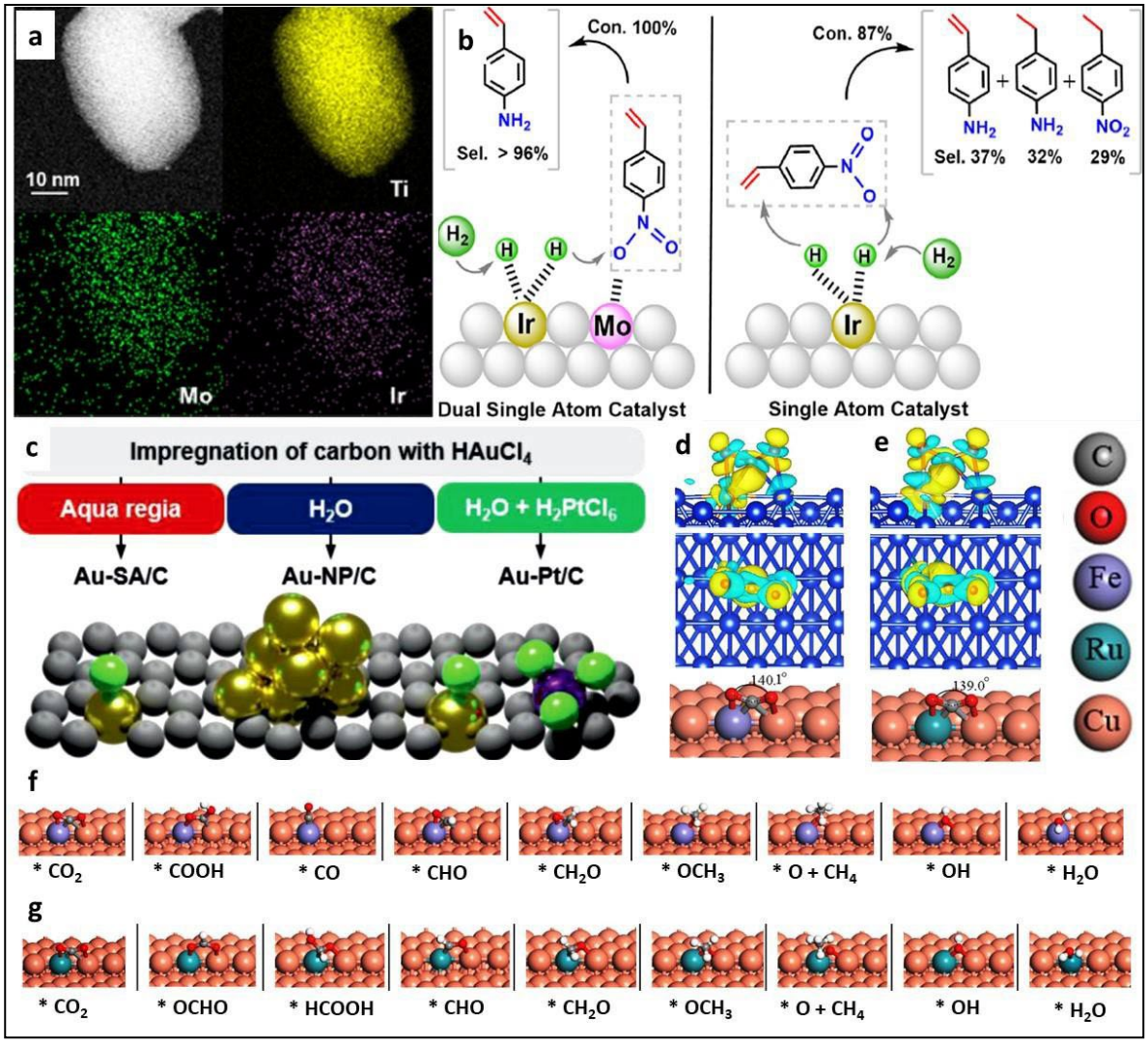

Figure 20. (a) Elemental mapping of Ir_1Mo_1/TiO_2, (b) Proposed reaction mechanism for4-NS reduction. Reproduced from Ref. [223] by permission of American Chemical Society. (c) Synthesis of Au-based SACs on carbon support. Reproduced from Ref. [224] by permission of WILEY-VCH.

Charge density difference for CO_2 adsorbed on (d) Fe@Cu(211) and (e) Ru@Cu(211) representing both side and top views where yellow indicates charge accumulation and cyan is for charge depletion. DFT study for CO_2 RR toward (f) CH_4 formation via *COOH path for Fe@Cu (211) and (g) CH_4 formation via *OCHO path on Ru@Cu (211). Reproduced from Ref. [225] by permission of American Chemical Society.

The M was replaced by eleven metal atom in place of M (Y, Fe, Co, Ni, Zn, Ru, Rh, Ag, Au, Pd, and Pt.), out of which the Ru@Cu(211) and Fe@Cu(211) were shown remarkable activity for endorsing CO_2 RR to form CH_4 due to the broken of the linked relation of the critical

intermediate formed during the reaction at the active sites. The adsorption of CO_2 and the charge accumulations are shown in Fig. 20 (d, e) for Ru@Cu(211) and Fe@Cu(211), respectively. The authors were able to identify the different mechanistic path as shown in Fig. 20 (f, g) for Ru@Cu(211) and Fe@Cu(211) bimetallic catalysts. It was observed that in both the reactions, the second and third intermediate formation was different from each other while all other phases were constant. Similarly, there are many reports established for bimetallic SACs formation for several catalytic applications. Hou et al. prepared bimetallic single-atom Pd_1Co_1/Al_2O_3 catalysts for benzene oxidation [226], and PdAu bimetallic SACs for dehydrogenation of ethanol was achieved[227]. Ag alloyed Pd SACs for hydrogenation reaction was performed [228]. From the above study on bimetallic SACs production, it can be stated that even though alloying of two metal enhances the yield and selectivity, but still it has significant challenge in metal quantity optimization. In another way the formation of bimetallic SACs without alloying one metal remains as a key concern.

9. Summary and challenges

This discipline has progressed at a breakneck pace since the concept of "single-atom catalysis" was initially proposed. An efficient, improved, and developed material is crucial for sustainable and versatile catalytic applications. Likewise, to synthesize the raw chemicals in industrial scale and for a non-hazardous photocatalytic process, there is a subsequent demand for suitable catalyst. SACs have proven to be the appropriate catalysts exhibiting extreme atom use efficacy, high reactivity, and selectivity due to the availability of low co-ordination states, single site effect, and suitable metal-support interaction. This review offers a complete summary of SACs based on variety of metal-support interactions. The study includes the synthesis of SACs using several suitable synthesis protocols as well as large scale production techniques followed by typical catalytic examples. A brief explanation about the stability of SACs accompanied by variety of electrocatalytic, photocatalytic and organic transformation applications are explained. For advancing the SACs research, role of mixed valency state of SACs are brought into notice and also the current review suggests the performance of bimetallic SACs towards catalysis so far. However, the overall study found some challenges that still needs further attention. These are stated as follows.

I. Advance synthesis of SACs: There is no uncertainty that novel manufacturing approaches will be vital to passage the utility of SACs from synthetic to real-world applications. But when it comes to manufacture more energetic and durable catalysts, the goal is to upsurge

the number of active positions while improving their reactivity. To address this issue, different active site development will be more efficient for creating asymmetric structural SACs. In another way, even though there are several synthesis approaches are considered for the large-scale production of SACs, those strategies are mainly performed using carbon-based porous substrates whereas other substrate like silica, alumina, and some biological support such as cellulose, chitosan etc. are not explored for large scale SACs production. Hence, an advance SACs synthesis method will be sufficient to tackle these challenges.

II. An economical SACs is required: Exhaust gases, volatile organic compounds, and ground-level ozone are key pollutants that have a significant impact on human health and the environment. It was observed that mainly expensive metals like Pt, Pd, and Rh, Ru etc. are commonly used, however, low-cost metal SACs have not been explored much. SACs could also be used in air filtration technologies to eliminate air pollutants in homes or businesses; a tower or air clean-up unit could be developed utilizing such economical catalysts.

III. SACs for electrochemical organic reactions: It is worth noting that SACs have been thoroughly investigated for electrocatalytic HER, OER, ORR, CO_2, CO, NO, N_2 reduction, CO oxidation etc. However, the usage of SACs for electrochemical organic reactions, on the other hand, has yet to be investigated.

IV. Versatile and multi-functional SACs is required: Because transition metals have multiple oxidation states, SACs with mixed valency states can function differently for catalytic applications and they can also demonstrate greater stability. The mixed valency state of SACs has demonstrated exceptional catalytic activity for O_2 mediated reactions, as previously stated. Despite the fact that this emphasises the importance of SACs dual site behaviour, there has been very little research on these topics. Hence, an versatile and multipurpose SACs formation needs to be explored thoroughly.

V. Exploring bimetallic SACs: Most importantly, instead of synthesizing only monometallic SACs, bimetallic SACs may act efficiently as well as in the favour of economy. The stability and synergistic effect may provide an alternate result in the field of catalysis. Our insightful study on bimetallic SAC conveyed that, in case of bimetallic SACs, metal content optimisation is not thoroughly performed. Hence, during the synthesis of SACs, it is more accurate to tune the metal compositions based on their physical and chemical phenomenon. However, why are just alloy morphologies formed? Why aren't other shapes formed? By advancing the bimetallic SACs themes, this field of research needs to be explored systematically. We believe that by combining unique synthetic methodologies, advanced characterisation tools, and theoretical modelling, it will be able to gain a better

understanding of SACs and realise aim of tweaking and creating catalysts on a single atomic scale.

Declaration of competing interest

The authors declare no competing financial interest.

ACKNOWLEDGMENTS

S.S. and A.K.S. are grateful to SERB, New Delhi, India, for funding to conduct the research (CRG/2018/003533) and Karnataka Science and Technology Promotion Society (KSTePS/VGST-RGS-F/2018-19/GRD No.831/315). The authors are thankful to Nano Mission (SR/NM/NS-20/2014) for the FESEM facility at Jain University, Bangalore, India.

References

[1] R.J. Farrauto, L. Dorazio, C.H. Bartholomew, Introduction to catalysis and industrial catalytic processes, John Wiley & Sons, 2016.

[2] J. Hagen, Industrial catalysis: a practical approach, John Wiley & Sons, 2015.

[3] C.M. Friend, B.J. Xu, Acc. Chem. Res. 50 (2017) 517-521, https://doi.org/10.1021/acs.accounts.6b00510.

[4] S. Swain, P. Bhol, M. Bhavya, S. Yadav, A. Altaee, M. Saxena, P.K. Misra, A.K. Samal, (2021) 135-168, https://doi.org/10.1002/9781119809036.ch5..

[5] M. Valden, X. Lai, D.W. Goodman, Science. 281 (1998) 1647-1650, https://doi.org/10.1126/science.281.5383.1647.

[6] X.-F. Yang, A. Wang, B. Qiao, J. Li, J. Liu, Zhang, Acc. Chem. Res. 46 (2013) 1740-1748, https://doi.org/10.1021/ar300361m.

[7] C. Zhang, J. Sha, H. Fei, M. Liu, S. Yazdi, J. Zhang, Q. Zhong, X. Zou, N. Zhao, H. Yu, ACS Nano. 11 (2017) 6930-6941, https://doi.org/10.1021/acsnano.7b02148.

[8] T. Maschmeyer, F. Rey, G. Sankar, J.M.J.N. Thomas, Nature. 378 (1995) 159-162, https://doi.org/10.1038/378159a0.

[9] D.V. Yandulov, R.R. Schrock, Science. 301 (2003) 76-78, https://doi.org/10.1126/science.1085326.

[10] Q. Fu, H. Saltsburg, M.J.S. Flytzani-Stephanopoulos, Science. 301 (2003) 935-938, https://doi.org/10.1126/science.1085721 .

[11] X. Zhang, H. Shi, B. Xu, Angew. Chem. Int. Ed. 117 (2005) 7294-7297, https://doi.org/10.1002/ange.200502101.

[12] B. Qiao, A. Wang, X. Yang, L.F. Allard, Z. Jiang, Y. Cui, J. Liu, J. Li, T. Zhang, Nat. Chem. 3 (2011) 634-641, https://doi.org/10.1038/nchem.1095.

[13] B. Qiao, J. Lin, A. Wang, Y. Chen, T. Zhang, J. Liu, Chinese J. Catal. 36 (2015) 1505-1511, https://doi.org/10.1016/S1872-2067(15)60889-0.

[14] B. Qiao, J. Liu, Y. Wang, Q. Lin, X. Liu, A. Wang, J. Li, T. Zhang, J. Liu, A.J.X.L. Catal, A. Wang, C.-Q. Xu, J. Li, T. Zhang, JJ Liu, Nano Res. 8 (2015) 2913-2924, https://doi.org/10.1007/s12274-015-0796-9.

[15] M. Moses-DeBusk, M. Yoon, L.F. Allard, D.R. Mullins, Z. Wu, X. Yang, G. Veith, G.M. Stocks, C.K. Narula, J. Am. Chem. Soc. 135 (2013) 12634-12645, https://doi.org/10.1021/ja401847c.

[16] X. Sun, J. Lin, Y. Zhou, L. Li, Y. Su, X. Wang, T.J.A.J. Zhang, AlChE Journal. 63 (2017) 4022-4031, https://doi.org/10.1002/aic.15759.

[17] S. Yang, J. Kim, Y.J. Tak, A. Soon, H. Lee, Angew. Chem. Int. Ed. 55 (2016) 2058-2062, https://doi.org/10.1002/anie.201509241.

[18] P. Liu, Y. Zhao, R. Qin, S. Mo, G. Chen, L. Gu, D.M. Chevrier, P. Zhang, Q. Guo, D. Zang, 352 (2016) 797-800, https://doi.org/10.1126/science.aaf5251.

[19] W. Liu, L. Zhang, W. Yan, X. Liu, X. Yang, S. Miao, W. Wang, A. Wang, T. Zhang, Chem. Sci. 7 (2016) 5758-5764, https://doi.org/10.1039/C6SC02105K.

[20] J. Li, S. Chen, N. Yang, M. Deng, S. Ibraheem, J. Deng, J. Li, L. Li, Z. Wei, Angew. Chem. Int. Ed. 58 (2019) 7035-7039, https://doi.org/10.1002/anie.201902109.

[21] M. Babucci, F.E. Sarac Oztuna, L.M. Debefve, A. Boubnov, S.R. Bare, B.C. Gates, U. Unal, A. Uzun, ACS Catal. 9 (2019) 9905-9913, https://doi.org/10.1021/acscatal.9b02231.

[22] Y. Cheng, S. Zhao, B. Johannessen, J.P. Veder, M. Saunders, M.R. Rowles, M. Cheng, C. Liu, M.F. Chisholm, R. De Marco, Adv. Mater. 30 (2018) 1706287, https://doi.org/10.1002/adma.201706287.

[23] B. Singh, M.B. Gawande, A.D. Kute, R.S. Varma, P. Fornasiero, P. McNeice, R.V. Jagadeesh, M. Beller, R. Zboril, Chem. Rev. 121 (2021) 13620-13697, https://doi.org/10.1021/acs.chemrev.1c00158.

[24] Z.-X. Wei, Y.-T. Zhu, J.-Y. Liu, Z.-C. Zhang, W.-P. Hu, H. Xu, Y.-Z. Feng, J.-M.Ma, Rare Metals. 40 (2021) 767-789, https://doi.org/10.1007/s12598-020-01592-1.

[25] B. Singh, V. Sharma, R.P. Gaikwad, P. Fornasiero, R. Zboril, M.B. Gawande, Small. 17 (2021) 2006473, https://doi.org/10.1002/smll.202006473.

[26] M.B. Gawande, P. Fornasiero, R. Zbořil, ACS Catal. 10 (2020) 2231-2259, https://doi.org/10.1021/acscatal.9b04217.

[27] A. Wang, J. Li, T.. Zhang, Nat. Rev. Chem. 2 (2018) 65-81, https://doi.org/10.1038/s41570-018-0010-1.

[28] E.C.H. Sykes, P. Christopher, J. Li, J. Chem. Phys. 155 (2021) 210401, https://doi.org/10.1063/5.0073628.

[29] S. Abbet, A. Sanchez, U. Heiz, W.-D. Schneider, A.M. Ferrari, G. Pacchioni, N. Rösch, J. Am. Chem. Soc. 122 (2000) 3453-3457, https://doi.org/10.1021/ja9922476.

[30] H. Wei, X. Liu, A. Wang, L. Zhang, B. Qiao, X. Yang, Y. Huang, S. Miao, J. Liu, T. Zhang, Nat. Commun. 5 (2014) 1-8, https://doi.org/10.1038/ncomms6634.

[31] L. Lin, W. Zhou, R. Gao, S. Yao, X. Zhang, W. Xu, S. Zheng, Z. Jiang, Q. Yu, Y.-W. Li, Nature. 544 (2017) 80-83, https://doi.org/10.1038/nature21672.

[32] J. Lin, B. Qiao, J. Liu, Y. Huang, A. Wang, L. Li, W. Zhang, L.F. Allard, X. Wang, T. Zhang, Angew. Chem. Int. Ed. 124 (2012) 2974-2978, https://doi.org/10.1002/ange.201106702.

[33] J.H. Kwak, L. Kovarik, J. Szanyi, ACS Catal. 3 (2013) 2449-2455, https://doi.org/10.1021/cs400381f.

[34] Q. Fu, Y. Meng, Z. Fang, Q. Hu, L. Xu, W. Gao, X. Huang, Q. Xue, Y.-P. Sun, F. Lu, ACS Appl. Mater. Interfaces. 9 (2017) 2469-2476, https://doi.org/10.1021/acsami.6b13570.

[35] I. Mustieles Marin, J.M. Asensio, B. Chaudret, ACS Nano. 15 (2021) 3550-3556, https://doi.org/10.1021/acsnano.0c09744.

[36] G. Gao, Y. Jiao, E.R. Waclawik, A. Du, J. Am. Chem. Soc. 138 (2016) 6292-6297, https://doi.org/10.1021/jacs.6b02692.

[37] X. Li, W. Bi, L. Zhang, S. Tao, W. Chu, Q. Zhang, Y. Luo, C. Wu, Y. Xie, Adv. Mat. 28 (2016) 2427-2431, https://doi.org/10.1002/adma.201505281.

[38] Z. Chen, L. Chen, C. Yang, Q. Jiang, J. Mater. Chem. A. 7 (2019) 3492-3515, https://doi.org/10.1039/C8TA11416A.

[39] J.A. Schwarz, C. Contescu, A. Contescu, Chem. Rev. 95 (1995) 477-510, https://doi.org/10.1021/cr00035a002.

[40] C.H. Choi, M. Kim, H.C. Kwon, S.J. Cho, S. Yun, H.-T. Kim, K.J. Mayrhofer, H. Kim, M. Choi, Nat. Commun. 7 (2016) 1-9, https://doi.org/10.1038/ncomms10922.

[41] L. Zhang, A. Wang, J.T. Miller, X. Liu, X. Yang, W. Wang, L. Li, Y. Huang, C.-Y. Mou, T. Zhang, ACS Catal. 4 (2014) 1546-1553, https://doi.org/10.1021/cs500071c.

[42] G. Kyriakou, M.B. Boucher, A.D. Jewell, E.A. Lewis, T.J. Lawton, A.E. Baber, H.L. Tierney, M. Flytzani-Stephanopoulos, E.C.H. Sykes, Science. 335 (2012) 1209-1212, https://doi.org/10.1126/science.1215864.

[43] W.E. Kaden, T. Wu, W.A. Kunkel, S. Anderson, Science. 326 (2009) 826-829, https://doi.org/10.1126/science.1180297.

[44] S. George, Chem. Rev. 110 (2010) 111-131, https://doi.org/10.1021/cr900056b.

[45] J. Liu, X. Sun, Nanotechnology. 26 (2014) 024001, https://doi.org/10.1088/0957-4484/26/2/024001.

[46] N. Cheng, Y. Shao, J. Liu, X. Sun, Nano Energy. 29 (2016) 220-242, https://doi.org/10.1016/j.nanoen.2016.01.016.

[47] S. Sun, G. Zhang, N. Gauquelin, N. Chen, J. Zhou, S. Yang, W. Chen, X. Meng, D. Geng, M. Banis, Sci. Rep. 3 (2013) 1-9, https://doi.org/10.1038/srep01775.

[48] L. Jiao, H.-L. Jiang, Chem. 5 (2019) 786-804, https://doi.org/10.1016/j.chempr.2018.12.011.

[49] X. Zhang, A. Chen, M. Zhong, Z. Zhang, X. Zhang, Z. Zhou, X.-H. Bu, Electrochemical Energy Reviews. 2 (2019) 29-104, https://doi.org/10.1007/s41918-018-0024-x.

[50] A.M. Abdel-Mageed, B. Rungtaweevoranit, M. Parlinska-Wojtan, X. Pei, O.M. Yaghi, R.J. Behm, J. Am. Chem. Soc. 141 (2019) 5201-5210, https://doi.org/10.1021/jacs.8b11386.

[51] Y. Shi, C. Zhao, H. Wei, J. Guo, S. Liang, A. Wang, T. Zhang, J. Liu, T. Ma, Adv. Mater. 26 (2014) 8147-8153, https://doi.org/10.1002/adma.201402978.

[52] J. Lin, A. Wang, B. Qiao, X. Liu, X. Yang, X. Wang, J. Liang, J. Li, J. Liu, T. Zhang, J. Am. Chem. Soc. 135 (2013) 15314-15317, https://doi.org/10.1021/ja408574m.

[53] J.-X. Liang, J. Lin, X.-F. Yang, A.-Q. Wang, B.-T. Qiao, J. Liu, T. Zhang, J. Li, J. Phys. Chem. C. 118 (2014) 21945-21951, https://doi.org/10.1021/jp503769d.

[54] J. Lin, B. Qiao, N. Li, L. Li, X. Sun, J. Liu, X. Wang, T. Zhang, Chem. Commun. 51 (2015) 7911-7914, https://doi.org/10.1039/C5CC00714C.

[55] U. Heiz, A. Sanchez, S. Abbet, W.-D. Schneider, J. Am. Chem. Soc. 121 (1999) 3214-3217, https://doi.org/10.1021/ja983616l.

[56] Z.-Y. Li, Z. Yuan, X.-N. Li, Y.-X. Zhao, S.-G. He, J. Am. Chem. Soc. 136 (2014) 14307-14313, https://doi.org/10.1021/ja508547z.

[57] L. Jiao, J.Regalbuto, J. Catal. 260 (2008) 329-341, https://doi.org/10.1016/j.jcat.2008.09.022.

[58] M. Hegde, G. Madras, K. Patil, Acc. Chem. Res. 42 (2009) 704-712, https://doi.org/10.1021/ar800209s.

[59] L. Fan, P.F. Liu, X. Yan, L. Gu, Z.Z. Yang, H.G. Yang, S. Qiu, X. Yao, Nat. Commun. 7 (2016) 1-7, https://doi.org/10.1038/ncomms10667.

[60] J. Jones, H. Xiong, A.T. DeLaRiva, E.J. Peterson, H. Pham, S.R. Challa, G. Qi, S. Oh, M.H. Wiebenga, X. Pereira Hernández, Science. 353 (2016) 150-154, https://doi.org/10.1126/science.aaf8800.

[61] J. Wang, Z. Huang, W. Liu, C. Chang, H. Tang, Z. Li, W. Chen, C. Jia, T. Yao, S. Wei, J. Am. Chem. Soc. 139 (2017) 17281-17284, https://doi.org/10.1021/jacs.7b10385.

[62] J. Li, M. Chen, D.A. Cullen, S. Hwang, M. Wang, B. Li, K. Liu, S. Karakalos, M. Lucero, H. Zhang, Nat. Catal. 1 (2018) 935-945, https://doi.org/10.1038/s41929-018-0164- 8.

[63] H. Zhang, J. Wei, J. Dong, G. Liu, L. Shi, P. An, G. Zhao, J. Kong, X. Wang, X. Meng, Angew. Chem. Int. Ed. 128 (2016) 14522-14526, https://doi.org/10.1002/ange.201608597.

[64] X. Zhang, J. Guo, P. Guan, C. Liu, H. Huang, F. Xue, X. Dong, S.J. Pennycook, M. Chisholm, Nat. Commun. 4 (2013) 1-7, https://doi.org/10.1038/ncomms2929.

[65] H. Li, L. Wang, Y. Dai, Z. Pu, Z. Lao, Y. Chen, M. Wang, X. Zheng, J. Zhu, W. Zhang, Nat. Nanotechnol. 13 (2018) 411-417, https://doi.org/10.1038/s41565-018-0089-z.

[66] C. Zhao, X. Dai, T. Yao, W. Chen, X. Wang, J. Wang, J. Yang, S. Wei, Y. Wu, Y. Li, J. Am. Chem. Soc. 139 (2017) 8078-8081, https://doi.org/10.1021/jacs.7b02736.

[67] P. Bera, K. Patil, M. Hegde, Phys. Chem. Chem. Phys. 2 (2000) 373-378, https://doi.org/10.1039/A907067B.

[68] M. Melchionna, P. Fornasiero, Chem. 5 (2019) 1927-1928, https://doi.org/10.1016/j.chempr.2019.07.005.

[69] S. Ji, Y. Chen, X. Wang, Z. Zhang, D. Wang, Y. Li, Chem. Rev. 120 (2020) 11900- 11955, https://doi.org/10.1021/acs.chemrev.9b00818.

[70] X.-F. Yang, A. Wang, B. Qiao, J. Li, J. Liu, T. Zhang, Acc. Chem. Res. 46 (2013) 1740-1748, https://doi.org/10.1021/ar300361m.

[71] K. Wang, X. Wang, X. Liang, ChemCatChem. 13 (2021) 28-58, https://doi.org/10.1002/cctc.202001255.

[72] L. Han, X. Liu, J. Chen, R. Lin, H. Liu, F. Lü, S. Bak, Z. Liang, S. Zhao, E. Stavitski, Angew. Chem. Int. Ed. 58 (2019) 2525-2525, https://doi.org/10.1002/anie.201900203.

[73] F. Li, G.-F. Han, H.-J. Noh, S.-J. Kim, Y. Lu, H.Y. Jeong, Z. Fu, J.-B. Baek, Energy Environ. Sci. 11 (2018) 2263-2269, https://doi.org/10.1039/C8EE01169A.

[74] S. Zhao, Y. Cheng, J.-P. Veder, B. Johannessen, M. Saunders, L. Zhang, C. Liu, M.F. Chisholm, R. De Marco, J. Liu, ACS Appl. Energy Mater. 1 (2018) 5286-5297, https://doi.org/10.1021/acsaem.8b00903.

[75] C. Yan, H. Li, Y. Ye, H. Wu, F. Cai, R. Si, J. Xiao, S. Miao, S. Xie, F. Yang, Y. Li, G. Wang, X. Bao, Energy Environ. Sci. 11 (2018) 1204-1210, https://doi.org/10.1039/C8EE00133B.

[76] J. Wu, H. Zhou, Q. Li, M. Chen, J. Wan, N. Zhang, L. Xiong, S. Li, B.Y. Xia, G. Feng, M. Liu, L. Huang, Adv. Energy Mater. 9 (2019) 1900149, https://doi.org/10.1002/aenm.201900149.

[77] L. Wang, M.-X. Chen, Q.-Q. Yan, S.-L. Xu, S.-Q. Chu, P. Chen, Y. Lin, H.-W. Liang, Sci. Adv. 5 (2019) eaax6322, https://doi.org/10.1126/sciadv.aax6322.

[78] C. Gao, S. Chen, Y. Wang, J. Wang, X. Zheng, J. Zhu, L. Song, W. Zhang, Y.. Xiong, Adv. Mater. 30 (2018) 1704624, https://doi.org/10.1002/adma.201704624.

[79] J. Kim, C.W. Roh, S.K. Sahoo, S. Yang, J. Bae, J.W. Han, H. Lee, Adv. Energy Mater. 8 (2018) 1701476, https://doi.org/10.1002/aenm.201701476.

[80] S.F.J. Hackett, R.M. Brydson, M.H. Gass, I. Harvey, A.D. Newman, K. Wilson, A.F. Lee, Angew. Chem. Int. Ed. 119 (2007) 8747-8750, https://doi.org/10.1002/ange.200702534.

[81] K.T. Rim, D. Eom, L. Liu, E. Stolyarova, J.M. Raitano, S.-W. Chan, M. Flytzani-Stephanopoulos, G. Flynn, J. Phys. Chem. C. 113 (2009) 10198-10205, https://doi.org/10.1021/jp8112599.

[82] S. Wang, A.Y. Borisevich, S.N. Rashkeev, M.V. Glazoff, K. Sohlberg, S.J. Pennycook, S. Pantelides, Nat. Mater. 3 (2004) 143-146, https://doi.org/10.1038/nmat1077.

[83] J.H. Kwak, J. Hu, D. Mei, C.-W. Yi, D.H. Kim, C.H. Peden, L.F. Allard, J. Szanyi, Science. 325 (2009) 1670-1673, https://doi.org/10.1126/science.1176745.

[84] Z. Huang, X. Gu, Q. Cao, P. Hu, J. Hao, J. Li, X. Tang, Angew. Chem. Int. Ed. 124 (2012) 4274-4279, https://doi.org/10.1002/ange.201109065.

[85] H. Zhang, T. Watanabe, M. Okumura, M. Haruta, N. Toshima, Nat. Mater. 11 (2012) 49-52, https://doi.org/10.1038/nmat3143.

[86] Z. Hu, H. Metiu, J. Phys. Chem. C. 115 (2011) 17898-17909, https://doi.org/10.1021/jp205432r.

[87] W. Song, A.P. Jansen, E.J.M. Hensen, Faraday Discuss. 162 (2013) 281-292, https://doi.org/10.1039/C3FD20129E .

[88] A. Bruix, Y. Lykhach, I. Matolínová, A. Neitzel, T. Skála, N. Tsud, M. Vorokhta, V. Stetsovych, K. Ševčíková, J. Mysliveček, 53 (2014) 10525-10530.

[89] A. Neitzel, A. Figueroba, Y. Lykhach, T. Skala, M. Vorokhta, N. Tsud, S. Mehl, K. Sevcikova, K.C. Prince, K.M. Neyman, Angew. Chem. Int. Ed. 120 (2016) 9852-9862, https://doi.org/10.1002/anie.201402342 .

[90] Z. Zhang, Y. Zhu, H. Asakura, B. Zhang, J. Zhang, M. Zhou, Y. Han, T. Tanaka, A. Wang, T. Zhang, Nat. Commun. 8 (2017) 1-10, https://doi.org/10.1038/ncomms16100.

[91] E.J. Peterson, A.T. DeLaRiva, S. Lin, R.S. Johnson, H. Guo, J.T. Miller, J. Hun Kwak, C.H. Peden, B. Kiefer, L. Allard, Nat. Commun. 5 (2014) 1-11, https://doi.org/10.1038/ncomms5885.

[92] D.A. Bulushev, M. Zacharska, A.S. Lisitsyn, O.Y. Podyacheva, F.S. Hage, Q.M. Ramasse, U. Bangert, L. Bulusheva, ACS Catal. 6 (2016) 3442-3451, https://doi.org/10.1021/acscatal.6b00476.

[93] H. Jing, P. Zhu, X. Zheng, Z. Zhang, D. Wang, Y. Li, Advanced Powder Materials. (2021), https://doi.org/10.1016/j.apmate.2021.10.004.

[94] S. Zhang, Z.-Q. Huang, Y. Ma, W. Gao, J. Li, F. Cao, L. Li, C.-R. Chang, Y. Qu, Nat. Commun. 8 (2017) 1-11, https://doi.org/10.1038/ncomms15266.

[95] Y. Chen, S. Ji, C. Chen, Q. Peng, D. Wang, Y. Li, Joule. 2 (2018) 1242-1264, https://doi.org/10.1016/j.joule.2018.06.019.

[96] R. Subbaraman, D. Tripkovic, D. Strmcnik, K.-C. Chang, M. Uchimura, A.P. Paulikas, V. Stamenkovic, N. Markovic, Science. 334 (2011) 1256-1260, https://doi.org/10.1126/science.1211934.

[97] H. Yin, S. Zhao, K. Zhao, A. Muqsit, H. Tang, L. Chang, H. Zhao, Y. Gao, Z. Tang, Nat. Commun. 6 (2015) 1-8, https://doi.org/10.1038/ncomms7430.

[98] S. Chen, J. Duan, Y. Tang, B. Jin, S. Qiao, Nano Energy. 11 (2015) 11-18, https://doi.org/10.1016/j.nanoen.2014.09.022.

[99] J. Duan, S. Chen, M. Jaroniec, S. Qiao, 5 (2015) 5207-5234, https://doi.org/10.1021/acscatal.5b00991.

[100] I.E.L Stephens, I.B Chorkendorff, Angew. Chem. Int. Ed. 50 (2011) 1476-1477, https://doi.org/10.1002/anie.201005921.

[101] X. Li, X. Yang, Y. Huang, T. Zhang, B. Liu, Adv. Mater. 31 (2019) 1902031, https://doi.org/10.1002/adma.201902031.

[102] N. Cheng, S. Stambula, D. Wang, M.N. Banis, J. Liu, A. Riese, B. Xiao, R. Li, T.-K. Sham, L.-M. Liu, Nat. Commun. 7 (2016) 1-9, https://doi.org/10.1038/ncomms13638.

[103] H.J. Qiu, Y. Ito, W. Cong, Y. Tan, P. Liu, A. Hirata, T. Fujita, Z. Tang, M. Chen, Angew. Chem. Int. Ed. 54 (2015) 14031-14035, https://doi.org/10.1002/anie.201507381.

[104] B. You, Y. Sun, ChemPlusChem. 81 (2016) 1045-1055, https://doi.org/10.1002/cplu.201600029.

[105] J. Kibsgaard, Z. Chen, B.N. Reinecke, T. Jaramillo, Nat. Mater. 11 (2012) 963-969, https://doi.org/10.1038/nmat3439.

[106] J.K. Nørskov, T. Bligaard, A. Logadottir, J. Kitchin, J.G. Chen, S. Pandelov, U. Stimming, J. Electrochem. Soc. 152 (2005) J23, https://doi.org/10.1149/1.1856988.

[107] Q. Wang, Z.L. Zhao, S. Dong, D. He, M.J. Lawrence, S. Han, C. Cai, S. Xiang, P. Rodriguez, B. Xiang, Nano Energy. 53 (2018) 458-467, https://doi.org/10.1016/j.nanoen.2018.09.003.

[108] L. Liang, H. Cheng, F. Lei, J. Han, S. Gao, C. Wang, Y. Sun, S. Qamar, S. Wei, Y. Xie, Angew. Chem. Int. Ed. 127 (2015) 12172-12176, https://doi.org/10.1002/ange.201505245.

[109] X. Li, P. Cui, W. Zhong, J. Li, X. Wang, Z. Wang, J. Jiang, Chem. Commun. 52 (2016) 13233-13236, https://doi.org/10.1039/C6CC07049C.

[110] C.A. Kent, J.J. Concepcion, C.J. Dares, D.A. Torelli, A.J. Rieth, A.S. Miller, P.G. Hoertz, T. Meyer, J. Am. Chem. Soc. 135 (2013) 8432-8435, https://doi.org/10.1021/ja400616a.

[111] H. Fei, J. Dong, Y. Feng, C.S. Allen, C. Wan, B. Volosskiy, M. Li, Z. Zhao, Y. Wang, H. Sun, Nat. Catal. 1 (2018) 63-72, https://doi.org/10.1038/s41929-017-0008-y.

[112] S.H. Talib, Z. Lu, X. Yu, K. Ahmad, B. Bashir, Z. Yang, J. Li, ACS Catal. 11 (2021) 8929-8941, https://doi.org/10.1021/acscatal.1c01294.

[113] M. Gao, W. Sheng, Z. Zhuang, Q. Fang, S. Gu, J. Jiang, Y. Yan, J. Am. Chem. Soc. 136 (2014) 7077-7084, https://doi.org/10.1021/ja502128j.

[114] J. Liu, M. Jiao, L. Lu, H.M. Barkholtz, Y. Li, Y. Wang, L. Jiang, Z. Wu, D.-j. Liu, L. Zhuang, Nat. Commun. 8 (2017) 1-10, https://doi.org/10.1038/ncomms15938.

[115] G. Wan, P. Yu, H. Chen, J. Wen, C.j. Sun, H. Zhou, N. Zhang, Q. Li, W. Zhao, B. Xie, Small. 14 (2018) 1704319, https://doi.org/10.1002/smll.201704319.

[116] Y.T. Kim, K. Ohshima, K. Higashimine, T. Uruga, M. Takata, H. Suematsu, T. Mitani, Angew. Chem. Int. Ed. 45 (2006) 407-411, https://doi.org/10.1002/anie.200501792.

[117] Z. Zhang, J. Liu, J. Wang, Q. Wang, Y. Wang, K. Wang, Z. Wang, M. Gu, Z. Tang, J. Lim, Nat. Commun. 12 (2021) 1-9, https://doi.org/10.1038/s41467-021-25562-y.

[118] E. Antolini, J. Power Sources. 170 (2007) 1-12, https://doi.org/10.1016/j.jpowsour.2007.04.009.

[119] A. von Weber, E.T. Baxter, S. Proch, M.D. Kane, M. Rosenfelder, H.S. White, S. Anderson, Phys. Chem. Chem. Phys. 17 (2015) 17601-17610, https://doi.org/10.1039/C5CP01824B.

[120] R. Liu, L.Q. Zhang, C. Yu, M.T. Sun, J.F. Liu, G. Jiang, Adv. Mater. 29 (2017) 1604571, https://doi.org/10.1002/adma.201604571.

[121] Y. Xiong, J. Dong, Z.-Q. Huang, P. Xin, W. Chen, Y. Wang, Z. Li, Z. Jin, W. Xing, Z. Zhuang, Nat. Nanotechnol. 15 (2020) 390-397, https://doi.org/10.1038/s41565-020-0665-x.

[122] Z. Li, Y. Chen, S. Ji, Y. Tang, W. Chen, A. Li, J. Zhao, Y. Xiong, Y. Wu, Y. Gong, Nat. Chem. 12 (2020) 764-772, https://doi.org/10.1038/s41557-020-0473-9.

[123] B.Q. Li, C.X. Zhao, S. Chen, J.N. Liu, X. Chen, L. Song, Q. Zhang, Adv. Mater. 31 (2019) 1900592, https://doi.org/10.1002/adma.201900592.

[124] T. Zheng, K. Jiang, N. Ta, Y. Hu, J. Zeng, J. Liu, H. Wang, Joule. 3 (2019) 265-278, https://doi.org/10.1016/j.joule.2018.10.015.

[125] T. Sheng, S.-G. Sun, Chem. Phys. Lett. 688 (2017) 37-42, https://doi.org/10.1016/j.cplett.2017.09.052.

[126] H.B. Yang, S.-F. Hung, S. Liu, K. Yuan, S. Miao, L. Zhang, X. Huang, H.-Y. Wang, W. Cai, R. Chen, Nat. Energy. 3 (2018) 140-147, https://doi.org/10.1038/s41560-017- 0078-8.

[127] Y.N. Gong, L. Jiao, Y. Qian, C.Y. Pan, L. Zheng, X. Cai, B. Liu, S.H. Yu, H.L. Jiang, Angew. Chem. Int. Ed. 59 (2019) 2705-2709, https://doi.org/10.1002/ange.201914977.

[128] J. Gu, C.-S. Hsu, L. Bai, H.M. Chen, X. Hu, Science. 364 (2019) 1091-1094, https://doi.org/10.1126/science.aaw7515.

[129] N. Zhang, X. Zhang, L. Tao, P. Jiang, C. Ye, R. Lin, Z. Huang, A. Li, D. Pang, H. Yan, Angew. Chem. Int. Ed. 60 (2021) 6170-6176, https://doi.org/10.1002/anie.202014718.

[130] X. Wang, Z. Chen, X. Zhao, T. Yao, W. Chen, R. You, C. Zhao, G. Wu, J. Wang, W. Huang, Angew. Chem. Int. Ed. 130 (2018) 1962-1966, https://doi.org/10.1002/ange.201712451.

[131] A.S. Varela, M. Kroschel, N.D. Leonard, W. Ju, J. Steinberg, A. Bagger, J. Rossmeisl, P. Strasser, ACS Energy Lett. 3 (2018) 812-817, https://doi.org/10.1021/acsenergylett.8b00273.

[132] X. Wang, W. Wang, M. Qiao, G. Wu, W. Chen, T. Yuan, Q. Xu, M. Chen, Y. Zhang, X. Wang, Sci. Bull. 63 (2018) 1246-1253, https://doi.org/10.1016/j.scib.2018.07.005.

[133] Q. Qin, T. Heil, M. Antonietti, M. Oschatz, Small. 2 (2018) 1800202, https://doi.org/10.1002/smtd.201800202.

[134] Z. Geng, Y. Liu, X. Kong, P. Li, K. Li, Z. Liu, J. Du, M. Shu, R. Si, J. Zeng, Adv. Mater. 30 (2018) 1803498, https://doi.org/10.1002/adma.201803498.

[135] H. Tao, C. Choi, L.-X. Ding, Z. Jiang, Z. Han, M. Jia, Q. Fan, Y. Gao, H. Wang, A. Robertson, Chem. 5 (2019) 204-214, https://doi.org/10.1016/j.chempr.2018.10.007.

[136] Y. Zhao, Y. Zhao, G. Waterhouse, L. Zheng, X. Cao, F. Teng, L. Wu, C. Tung, Adv. Mater. 29 (2017) 1703828, https://doi.org/10.1002/adma.201703828.

[137] J. Zhao, J. Zhao, Q. Cai, Phys. Chem. Chem. Phys. 20 (2018) 9248-9255, https://doi.org/10.1039/C7CP08626A.

[138] C. Ling, X. Bai, Y. Ouyang, A. Du, J. Wang, J. Phys. Chem. C. 122 (2018) 16842-16847, https://doi.org/10.1021/acs.jpcc.8b05257.

[139] Y. Xin, N. Zhang, Q. Li, Z. Zhang, X. Cao, L. Zheng, Y. Zeng, J. Anderson, Appl. Catal. B. 229 (2018) 81-87, https://doi.org/10.1016/j.apcatb.2018.02.012.

[140] J. Wu, Y. Li, Y. Yang, Q. Zhang, L. Yun, S. Wu, C. Zhou, Z. Jiang, X. Zhao, J. Mater. Chem. A. 7 (2019) 7202-7212, https://doi.org/10.1039/C8TA11528A.

[141] L. Wang, S. Zhang, Y. Zhu, A. Patlolla, J. Shan, H. Yoshida, S. Takeda, A.I. Frenkel, F. Tao, ACS Catal. 3 (2013) 1011-1019, https://doi.org/10.1021/cs300816u.

[142] S. Zhang, Y. Tang, L. Nguyen, Y.-F. Zhao, Z. Wu, T.-W. Goh, J.J. Liu, Y. Li, T. Zhu, W. Huang, ACS Catal. 8 (2018) 110-121, https://doi.org/10.1021/acscatal.7b01788.

[143] L. Nie, D. Mei, H. Xiong, B. Peng, Z. Ren, X.I.P. Hernandez, A. DeLaRiva, M. Wang, M.H. Engelhard, L. Kovarik, Science. 358 (2017) 1419-1423, https://doi.org/10.1126/science.aao2109.

[144] M. Yoo, Y.-S. Yu, H. Ha, S. Lee, J.-S. Choi, S. Oh, E. Kang, H. Choi, H. An, K.-S. Lee, Energy Environ. Sci. 13 (2020) 1231-1239, https://doi.org/10.1039/C9EE03492G.

[145] J. Resasco, L. DeRita, S. Dai, J.P. Chada, M. Xu, X. Yan, J. Finzel, S. Hanukovich, A.S. Hoffman, G.W Graham, S.R. Bare, X. Pan, P. Christopher, J. Am. Chem. Soc. 142 (2019) 169-184, https://doi.org/10.1021/jacs.9b09156.

[146] S. Zhao, F. Chen, S. Duan, B. Shao, T. Li, H. Tang, Q. Lin, J. Zhang, L. Li, J. Huang, Nat. Commun. 10 (2019) 1-9, https://doi.org/10.1038/s41467-019-11871-w.

[147] C. Wang, X.-K. Gu, H. Yan, Y. Lin, J. Li, D. Liu, W.-X. Li, J. Lu, ACS Catal. 7 (2017) 887-891, https://doi.org/10.1021/acscatal.6b02685.

[148] G. Xu, F. Liu, Z. Lu, S.H. Talib, D. Ma, Z. Yang, Phys. E: Low-Dimens. Syst. Nanostructures. 130 (2021) 114676, https://doi.org/10.1016/j.physe.2021.114676.

[149] V. Muravev, G. Spezzati, Y.-Q. Su, A. Parastaev, F.-K. Chiang, A. Longo, C. Escudero, N. Kosinov, E. Hensen, Nat. Catal. 4 (2021) 469-478, https://doi.org/10.1038/s41929-021-00621-1.

[150] A.A. Herzing, C.J. Kiely, A.F. Carley, P. Landon, G. Hutchings, Science. 321 (2008) 1331-1335, 10.1126/science.1159639.

[151] W.-C. Ding, X.-K. Gu, H.-Y. Su, W.-X. Li, J. Phys. Chem. C. 118 (2014) 12216-12223, https://doi.org/10.1021/jp503745c.

[152] P. Hu, Z. Huang, Z. Amghouz, M. Makkee, F. Xu, F. Kapteijn, A. Dikhtiarenko, Y. Chen, X. Gu, X. Tang, Angew. Chem. Int. Ed. 126 (2014) 3486-3489, https://doi.org/10.1002/ange.201309248.

[153] Q. Wang, K. Domen, Chem. Rev. 120 (2019) 919-985, https://doi.org/10.1021/acs.chemrev.9b00201.

[154] Y. Wang, H. Suzuki, J. Xie, O. Tomita, D.J. Martin, M. Higashi, D. Kong, R. Abe, J. Tang, Chem. Rev. 118 (2018) 5201-5241, https://doi.org/10.1021/acs.chemrev.7b00286.

[155] Y. Wang, Y. Zheng, C. Han, W. Chen, Nano Res. 14 (2021) 1682-1697, https://doi.org/10.1007/s12274-020-2919-1.

[156] F.E. Osterloh, Chem. Rev. 42 (2013) 2294-2320, https://doi.org/10.1039/C2CS35266D.

[157] B.-H. Lee, S. Park, M. Kim, A.K. Sinha, S.C. Lee, E. Jung, W.J. Chang, K.-S. Lee, J.H. Kim, S.-P. Cho, Nat. Mater. 18 (2019) 620-626, https://doi.org/10.1038/s41563-019-0344-1.

[158] X. Fang, Q. Shang, Y. Wang, L. Jiao, T. Yao, Y. Li, Q. Zhang, Y. Luo, H.L. Jiang, Adv. Mater. 30 (2018) 1705112, https://doi.org/10.1002/adma.201705112.

[159] X. Jin, R. Wang, L. Zhang, R. Si, M. Shen, M. Wang, J. Tian, J. Shi, Angew. Chem. Int. Ed. 132 (2020) 6894-6898, https://doi.org/10.1002/ange.201914565.

[160] H. Zhang, Y. Dong, S. Zhao, G. Wang, P. Jiang, J. Zhong, Y. Zhu, Appl. Catal. B.261 (2020) 118233, https://doi.org/10.1016/j.apcatb.2019.118233.

[161] F. Zeng, W.-Q. Huang, J.-H. Xiao, Y. Li, W. Peng, W. Hu, K. Li, G.-F. Huang, J. Phys. D: Appl. Phys. 52 (2018) 025501, https://doi.org/10.1088/1361-6463/aae81a.

[162] T. Tong, B. Zhu, C. Jiang, B. Cheng, J. Yu, Appl. Surf. Sci. 433 (2018) 1175-1183, https://doi.org/10.1016/j.apsusc.2017.10.120.

[163] X. Wu, H. Zhang, J. Dong, M. Qiu, J. Kong, Y. Zhang, Y. Li, G. Xu, J. Zhang, J. Ye, Nano Energy. 45 (2018) 109-117, https://doi.org/10.1016/j.nanoen.2017.12.039.

[164] X. Liu, S. Inagaki, J. Gong, Angew. Chem. Int. Ed. 55 (2016) 14924-14950, https://doi.org/10.1002/anie.201600395.

[165] X. Li, J. Yu, M. Jaroniec, X. Chen, Chem. Rev. 119 (2019) 3962-4179, https://doi.org/10.1021/acs.chemrev.8b00400.

[166] P. Huang, J. Huang, S.A. Pantovich, A.D. Carl, T.G. Fenton, C.A. Caputo, R.L. Grimm, A.I. Frenkel, G. Li, J. Am. Chem. Soc. 140 (2018) 16042-16047, https://doi.org/10.1021/jacs.8b10380.

[167] J. Di, C. Chen, S.-Z. Yang, S. Chen, M. Duan, J. Xiong, C. Zhu, R. Long, W. Hao, Z. Chi, Nat. Commun. 10 (2019) 1-7, https://doi.org/10.1038/s41467-019-10392-w.

[168] J. Yang, Y. Guo, W. Lu, R. Jiang, J. Wang, Adv. Mater. 30 (2018) 1802227, https://doi.org/10.1002/adma.201802227.

[169] S. Liu, Y. Wang, S. Wang, M. You, S. Hong, T.-S. Wu, Y.-L. Soo, Z. Zhao, G. Jiang, Q. Jieshan, B. Wang, Z. Sun, ACS Sustainable Chem. Eng. 7 (2019) 6813-6820, https://doi.org/10.1021/acssuschemeng.8b06134.

[170] X.-W. Guo, S.-M. Chen, H.-J. Wang, Z.-M. Zhang, H. Lin, L. Song, T.-B. Lu, J. Mater. Chem. A. 7 (2019) 19831-19837, https://doi.org/10.1039/C9TA06653E .

[171] W. Wu, E. Cui, Y. Zhang, C. Zhang, F. Zhu, C.-H. Tung, Y. Wang, ACS Catal. 9 (2019) 6335-6341, https://doi.org/10.1021/acscatal.9b01929.

[172] C.-C. Wang, J.-R. Li, X.-L. Lv, Y.-Q. Zhang, G.J.E. Guo, Energy Environ. Sci. 7 (2014) 2831-2867, https://doi.org/10.1039/C4EE01299B.

[173] F. Wang, Y. Wang, Y. Li, X. Cui, Q. Zhang, Z. Xie, H. Liu, Y. Feng, W. Lv, G. Liu, Dalton Trans. 47 (2018) 6924-6933, https://doi.org/10.1039/C8DT00919H.

[174] P. Xie, T. Pu, A. Nie, S. Hwang, S.C. Purdy, W. Yu, D. Su, J.T. Miller, C. Wang, ACS Catal. 8 (2018) 4044-4048, https://doi.org/10.1021/acscatal.8b00004.

[175] X. Zhang, Z. Sun, B. Wang, Y. Tang, L. Nguyen, Y. Li, F.F. Tao, J. Am. Chem. Soc. 140 (2018) 954-962, https://doi.org/10.1021/jacs.7b09314.

[176] L. Wang, W. Zhang, S. Wang, Z. Gao, Z. Luo, X. Wang, R. Zeng, A. Li, H. Li, M. Wang, X. Zheng, J. Zhu, W. Zhang, C. Ma, R. Si, J. Zeng, Nat. Commun. 7 (2016) 14036, https://doi.org/10.1038/ncomms14036.

[177] J. Shan, M. Li, L.F. Allard, S. Lee, M. Flytzani-Stephanopoulos, Nature, 551 (2017) 605-608, https://doi.org/10.1038/nature24640.

[178] Y. Tang, Y. Li, V. Fung, D.-e. Jiang, W. Huang, S. Zhang, Y. Iwasawa, T. Sakata, L. Nguyen, X. Zhang, A.I. Frenkel, F. Tao, Nat. Commun. 9 (2018) 1231, https://doi.org/10.1038/s41467-018-03235-7.

[179] P. Zhao, L. Ye, Z. Sun, B.T.W. Lo, H. Woodcock, C. Huang, C. Tang, A.I. Kirkland, D. Mei, S.C. Edman Tsang, J. Am. Chem. Soc. 140 (2018) 6661-6667, https://doi.org/10.1021/jacs.8b03012.

[180] E. Fernández, M.A. Rivero-Crespo, I. Domínguez, P. Rubio-Marqués, J. Oliver-Meseguer, L. Liu, M. Cabrero-Antonino, R. Gavara, J.C. Hernández-Garrido, M. Boronat, A. Leyva-Pérez, A. Corma, J. Am. Chem. Soc. 141 (2019) 1928-1940, https://doi.org/10.1021/jacs.8b07884.

[181] E.-K. Lee, S.-A. Park, H. Woo, K. Hyun Park, D.W. Kang, H. Lim, Y.-T. Kim, J. Catal. 352 (2017) 388-393, https://doi.org/10.1016/j.jcat.2017.05.005.

[182] Z. Chen, E. Vorobyeva, S. Mitchell, E. Fako, M.A. Ortuño, N. López, S.M. Collins, P.A. Midgley, S. Richard, G. Vilé, J. Pérez-Ramírez, Nat. Nanotechnol. 13 (2018) 702-707, https://doi.org/10.1038/s41565-018-0167-2.

[183] H. Miura, K. Endo, R. Ogawa, T. Shishido, ACS Catal. 7 (2017) 1543-1553, https://doi.org/10.1021/acscatal.6b02767.

[184] L. Ye, X. Duan, S. Wu, T.-S. Wu, Y. Zhao, A.W. Robertson, H.-L. Chou, J. Zheng, T. Ayvalı, S. Day, C. Tang, Y.-L. Soo, Y. Yuan, S. Tsang, Nat. Commun. 10 (2019) 914, https://doi.org/10.1038/s41467-019-08827-5.

[185] K. Zhou, W. Wang, Z. Zhao, G. Luo, J.T. Miller, M.S. Wong, F. Wei, ACS Catal. 4 (2014) 3112-3116, https://doi.org/10.1021/cs500530f.

[186] J. Shan, F.R. Lucci, J. Liu, M. El-Soda, M.D. Marcinkowski, L.F. Allard, E.C.H. Sykes, M. Flytzani-Stephanopoulos, Surf. Sci. 650 (2016) 121-129, https://doi.org/10.1016/j.susc.2016.02.010.

[187] A. Modak, J. Mondal, A. Bhaumik, Appl. Catal. A. General, 459 (2013) 41-51, https://doi.org/10.1016/j.apcata.2013.03.036.

[188] C. Wang, G. Garbarino, L.F. Allard, F. Wilson, G. Busca, M. Flytzani-Stephanopoulos, ACS Catal. 6 (2016) 210-218, https://doi.org/10.1021/acscatal.5b01593.

[189] C. Wang, M. Yang, M. Flytzani-Stephanopoulos, AlChE Journal. 62 (2016) 429-439, https://doi.org/10.1002/aic.15134.

[190] M. Mavrikakis, M.A. Barteau, J. Mol. Catal. A Chem. 131 (1998) 135-147, https://doi.org/10.1016/S1381-1169(97)00261-6.

[191] V. Fung, F. Tao, D.-e. Jiang, Phys. Chem. Chem. Phys. 20 (2018) 22909-22914, https://doi.org/10.1039/C8CP03191F.

[192] P. Tomkins, M. Ranocchiari, J.A. van Bokhoven, Acc. Chem. Res. 50 (2017) 418-425, https://doi.org/10.1021/acs.accounts.6b00534.

[193] T. Ikuno, J. Zheng, A. Vjunov, M. Sanchez-Sanchez, M.A. Ortuño, D.R. Pahls, J.L. Fulton, D.M. Camaioni, Z. Li, D. Ray, B.L. Mehdi, N.D. Browning, O.K. Farha, J.T. Hupp, C.J. Cramer, L. Gagliardi, J.A. Lercher, J. Am. Chem. Soc. 139 (2017) 10294-10301, https://doi.org/10.1021/jacs.7b02936.

[194] W. Liu, L. Zhang, X. Liu, X. Liu, X. Yang, S. Miao, W. Wang, A. Wang, T. Zhang, J. Am. Chem. Soc. 139 (2017) 10790-10798, https://doi.org/10.1021/jacs.7b05130.

[195] T. Zhang, D. Zhang, X. Han, T. Dong, X. Guo, C. Song, R. Si, W. Liu, Y. Liu, Z. Zhao, J. Am. Chem. Soc. 140 (2018) 16936-16940, https://doi.org/10.1021/jacs.8b10703.

[196] D. Deng, X. Chen, L. Yu, X. Wu, Q. Liu, Y. Liu, H. Yang, H. Tian, Y. Hu, P. Du, R. Si, J. Wang, X. Cui, H. Li, J. Xiao, T. Xu, J. Deng, F. Yang, P.N. Duchesne, P. Zhang, J. Zhou, L. Sun, J. Li, X. Pan, X. Bao, Sci. Adv. 1 (2015) e1500462, https://doi.org/10.1126/sciadv.1500462.

[197] M. Zhang, Y.-G. Wang, W. Chen, J. Dong, L. Zheng, J. Luo, J. Wan, S. Tian, W.-C. Cheong, D. Wang, Y. Li, J. Am. Chem. Soc. 139 (2017) 10976-10979, https://doi.org/10.1021/jacs.7b05372.

[198] X.-P. Yin, H.-J. Wang, S.-F. Tang, X.-L. Lu, M. Shu, R. Si, T.-B. Lu, Angew. Chem. Int. Ed. 57 (2018) 9382-9386, https://doi.org/10.1002/anie.201804817.

[199] Q. Li, W. Chen, H. Xiao, Y. Gong, Z. Li, L. Zheng, X. Zheng, W. Yan, W.-C. Cheong, R. Shen, N. Fu, L. Gu, Z. Zhuang, C. Chen, D. Wang, Q. Peng, J. Li, Y. Li, Adv. Mater. 30 (2018) 1800588, https://doi.org/10.1002/adma.201800588.

[200] P. Chen, T. Zhou, L. Xing, K. Xu, Y. Tong, H. Xie, L. Zhang, W. Yan, W. Chu, C. Wu, Y. Xie, Angew. Chem. Int. Ed. 56 (2017) 610-614, https://doi.org/10.1002/ange.201610119.

[201] G. Liu, A.W. Robertson, M.M.-J. Li, W.C.H. Kuo, M.T. Darby, M.H. Muhieddine, Y.-C. Lin, K. Suenaga, M. Stamatakis, J.H. Warner, S.C.E. Tsang, Nat. Chem. 9 (2017) 810-816, https://doi.org/10.1038/nchem.2740.

[202] J. Kibsgaard, Z. Chen, B.N. Reinecke, T.F. Jaramillo, Nat. Mater. 11 (2012) 963-969, https://doi.org/10.1038/nmat3439.

[203] X. Li, X. Yang, Y. Huang, T. Zhang, B. Liu, Adv. Mater. 31 (2019) 1902031, https://doi.org/10.1002/adma.201902031.

[204] H. Wei, X. Liu, A. Wang, L. Zhang, B. Qiao, X. Yang, Y. Huang, S. Miao, J. Liu, T. Zhang, Nat. Commun. 5 (2014) 5634, https://doi.org/10.1038/ncomms6634.

[205] J. Lin, A. Wang, B. Qiao, X. Liu, X. Yang, X. Wang, J. Liang, J. Li, J. Liu, T. Zhang, J. Am. Chem. Soc. 135 (2013) 15314-15317, https://doi.org/10.1021/ja408574m.

[206] M.-M. Millet, G. Algara-Siller, S. Wrabetz, A. Mazheika, F. Girgsdies, D. Teschner, F. Seitz, A. Tarasov, S.V. Levchenko, R. Schlögl, E. Frei, J. Am. Chem. Soc. 141 (2019) 2451-2461, https://doi.org/10.1021/jacs.8b11729.

[207] Y. Zhao, H. Zhou, W. Chen, Y. Tong, C. Zhao, Y. Lin, Z. Jiang, Q. Zhang, Z. Xue, W.-C. Cheong, B. Jin, F. Zhou, W. Wang, M. Chen, X. Hong, J. Dong, S. Wei, Y. Li, Y. Wu, J. Am. Chem. Soc. 141 (2019) 10590-10594, https://doi.org/10.1021/jacs.9b03182.

[208] Y. Wang, K. Qi, S. Yu, G. Jia, Z. Cheng, L. Zheng, Q. Wu, Q. Bao, Q. Wang, J. Zhao, X. Cui, W. Zheng, Nano-Micro Lett. 11 (2019) 102, https://doi.org/10.1007/s40820-019-0324-7.

[209] T. Yamada, T. Kojima, E. Abe, S. Kameoka, Y. Murakami, P. Gille, A.P. Tsai, J. Am. Chem. Soc. 140 (2018) 3838-3841, https://doi.org/10.1021/jacs.7b13658.

[210] L. Lin, W. Zhou, R. Gao, S. Yao, X. Zhang, W. Xu, S. Zheng, Z. Jiang, Q. Yu, Y.-W. Li, C. Shi, X.-D. Wen, D. Ma, Nature, 544 (2017) 80-83, https://doi.org/10.1038/nature21672.

[211] R. Lang, T. Li, D. Matsumura, S. Miao, Y. Ren, Y.-T. Cui, Y. Tan, B. Qiao, L. Li, A. Wang, X. Wang, T. Zhang, Angew. Chem. Int. Ed., 55 (2016) 16054-16058, https://doi.org/10.1002/anie.201607885.

[212] Y. Zhao, J. Liang, C. Wang, J. Ma, G.G. Wallace, Adv. Energy Mater. 8 (2018) 1702524, https://doi.org/10.1002/aenm.201702524.

[213] F. Wang, Y. Wang, Y. Feng, Y. Zeng, Z. Xie, Q. Zhang, Y. Su, P. Chen, Y. Liu, K. Yao, W. Lv, G. Liu, Appl. Catal. B. 221 (2018) 510-520, https://doi.org/10.1016/j.apcatb.2017.09.055.

[214] Z. Chen, S. Pronkin, T.-P. Fellinger, K. Kailasam, G. Vilé, D. Albani, F. Krumeich, R. Leary, J. Barnard, J.M. Thomas, J. Pérez-Ramírez, M. Antonietti, D. Dontsova, ACS Nano.10 (2016) 3166-3175, https://doi.org/10.1021/acsnano.5b04210.

[215] G. Wang, T. Zhang, W. Yu, R. Si, Y. Liu, Z. Zhao, ACS Catal. 10 (2020) 5715-5722, https://doi.org/10.1021/acscatal.0c01099.

[216] M. Ou, S. Wan, Q. Zhong, S. Zhang, Y. Wang, Int. J. Hydrog. Energy. 42 (2017) 27043-27054, https://doi.org/10.1016/j.ijhydene.2017.09.047.

[217] H. Li, Y. Wu, C. Li, Y. Gong, L. Niu, X. Liu, Q. Jiang, C. Sun, S. Xu, Appl. Catal. B. 251 (2019) 305-312, https://doi.org/10.1016/j.apcatb.2019.03.079.

[218] Y. Wang, X. Zhao, D. Cao, Y. Wang, Y. Zhu, Appl. Catal. B. 211 (2017) 79-88, https://doi.org/10.1016/j.apcatb.2017.03.079.

[219] A. Bakandritsos, R.G. Kadam, P. Kumar, G. Zoppellaro, M. Medved', J. Tuček, T. Montini, O. Tomanec, P. Andrýsková, B. Drahoš, Adv. Mater. 31 (2019) 1900323, https://doi.org/10.1002/adma.201900323.

[220] V. Urbanová, K. Holá, A.B. Bourlinos, K. Čépe, A. Ambrosi, A.H. Loo, M. Pumera, F. Karlický, M. Otyepka, R. Zbořil, Adv. Mater. 27 (2015) 2305-2310, https://doi.org/10.1002/adma.201500094.

[221] J. Tuček, K. Holá, A.B. Bourlinos, P. Błoński, A. Bakandritsos, J. Ugolotti, M. Dubecký, F. Karlický, V. Ranc, K. Čépe, Nat. Commun. 8 (2017) 1-12, https://doi.org/10.1038/ncomms14525.

[222] G.-P. Gao, S.-H. Wei, X.-M. Duan, J. Phys. Chem. C. 116 (2012) 24930-24934, https://doi.org/10.1021/jp306620b.

[223] J. Fu, J. Dong, R. Si, K. Sun, J. Zhang, M. Li, N. Yu, B. Zhang, M.G. Humphrey, Q. Fu, ACS Catal. 11 (2021) 1952-1961, https://doi.org/10.1021/acscatal.0c05599.

[224] S.K. Kaiser, A.H. Clark, L. Cartocci, F. Krumeich, J. Pérez-Ramírez, Small. 17 (2021) 2004599, https://doi.org/10.1002/smll.202004599.

[225] Y. Feng, W. An, Z. Wang, Y. Wang, Y. Men, Y.J.A.S.C. Du, ACS Sustainable Chem. Eng. 8 (2019) 210-222, https://doi.org/10.1021/acssuschemeng.9b05183.

[226] Z. Hou, L. Dai, Y. Liu, J. Deng, L. Jing, W. Pei, R. Gao, Y. Feng, H. Dai, Appl. Catal. B. 285 (2021) 119844, https://doi.org/10.1016/j.apcatb.2020.119844.

[227] M. Ouyang, K.G. Papanikolaou, A. Boubnov, A.S. Hoffman, G. Giannakakis, S.R. Bare, M. Stamatakis, M. Flytzani-Stephanopoulos, E.C.H. Sykes, Nat. Commun. 12 (2021) 1-11, https://doi.org/10.1038/s41467-021-21555-z.

[228] G.X. Pei, X.Y. Liu, A. Wang, A.F. Lee, M.A. Isaacs, L. Li, X. Pan, X. Yang, X. Wang, Z. Tai, ACS Catal. 5 (2015) 3717-3725, https://doi.org/10.1021/acscatal.5b00700.

TOC

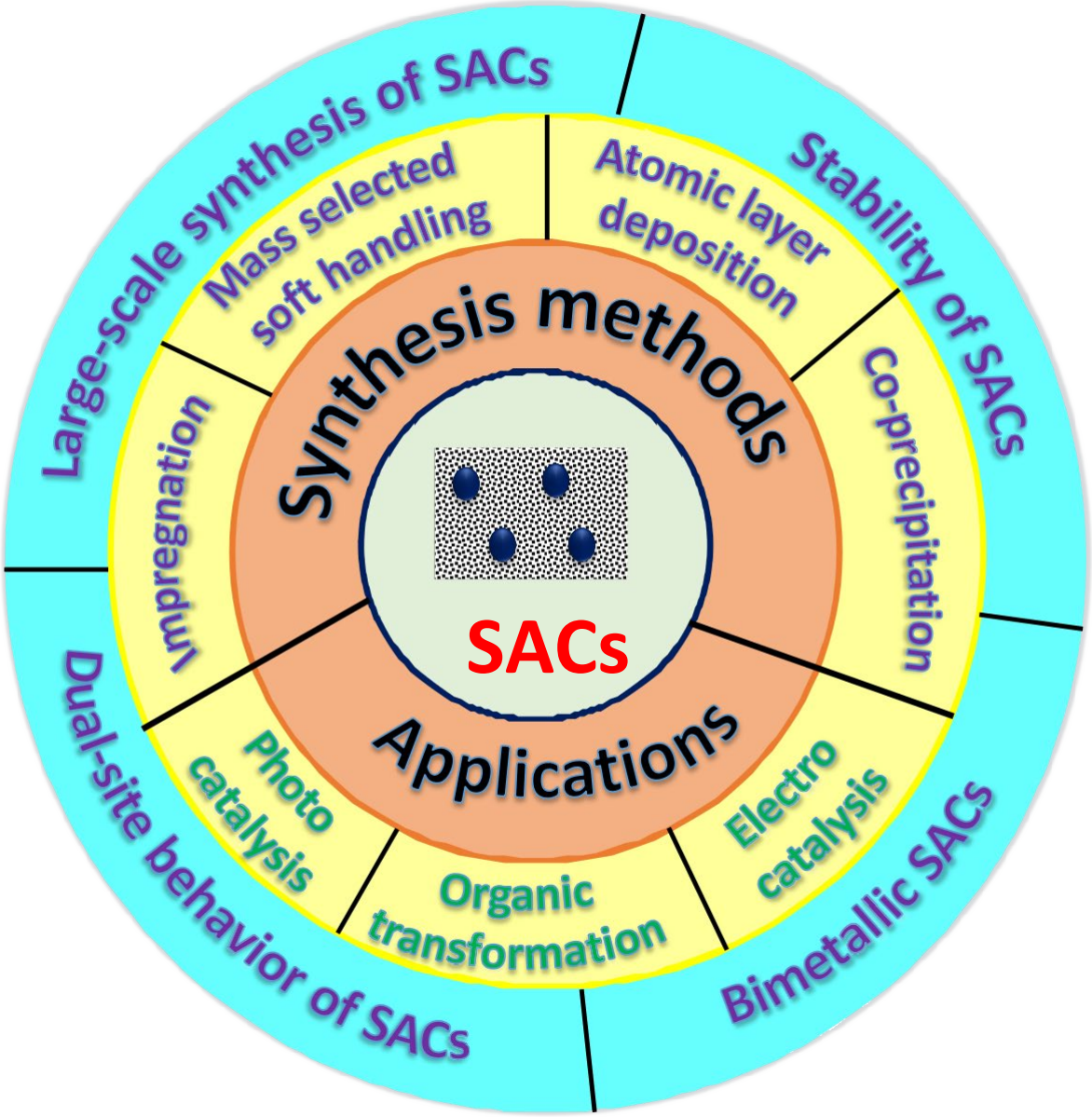
Large-scale synthesis of SACs
Stability of SACs
Dual-site behavior of SACs
Bimetallic SACs
Synthesis methods
Mass selected soft handling
Atomic layer deposition
Impregnation
Co-precipitation
SACs
Applications
Photo catalysis
Organic transformation
Electro catalysis

Conflict of interest

Title: A Comprehensive study on Heterogeneous Single Atom Catalysis: Current Progress, and Challenges

Authors:

Swarnalata Swain-Draft preparation

Ali Altaee, Manav Saxena and Akshaya K Samal-Reviewing, final drafting and supervision

The authors declare that there is no conflict of interest.